Structural collapse:
The sources and effects of volcano flank instability, a case study from the Canary Islands

Dissertation zur Erlangung des Doktorgrades
der Mathematisch-Naturwissenschaftlichen Fakultät
der Christian-Albrechts-Universität zu Kiel

vorgelegt von
Thomas R. Walter
geboren in Konstanz

Kiel, März 2002

Chicken or egg ?

Referent: Prof. Hans-Ulrich Schmincke, PhD

Koreferent: Priv. Doz. Dr. Matthias Hort

Tag der mündlichen Prüfung: _____

Zum Druck genehmigt: _____

Der Dekan

Hiermit erkläre ich an Eides statt, dass die vorliegende Abhandlung, abgesehen der Beratung durch meine akademischen Lehrer, nach Inhalt und Form meine eigene Arbeit darstellt. Ferner habe ich weder diese noch eine ähnlich Arbeit an einer anderen Abteilung oder Hochschule im Rahmen eines Prüfungsverfahrens vorgelegt.

Thomas R. Walter

Table of contents

Conception and preface i
Introduction iv
Einleitung vi

Part I: Volcano flank instability by caldera formation

Chapter 1: Formation of caldera periphery faults 1
Formation of caldera periphery faults: an experimental study 2
Abstract 2
Introduction 2
Experimental set-up 3
Results 7
Pure doming 7
Pure evacuation collapse 8
Doming and collapse 10
Summary and discussion 12
Doming 13
Evacuation collapse 13
Combined doming and evacuation collapse 14
Effect of the initial edifice geometry 15
Natural examples 17
Tumescence 17
Evacuation collapse 17
Multi-stage caldera activity 18
Conclusion 19
Acknowledgements 19
References 20

Chapter 2: Cyclic caldera collapse 22
Cyclic caldera collapse: piston or piecemeal subsidence? 23
Abstract 23
Introduction 23
Field observation 24
Experiments 27
Discussion 30
Acknowledgements 30
References 31

Chapter 3: Mirrors of shallow magma reservoirs 32
Collapse calderas – mirrors of shallow magma reservoirs 33
Abstract 33
Introduction 33
Caldera formation experiments 34
Comparison with natural calderas 36
Tejeda Caldera on Gran Canaria 36
Rabaul Caldera, Papua New Guinea 37
Discussion 37
Implications for natural calderas 37
Las Cañadas Caldera, Tenerife 37
Olympus Mons, Mars 39
Galapagos Calderas 39
Limitations 40
Conclusion 40
Acknowledgements 41
References 41

Part II: Volcano flank instability and dike intrusions

Chapter 4: Recurrent flank collapse in Teno 42
Rifting, recurrent landsliding and Miocene structural reorganization in Teno, NW-Tenerife (Canary Islands) 43
Abstract 43
Introduction 43
Volcano-tectonic evolution of Tenerife 45
The structure of Teno 46
Los Gigantes collapse 48
Carrizales collapse 50
Teno rift zones 51
Mazca Rift Zone 52
Teno Bajo Rift Zone 53
The fracture belt(s) 57
Discussion 58
Conclusion 61
Acknowledgements 61
References 62

Chapter 5: Rift architecture in volcanoes 63
Rift architecture in volcanoes: from single rift to triaxial rifts 64
Abstract 64
Introduction 64
The progress of rifting: persistence or feebleness? 65
Geological setting of Anaga (Tenerife) 66
Anaga rift zones 68
Taganana area – the roots of a landslide? 69
Physical models 71
Experimental setup and procedure 71
Discussion 73
Conclusion 74
Acknowledgements 75
References 75

Chapter 6: Creeping – collapse – rifting 77
Creeping - collapse - rifting: the structural feedback on volcanoes 78
Abstract 78
Introduction 78
Volcano instability and rifting 79
Gravity-driven volcano deformation 80
Experimental procedure 82
Stable situation 84
Unstable situation 85
How many axes? 88
Implications 90
La Palma: Taburiente shield volcano 91
Discussion 94
Summary and conclusion 96
Acknowledgements 97
References 97

Appendix

Conference contributions 99
Flank destabilization of cyclic caldera volcanoes 100
Rift architecture in volcanoes: from single rift to triaxial rifts 101
Modeling volcano structures 102
Flank creep, sector collapse and the formation of volcanic rift zones 103
Acknowledgements 104
Curriculum Vitae 105

List of Figures

I.1. Experimental set-up 4
I.2. Doming experiments 7
I.3. Pure evacuation collapse 9
I.4. Plot for pure evacuation experiments 10
I.5. Chamber inflation and subsequent deflation 11
I.6. Experiments with cone morphology 12
I.7. Plot of multi-stage flour experiments 13
I.8. Sections through the edifice 14
I.9. Reconstruction of characteristic structures 16

II.1. Structural map of Gran Canaria 25
II.2. Experimental setup and results 29

III.1. Illustration of caldera formation 34
III.2. Derived relationship between reservoir size, depth and caldera diameter 35
III.3. Caldera examples: Gran Canaria, Tenerife, Rabaul Caldera 38
III.4. Olympus Mons Caldera, Mars 39

IV.1. Structural axes of Tenerife 45
IV.2. Photographs of Teno unconformities 48
IV.3. Maps of Teno 49
IV.4. Photographs of fracture belt near Los Carrizales 51
IV.5. Schmidt's projections, rose and contour diagrams for dikes and fractures 54
IV.6. Photo plate, Teno 56
IV.7. Dike swarm of Teno Bajo Rift 57
IV.8. Comparison to Etna–Stromboli 59
IV.9. Cycle of volcano construction and destruction 60

V.1. Location of the study area Anaga (NE Tenerife) 67
V.2. Dikes of the oldest dike swarm of the Taganana rift zone 69
V.3. Sheared dikes 70
V.4. Experimental setup 71
V.5. Photographs and sketches of the experiments 72

VI.1. Rift zone lengths as a function of volcano height 79
VI.2. Types of gravity-driven volcano deformation 81
VI.3. Geometry of the cones 82
VI.4. Photographs of gelatine experiments 83
VI.5. Stable situation plot 85
VI.6. Summarized arrangement of hydrofractures 87

VI.7. Amount of rift zones as a function of total number of experiments 88
VI.8. Canary Islands, structural axes and landslides 90
VI.9. Least effort model 91
VI.10. Structural evolution of La Palma 93
VI.11. Four main types of rift zones related to sector creep 96

List of Tables

I.1. Selected experiments and measured geometric structures 6
II.1. Geometric relations of experiments versus Gran Canaria 28
III.1. Experimental scaling 36
IV.1. Structural evolution of Teno 47

Conception and Preface

The main aim of this thesis is to elucidate structural mechanisms that destabilize volcano flanks and the mutual effects of edifice growth and its gravity-driven destruction. Pertinent morphological depressions resulting from lateral and vertical collapses were studied in the Canary Islands. Questions include (i) the evolutionary stage at which a volcanic island becomes critically unstable, (ii) where and why do giant landslides form, and (iii) what is the genetic and temporal relationship between intrusions and flank instability?
The principal localities studied are Gran Canaria and Tenerife, both islands experienced large-scale flank failures during their growth. Field and analytical evidence reveals the structural disparity of the caldera-type edifice (Gran Canaria) and rift-type edifice (Tenerife) and illustrates the mechanisms of flank destabilization. The multifaceted interaction of magma intrusion and decline of a volcano's stability was studied in analog experiments.
Since the constructional contrasts between Gran Canaria and Tenerife illustrate different types of instability, this thesis is separated into two main sections:

(I) Volcano flank instability by caldera formation (caldera-type volcanoes) (Chapters 1, 2 and 3), and

(II) Volcano flank instability and dike intrusions (rift-type volcanoes) (Chapters 4, 5 and 6).

All chapters are manuscripts written for peer-review publication in scientific journals. Each chapter contains separate sections on introduction, geological setting, data acquisition and discussion, and a separate reference list. Chapters 1 and 2 are already published; chapter 4 has been accepted for publication. Chapters 3 and 5 are submitted to a journal, and might be subject to changes; Chapter 6 is in preparation. All chapters are collaborative studies. First authorship manuscripts form chapters 1, 3, 4, 5, and 6. My contribution to the individual chapters was 60% (Chapter 1), 40% (Chapter 2), 70% (Chapter 3), 80% (Chapter 4), 70% (Chapter 5), and 80% (Chapter 6).

Part I: Volcano flank instability by caldera formation

Chapter 1

Walter TR and Troll VR (2001): Formation of caldera periphery faults: an experimental study. *Bulletin of Volcanology* 63: 191-203.

Summary: This chapter deals with experimentally simulated dynamic processes of inflating and emptying magma reservoirs and related volcano flank deformation. In scaled sandbox experiments, volcano flank structures are studied with respect to volcano morphology, magma reservoir shape and position; associated fault domains are categorized. It is shown how active flank faulting, sector detachment and thus flank collapses are related to caldera-forming events.

Chapter 2

Troll VR, Walter TR and Schmincke H-U (2002): Cyclic caldera collapse: piston or piecemeal subsidence? Field and experimental evidence. *Geology* 30: 135-138.

Summary: The formation of destabilizing mechanisms on the volcanic flanks of Gran Canaria is demonstrated. Detailed field work revealed the longevity and stages of fault reactivation, and the systematic dike patterns around the islands' flanks, providing the natural counterpart to analog experiments that were directly scaled to the dimensions of Gran Canaria. The chapter discusses the structural influence of the shallow expanding and contracting magma reservoir, predominant fault formation on the island, and implies mechanisms jointly responsible for structural collapses during the Miocene shield-building stage.

Chapter 3

Walter TR, Troll VR, Amelung F, Seyfried R: Collapse calderas – mirrors of shallow magma reservoirs. Submitted to *Geophysical Research Letters*.

Summary: This paper aims to constrain the internal volcano structure beneath calderas. Based on experimental modeling, a simple quadratic equation is given to estimate the dependencies of magma reservoir depth, reservoir diameter and caldera size. The size of a magma reservoir is one of the most debated questions in volcanology. The experimental data presented allows inferences for reservoir sizes of various caldera-type volcanoes (e.g. Gran Canaria, Rabaul, Galapagos or Olympus Mons). A further application is illustrated for Tenerife: the 16-km-wide Las Cañadas caldera is underlain by a reservoir of only 4 km diameter. This chapter shows that a collapse caldera on Tenerife was mechanically an unlikely incident. It is argued that erosion and huge landslides were extensively involved in the formation of the morphological basin of Tenerife. This study may help to identify other huge landslide scarps, previously interpreted as collapse calderas.

Part II: Volcano flank instability and dike intrusions

Chapter 4

Walter TR and Schmincke H-U (2002): Rifting, recurrent flank collapse and structural reorganization in Teno, NW-Tenerife (Canary Islands). *International Journal of Earth Sciences (Geologische Rundschau)* (in press).

Summary: This paper provides insights into related structures in the deeply eroded Miocene composite shield volcano "Teno" on northwestern Tenerife. Based on structural field work, periodic northward-directed volcano instability is characterized. This chapter focuses on the configuration of rift zones and of individual dikes and fractures. Dike directions changed after sector collapse events, implying a near-surface stress-field modification. Decompression and shearing caused intense crushing, forming a "fractured belt" that surrounds the landslide scarps. This fracture belt is described in detail based on several profiles and structural (data analysis) methods. Mechanisms of episodic stages of volcano sector collapses are discussed.

Chapter 5

Walter TR, Troll VR, Belousov A, Schmincke H-U: Rift architecture in volcanoes: from single rift to triaxial rifts. Submitted to *Physics and Chemistry of Dykes*, edited by MK Watkeys, Balkema Press, Spec. Vol.

Summary: This work combines field analysis and analog modeling, showing the non-durability of rift zones, exemplified by the Miocene shield "Anaga" in northeastern Tenerife. The early structure of Anaga was dominated by a single rift, significantly changing to triaxial rift-geometry as the northern sector (Taganana area) became unstable. The question is posed, using analog experiments, if rifting decouples the stress field and causes flank destabilization, or if weak volcano flanks may have a deep-reaching effect on rift zones. One of the results of this study is that volcano rift zones are not long-term stable structures. Instead, the dynamic feedback of volcano spreading, accompanied stress field changes and rift adjustment governed the structural evolution of Anaga.

Chapter 6

Walter TR, Troll VR and Schmincke H-U: Creeping - collapse - rifting: the structural feedback on volcanoes. In preparation for *Journal of Geophysical Research*.

Summary: This study aims to improve our understanding of volcano sector-creep prior to structural collapse, focusing on associated configuration of rift zones. This manuscript summarizes the results of extensive experiments on hydro-fracture propagation in elastic materials. Structures of the western Canary Islands, such as on La Palma are discussed. It is shown that rift zones (the most dominant volcanic island structures) could form, establish and change as a consequence of stress-field changes close to unstable creeping volcanic flanks. This chapter focuses on destructive–constructive interaction processes and provides a clue to locate weak substratum and local flank instabilities on volcanoes.

Introduction

The Canary Islands comprise seven islands with individual and long-term volcanic record, all of them but La Gomera having been active in the past 5ka (Schmincke 1994). Seaward-facing escarpments, up to more than one kilometer deep and tens of kilometers long, are prominent morphological features on these volcanic islands, as well on many volcanic edifices worldwide. Alexander v. Humboldt (1814), one of the first explorers on the Canary Islands, paid attention to the geological evolution of such scar-like valleys on Tenerife. A few years later a discussion of the development of the common morphological depressions of the Canary Islands ensued: Léopold von Buch (1825) applied the term "elevated crater" (caldera) to a more than 2000 m deep scarp in northern La Palma. Charles Lyell, on the other hand, postulated in 1855 that significant erosion was involved in the formation of the Taburiente Caldera on La Palma and Las Cañadas Caldera on Tenerife. Other huge morphological depressions, such as the scar-like Orotava valley on southeastern Tenerife were likewise interpreted as formed by erosion (Fritsch & Reiss 1868). About hundred years later, Bravo (1952, 1962) was one of the first to consider the steep scars of Las Cañadas Caldera, Orotava and Güímar valleys on Tenerife as the results of gravitational block sliding. Such a landslide-hypothesis, however, was broadly doubted because of the implied huge volumes (tens of cubic kilometers) of material to fail from the volcanic flanks into the sea.

Since the spectacular and well-witnessed landslide which triggered the climactic 1980 Mt. Helens eruption (Lipman & Mullineaux 1982), the unstable nature and structural collapse of volcanic edifices have become recognized and attracted attention globally (e.g. Duffield et al. 1981; Siebert 1984; Holcomb & Searle 1984; Moore et al. 1994). Evidences for giant landslides have been identified in the following years at many volcanoes (Siebert 1984). About 75% of the Andean volcanoes taller than 2.5 km collapsed (Francis 1994). Around 100 debris avalanches –the resulting landslide deposit– have been documented around Quaternary Japanese volcanoes (Inokuchi 1988). At least three major 20^{th} century collapses are reported from Kamchatka (Belousov 1994). Extensive submarine deposits associated with about 70 giant landslides of Hawaiian ocean island volcanoes were mapped, some of the landslides attained lengths of over 200 km, volumes exceeding 5000 km^3 (Moore et al 1994). All these facts show that the instability and collapse of volcanic flanks is ubiquitous.

Based on submarine studies around the Canaries, enormous volumes (10^3-10^4 km^3) of landslide deposits were verified (Watts & Masson 2001), the mean landslide frequency being there ca. 125-170 ka (Krastel et al. 2001, Masson et al. 2002). The upper submarine slide deposits north of Tenerife are correlated to very recent events, implying that volcano instability is still active (Watts & Masson 2001). Also subaerial studies reveal the high frequency and hazard potential of sector collapses, producing scarps much above the sea level (e.g. Navarro & Coello 1989; Carracedo 1994; Hürlimann et al. 1999).

The sources of subaerial and submarine volcano flank destabilization are largely speculative. Although large temporal and spatial variety of volcanic Islands (cf. Canaries –

Hawaii), the sizes, types and incidences of sector collapse events are generally very similar (Carracedo 1994; Krastel et al. 2001). This implies common factors to be responsible. Gravity force itself may cause volcano spreading and tensional flank-slip along discrete detachment surfaces (Delaney & Denlinger 1999; van Wyk de Vries et al. 1997; Borgia et al. 2000). These forces are moreover biased by dike[1] intrusions that nucleate in swarms and rift zones. High magmatic or hydraulic pressures within rift zones may push a volcano segment seaward and thus trigger décollement of huge volcanic sectors (Siebert 1984; Walker 1992; Iverson 1995; Elsworth & Voight 1996). Based on numerical calculations we know that a volcano is in critical balance of its load, intrusions and the mechanical properties of the rocks (Dieterich 1988; Iverson 1995). Intrusive doming increases the instability of volcanic flanks, which are triggered to fail by e.g. earthquakes and tremors, fault reactivation or oversteepening (Voight & Elsworth, 2000). Decrease of the cohesion and internal friction coefficient of rocks by, e.g alteration or high pore pressures, ease fault formation (Iverson 1995). Therefore, the distribution of weak layers inside a volcano or easy deformable substratum is of importance, facilitating volcano deformation and sector collapse (Nakamura 1980; Clague & Denlinger 1994).

Since weak materials focus the volcano strain, but the volcano deformation directs dike intrusions, which again alters the stress field, a steady stress/strain balance and structural feedback is given. Rift zones are accordingly the cause but also the result of volcano deformation (the chicken or egg problem).

To reconstruct the volcanotectonic stress field, several chapters of the present study are based upon statistically analyzed dike and fracture patterns. The adjacent islands Tenerife and Gran Canaria harbor dikes and dike swarms in different structural arrangements. On Gran Canaria, during the shield building stage and formation of the central Tejeda Caldera dikes grouped in radial and concentric trends. On Tenerife, in contrast, dikes formed rift zones, i.e. structural axes, aligned eruption vents and thus topographic ridges. The location, direction, and frequency of sector collapses are largely influenced by those rift zones. Sector collapses on Gran Canaria are not related to similar rift zones, hence the structural comparison and case studies of these two volcano-types help to better understand the temporal and spatial emergence of unstable volcano flanks and structural collapses. It is shown that local volcano stress fields and volcanotectonics play a fundamental role in the development of rift zones and sector failure on rift-type volcanoes (Tenerife), while magma reservoir dynamics controls the flank instability on caldera-type volcanoes (Gran Canaria).

[1] Dikes are thought to propagate as magmatic pressure-driven, liquid-filled fractures. They are thus orientated perpendicular to the main extensional stress direction. Analyzing dike arrangements therefore allows to infer the paleostress environment of the time of emplacement. If the magmatic pressure does not exceed strength criteria of the rocks, the tendency to intrude existing planes of weakness is enhanced.

Einleitung

Die Kanaren umfassen sieben Inseln, gekennzeichnet durch eine sehr lange Entwicklungsgeschichte, wobei alle Inseln, außer La Gomera, in den letzten 5000 Jahren aktiv waren (Schmincke 1994). Gewaltige, zur See gerichtete „Täler", oft über einen Kilometer tief und mehrere Zehnerkilometer lang, sind an Vulkangebäuden allgemein äußerst auffallend.

Auf den Kanaren begann die Diskussion über die Entstehung solcher morphologisch auffälliger Kar-ähnlicher Täler schon bei A.v. Humboldt (1814). Wenige Jahre später entbrannte die bis heute andauernde Diskussion zu ihrer Entstehung: Léopold von Buch definierte 1825 den Begriff „Caldera" (Erhebungskrater), während Charles Lyell (1855) eher Erosion als Hauptursache für die Entstehung der Calderen von Taburiente (La Palma) und Las Cañadas (Tenerife) deutete. Auch andere große morphologische Senken, wie das Orotavatal im Südosten Tenerifes wurden durch Erosion erklärt (Fritsch und Reiss 1868). Erst ca. hundert Jahre später erwägt Bravo (1952, 1962), die steilen riesigen Senken der Las Cañadas Caldera, sowie die Täler von Orotava und Güímar auf Tenerife könnten das Resultat von gravitativen Blockrutschungen sein. Vielfach wurde die derart kühne Hangrutsch-Hypothese angezweifelt, da es unmöglich schien dass ganze Vulkanflanken ins Meer stürzen könnten.

Erst seit dem bezeugten Abbruch der Mount St. Helens Nordflanke im Jahre 1980 (Lipman & Mullineaux 1982), begann man die Gefahr von Flankenkollapsen, bei denen sich u.a. Massenbewegungen mehrerer Kubikkilometer ereignen, zu untersuchen und zu verstehen. Seither mehren sich Hinweise darauf, dass fast alle ozeanischen Vulkane während ihres raschen Aufbaustadiums deformiert und destabilisiert werden und an ihren Flanken episodisch kollabieren (z.B. Duffield et al. 1981; Siebert 1984; Holcomb & Searle 1984; Moore et al. 1994). So zeigen 75% der Andenvulkane über 2,5 km Höhe Hinweise auf einstige Flankenkollapse (Francis 1994). Ca. 100 Schuttstromablagerungen – resultierende Ablagerungen von Flankenkollapsen – wurden um die quartären Vulkane Japans identifiziert (Inokuchi 1988). Drei große Flankenkollapse des 20. Jh. wurden alleine von Kamchatka beschrieben (Belousov 1994). Über 70 voluminöse submarine Hangrutsch-Ablagerungen wurden um die Hawaiianischen Inseln kartiert, z.T. über 200 km lang bei bis 5000 km³ Volumen (Moore et al. 1994). All diese Nachweise offenbaren wie gegenwärtig Instabilität und Kollapsgefahren an Vulkanen sind.

Untersuchungen des Meeresbodens im Raum der Kanaren konnten große Hangrutschungen (10^3-10^4 km³) nicht nur an den Flanken der älteren (15-20 Ma), sondern auch an den noch aktiven Inseln aufzeigen, dort mit einer mittleren Häufigkeit von einem Hangrutsch pro 125-170 ka (Krastel et al. 2001, Masson et al. 2002). Junge Hangrutschablagerungen vor Nord-Tenerife lassen vermuten, dass Massenverlagerungen den Vulkankomplex auch heute noch verändern (Watts & Masson 2001). Auch an Land mehren sich die Hinweise auf episodisch wiederkehrende Flankenkollapse (z.B. Navarro & Coello 1989; Carracedo 1994; Hürlimann et al. 1999).

Die Ursachen für die Destabilisierung von subaerischen und submarinen Flanken sind im wesentlichen unbekannt bzw. spekulativ. Da das zeitliche Auftreten von Flankenkollapsen an verschiedenen Inselketten äußerst unterschiedlich sein kann (Kanaren - Hawaii), dennoch ihre Ausbildung und Art ähnlich ist (Carracedo 1994; Krastel et al. 2001), müssen die Hauptfaktoren für die Instabilität vulkanischer Gebäude in ihrem Aufbau und internen Spannungsfeld liegen (Voight & Elsworth 2000). Es wird diskutiert, dass Vulkane alleine durch das eigene Gewicht deformieren (*spreading*) und die Vulkanflanken nach außen gleiten (Delaney & Denlinger 1999; van Wyk de Vries et al. 1997; Borgia et al. 2000). Die auf die Vulkanflanken einwirkenden Kräfte sind zudem in ihrer Richtung und Größe während magmatisch aktiver Phasen durch die Intrusion vulkanischer Gänge[2] (*dikes*) ständig veränderbar. Mit Hangbewegungen koexistierende Gangintrusionen oder Riftzonen lassen vermuten, dass die hohen magmatischen Drücke imstande sind eine ganze Vulkanflanke nach außen zu pressen (Siebert 1984; Walker 1992; Iverson 1995; Elsworth & Voight 1996). Nach numerischen Kräftefeldsimulationen befindet sich ein Vulkan in einem kritischen Gleichgewicht des Eigengewichtes, dem Winkel der inneren Reibung der Gesteine, sowie der Reibung/Festigkeit an der Vulkanbasis (Dieterich 1988; Iverson 1995). Eine wichtige Rolle kommt weichen Lagen zu, welche das Vulkangebäude mechanisch lockern (Nakamura 1980; Clague & Denlinger 1994; Iverson 1995). Domung, Intrusion und vor allem die Eigenlast bilden demnach die kritischen Spannungen, die letztlich durch sogenannte Trigger, wie z.B. Erdbeben, reaktivierte Störungen und Schwächezonen, Übersteilung, etc., "überkritisch" und ausgelöst werden (Voight & Elsworth, 2000).

Um das kontrollierende vulkantektonische Spannungsfeld zu rekonstruieren, wurden in dieser Arbeit systematisch Gänge analysiert, sowie statistische Methoden herangezogen zur Klärung der Bildung von Riftzonen, Störungs- und Kluftsystemen. An den ca. 70 km auseinanderliegenden Inseln Gran Canaria und Tenerife treten Gänge in strukturell grundsätzlich unterschiedlichen Schwärmen auf. Auf Gran Canaria sind die Gänge der Schildphase insgesamt radial und konzentrisch um die zentrale Tejeda Caldera angeordnet. Die Struktur von Gran Canaria wurde durch eine flachkrustale Magmakammer geprägt. Auf Tenerife definieren hingegen zumeist parallel intrudierte Gänge strukturelle Achsen, die, bedingt durch die dort fokussierte magmatische Aktivität, morphologische Rücken bildeten. Die Anzahl, Größe und Richtung von Flankenkollapsen an Tenerife (und den anderen westlichen Kanarischen Inseln) scheint bestimmt von der Lage und Ausgeprägtheit von jeweils zwei benachbarten Riftzonen, wobei die dazwischenliegenden Bereiche besonders instabil sind. Da aber auf Gran Canaria keine vergleichbaren Riftzonen erkennbar, und dennoch Flankenkollapse nachgewiesen sind, müssen weitere Prozesse den Zusammenhalt verringern. Wie in der vorliegenden Arbeit verdeutlicht

[2] Da magmatische Gänge durch unter Überdruck propagierende, flüssigkeitsgefüllte Brüche darstellen, intrudieren sie längs einer Richtung senkrecht zur größten Extensionsrichtung und erlauben so eine Paläospannungsanalyse. Falls jedoch der magmatische Druck nicht ausreicht, um neue Brüche zu erzeugen und präexistente tektonische Strukturen und Schwächezonen vorherrschen, tendieren Gänge und Gangschwärme dazu, in diese Zonen des geringeren Widerstandes zu intrudieren.

wird, haben vielmehr Prozesse des lokalen Spannungsfeldes und der lokalen Vulkantektonik eine wichtige Rolle für die Riftzonenentwicklung.
Die initialen und destabilisierenden Mechanismen an Calderavulkanen und Riftvulkanen wurden wegen der strukturellen Unterschiedlichkeiten im Rahmen dieser Dissertation insbesondere untersucht. Die vorliegende Abhandlung ist demgemäss gegliedert in zwei Teile; Teil I behandelt Flankenstrukturen und Implikationen an Calderavulkanen (am Beispiel Gran Canaria), in Teil II werden Entwicklungsgänge an Riftzonenvulkanen ausgearbeitet, sowie auf rückwirkende und interagierende Prozesse im Speziellen eingegangen (z.B. Tenerife, La Palma). Jeweils bilden drei veröffentlichungsreife, bzw. bereits veröffentlichte Manuskripte, unterschiedliche Aspekte in separaten Kapiteln.

Zitate/References:

Borgia A, Delaney P, Denlinger RP (2000) Spreading Volcanoes. Ann Rev Earth Planet Sci 28: 539-570.

Buch L von (1825) Pysikalische Beschreibung der Canarischen Inseln. Königl Akad Wiss, Berlin: 201p.

Bravo T (1952) Aportación al estudio geomorfológica y geológico de la costa de la fosa tectónica del valle de la Orotava. Bol R Soc Esp Hist Nat, Tomo L, 1-30.

Bravo T (1962) El circo de la Las Cañadas y su dependencia. Bol R Soc Esp Hist Nat G 60, 93-109.

Carracedo JC (1994) The Canary Islands: An example of structural control on the growth of large oceanic-island volcanoes. J Volcanol Geotherm Res 60: 225-241.

Clague DA, Denlinger RP (1994) The role of olivine cumulates in destabilizing the flanks of Hawaiian volcanoes. Bull Volcanol 56: 425-434.

Delaney P, Denlinger R P (1999) Stabillization of volcanic flanks by dike intrusion: an example from Kilauea. Bull Volcanol 61: 356-362.

Dieterich JH (1988) Growth and persistence of Hawaiian volcanic rift zones. J Geophys Res 93: 4258-4270.

Duffield WA, Stieltjes L, Varet J (1981) Huge landslide blocks in the growth of Piton de la Fournaise La Reunion and Kilauea Volcano Hawaii J Volc Geotherm Res 12: 147-160.

Elsworth D, Voight B (1996) Evaluation of volcano flank instability triggered by dyke intrusion. In: Volcano Instability on the Earth and Terrestrial Planets (Hrsg. WJ McGuire, AP Jones und J Neuberg). Geol Soc of London Spec Publ No 110: 45-53.

Francis PW (1994) Large volcanic debris avalanches in the central Andes. In: Proceedings of International Conference on Volcano Instability on the earth and other planets. Geol Soc Ldn.

von Fritsch R, Reiss W (1868) Geologische Beschreibung der Insel Tenerife. Wurster und Co. Winterthur: 494p.

Holcomb RT, Searle RC (1991) Large landslides from oceanic volcanoes. Mar Geotechnol 10: 19-32.

Humboldt Av (1814) Voyages aux régions equinoxiales du nouveau continent 1799-1804. Dufour et Cie Paris 1: 1-200.

Hürlimann M, Ledesma A, Marti J (1999) Conditions favouring catastrophic landslides on Tenerife (canary Islands). Terra Nova 11: 106-111.

Inokuchi T (1988) Gigantic landslides and debris avalanches on volcanoes in Japan. In: Proceedings of the Kagoshima International Conference on Volcanoes. Nat Inst Res Admin Jpn 456-459.

Iverson RM (1995) Can magma-injection and groundwater forces cause massive landslides on Hawaiian volcanoes? J Volcanol Geotherm Res 66: 295-308.

Krastel S, Schmincke H-U (2001) Crustal structure of northern Gran Canaria deduced from active seismic tomography. J Geohys Res 106, 3977-3997.

Lipman PW, Mullineaux DR (1982) The 1980 eruptionas of Mount st. Helens, Washington. Geol Surv Prof Pap 1250: 844pp.

Lyell C (1855) A manual of elementary geology. 5th Ed. (John Murray) London: 498p.

Masson DG, Watts AB, Gee MJR, Urgeles R, Mitchell NC, Le Bas TP, Canals M (2002) Slope failures on the flanks of the western Canary Islands. Earth Sci. Rev. 57, 1-35.

Moore JG, Normark WR, Holcomb RT (1994) Giant Hawaiian landslides. Ann Rev Earth Planet Sci 22: 119-144.

Nakamura K (1980) How do long rift zones develop in Hawaiian volcanoes? - A possible role of thick oceanic sediments. Volcanol Soc Jpn Bull 25: 255-269.

Navarro JM, Coello J (1989) Depression originated by landslide processes in Tenerife. ESF Meeting on Canarian Volcanism 159-152.

Siebert L (1984) Large volcanic debris avalanches: characteristics of source areas, deposits, and associated eruptions. J Volcanol Geotherm Res 22: 163-197.

Schmincke H-U (1994) Geological field guide of Gran Canaria: Part I and II. Pluto Press: 1-64.

Walker GPL (1992) Coherent intrusion complexes in large basaltic volcanoes - a new structural model. J Volcanol Geotherm Res 50: 41-54

van Wyk de Vries B, Francis PW (1997) Catastrophic collapse at stratovolcanoes induced by gradual volcano spreading. Nature 387: 387-390.

Voight B, Elsworth D (2000) Instability and collapse of hazardous gas-pressurized lava domes. Geophys Res Lett 27.

Watts AB, Masson DG (2001) New sonar evidence for recent catastrophic collapses of the north flank of Tene-

Part I: Volcano flank instability by caldera formation

Chapter 1

Formation of caldera periphery faults

Formation of caldera periphery faults: an experimental study

Thomas R. Walter, Valentin R. Troll
Abt. Vulkanologie & Petrologie, GEOMAR, Wischhofstrasse 1-3, 24148 Kiel, Germany

Abstract. Changing stresses in multi-stage caldera volcanoes were simulated in scaled analogue experiments aiming to reconstruct the mechanism(s) associated with caldera formation and the corresponding zones of structural weakness. We evaluate characteristic structures resulting from doming (chamber inflation), evacuation collapse (chamber deflation) and cyclic resurgence (inflation and deflation), and we analyse the consequential fault patterns and their statistical relationship to morphology and geometry. Doming results in radial fractures and subordinate concentric reverse faults which propagate divergently from the chamber upwards with increasing dilation. The structural dome so produced is characterised by steepening in the periphery, whereas the broadening apex subsides. Pure evacuation causes the chamber roof to collapse along adjacent bell-shaped reverse faults. The distribution of concentric faults is influenced by the initial edifice morphology; steep and irregular initial flanks result in a tilted or chaotic caldera floor. The third set of experiments focused on the structural interaction of cyclic inflation and subsequent moderate deflation. Following doming, caldera subsidence produces concentric faults that characteristically crosscut radial cracks of the dome. The flanks of the edifice relax, resulting in discontinuous circumferential faults that outline a structural network of radial and concentric faults; the latter form locally uplifted and tilted wedges (halfgrabens) that grade into horst-and-graben structures. This superimposed fault pattern also extends inside the caldera. We suggest that major pressure deviations in magma chamber(s) are reflected in the fault arrangement dissecting the volcano flanks and may be used as a first-order indication of the processes and mechanisms involved in caldera formation.

Keywords. Multi-stage caldera volcanoes - Caldera periphery faults - Volcano fractures - Flank instability

Introduction

Large, multi-stage "ash-flow calderas" are thought to form mainly during voluminous ignimbrite eruptions (e.g. Smith and Bailey 1968; Schmincke 1969; Williams and McBirney 1979; Druitt and Sparks 1984; Newhall and Dzurisin 1988; Lipman 1997). Rapid decompression of a shallow magma chamber during large eruptions causes deflation and the chamber roof subsides into the "void" thus created (Smith and Bailey 1968; Druitt and Sparks 1984). In addition to extensive field studies of caldera volcanoes (see Lipman

1997, and references therein), caldera formation has been studied theoretically and experimentally (Wisser 1927; Prucha 1965; Komuro et al. 1984; Komuro 1987; Gudmundsson 1988; Marti et al. 1994; Branney 1995; Gudmundsson et al. 1997; Odonne et al. 1999; Roche et al.2000; Marti et al. 2000). Caldera volcanoes illustrate structural elements of several types, with arrangements and quantities depending on, for example, the physical properties of the country rocks, pre-existing tectonic structures or a regional stress field, the geometry and dynamics of the magma chamber and the volcanic load. Inflation of a magma chamber causes volumetric spreading and swelling, combined with the effect of hundreds to thousands of intrusions, distributed mainly in radial or circumferential order (Komuro et al. 1984; Walker 1999). Also, radial and circumferential fractures develop in scaled experiments by inflation of an analogue reservoir (e.g. Marti et al. 1994), which contrasts with the exclusively concentric structures of pure evacuation collapse (Komuro 1987; Roche et al. 2000). Caldera volcanoes with several episodes of chamber inflation and evacuation collapse are thus likely to produce intersecting structural systems (Komuro 1987; Marti et al. 1994). The inflation of a chamber as a result of pressure increase (e.g. due to replenishment) is detected by uplift of the ground surface, accompanied by magma chamber wall burst and dyke growth (McLeod and Tait 1999). Tilt measurements on active volcanoes show that they undergo repeated inflation and deflation. Volcano inflation is slow, whereas deflation is very rapid, but the amounts of inflation and deflation are generally very similar (Swanson 1982).

Moreover, complex caldera periphery dykes and faults are common and surround caldera volcanoes on earth (Smith and Bailey 1968) and other planets (Thomas et al. 1990). The formation of this peripheral system, however, has received little attention in the literature and remains poorly understood. Since intracaldera structural relations are normally hidden, the extracaldera periphery fault system may help to reconstruct the evolution of such calderas in the field.

To better understand peripheral caldera faults and their relations to magma chamber dynamics, we experimentally studied the overall caldera fracture system for the cases of (a) pure doming, (b) pure evacuation collapse and (c) the combination of both. Herein, we focus on the geometry and propagation of the fractures produced by these scenarios and their relationship to chamber depth, chamber size, material properties and edifice morphology. We refer to natural examples where the arrangement of faults and dykes indicates the mechanism(s) from which those patterns originate.

Experimental set-up

Inflatable reservoirs were constructed by attaching two equivalent-sized mats of very thin stretchy rubber at the outer rims. In the lower mat, we inserted an inlet and connected a pipe system, through which inflation and evacuation of a balloon was accomplished. An

outflow valve was joined to the pipe. The volume of air/water within the balloon-pipe system was held constant for various initial geometric parameters. The balloon(s) were sill-like in shape with radii ranging from 6 to 12 cm and were inflated up to a height of 6 cm. To test the influence of the shape of the reservoir, experiments were also carried out using oval-shaped balloons.

A glass tank with the dimension of approximately 1 m^3 was filled to a depth of several tens of centimetres with granular analogue material. The balloon was placed in the centre of the box and a mound was constructed above, so as to simulate a volcanic cone (Fig. 1).

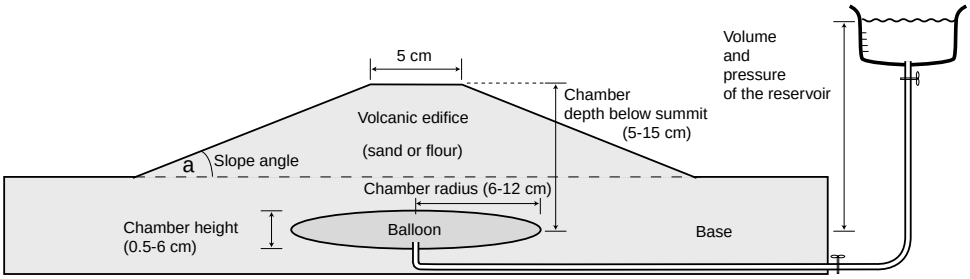

Fig. 1. *Experimental set-up: the geometry was systematically changed for slope angle, cone height, chamber depth below the summit and the chamber size (height, width). See text for details*

In separate set-ups, we varied the shape and size of the reservoir and the cone, in order to evaluate the relevance of individual geometric parameters for the models. More than 30 different geometries defined by these parameters were examined.

Analogue models were geometrically scaled to fit natural ocean-island volcanoes (cf. Schmincke 1976; Ye et al. 1999), where regional tectonic influences are believed to be small. The general set-up of the experiments simulated sill-like shallow magma chambers situated at depths between 5 and 15 km below the surface of a volcanic edifice. The geometric scaling factor was 10^{-5}, so that 1 cm in the experiment is approximately equivalent to 1 km in nature. The geometric similarity of the models is based on the ratios of the external forces, gravity forces, internal friction forces and resistant forces against failure. Experimental scaling followed Hubbert (1937), Sanford (1959) and Komuro et al. (1984), using the suggested ratios of external forces to gravity force and of internal friction to resistant forces. The generality and relation of the experimentally derived fault sites was established by using two analogue materials, medium-grained sand and wheat flour. Both analogue materials were measured mechanically in direct shear tests. Dry medium-grained sand is characterised by low cohesion and obeys the Mohr-Coulomb failure criterion (cf. Hubbert 1951; Byerlee 1978; Mandl 1988) with scaled yield strength and internal friction angles (ϕ) resembling those of volcanic rocks (e.g. for basalt $\phi_B = 30\text{-}45°$).

Sand has been widely used as a modelling material (Hubbert 1937, 1951; Sanford 1959; Ramberg 1981); its mechanical properties are well known (see Cobbold and Castro 1999 for review). We used sieved quartz sand with a mean diameter of 500 μm mixed with a subordinate amount of clay minerals, a bulk density of 1.5-1.7 g cm^{-3} (depending on consolidation) and a coefficient of internal friction (μ) of $\mu_S = 0.6$ (i.e. $\phi_S = 31°$). The cohesion (C) of sand was controlled by the pore-water pressure, and determined in direct shear tests and undrained triaxial tests. The natural cohesion is in the range of 10^5-10^7 Pa (e.g. Hoshino et al. 1972; Glicken et al. 1980). Higher standards of 10^7 Pa represent values of small laboratory samples, whereas 10^6 Pa approaches the cohesion lowered by large-scale inhomogeneity effects (Schultz 1996). An analogue material with an average mean cohesion scaling to ca. $5x10^6$ Pa was therefore chosen to be appropriate. The pore-water pressure in sand was accordingly held at a value so that the cohesion was approximately $5x10^1$ Pa ($C_S = 40$-50 Pa). Once dilated, the cohesion of sand decreases and allows fault reactivation (Krantz 1991). Elastic strain, however, cannot be studied in sand models (Cobbold and Castro 1999).

The second analogue material was dry flour (grain size 100-200 μm). Its mechanical properties were found to be complementary to medium-grained sand in being more cohesive ($C_F = 35$ Pa) relative to its density (~ 0.57 g cm^{-3}). Dry flour, therefore, deforms little under its own weight and offers the possibility to study the geometry and propagation of faults in detail; tensional strength was not to scale. The coefficient of internal friction for flour is $\mu_F = 0.65$ ($\phi_F = 33°$).

Edge effects were kept at a minimum by using a very big glass tank and a highly elastic and thin balloon material, where the finite size of the balloon allowed control of its deformation. On the other hand, however, to deform the elastic walls of the balloon during inflation, its internal pressure needed to be high relative to the load (i.e. lithostatic pressure). As a result, the balloons entail the deformation of the roof, not the contrary. Eruptions during high magma-chamber pressures could not form, so that the wide range of modelled doming discussed here possibly includes some structural end members, not observed in nature.

We used three methods to obtain and compare three-dimensional data on the orientation and propagation of faults: a) The depth of the balloon was systematically changed within a set of models of the same morphology, b) models were saturated in water and sectioned after deformation, and c) a set of experiments was performed against a transparent glass pane.

The surface deformation was filmed and photographed and the length, distance and displacement of each fault type was measured and recorded (Table 1). The positions of the observed circumferential (concentric) faults are described as a function of the volcano perimeter and the total distances from the centre.

Model description	Chamber depth	Initial slope inclination, 0 = plateau	Steepness after doming	Radial cracks diameter	Apical graben diameter	Subsidence apical graben	Concentric peripheral fault diameter	Concentric peripheral fault length	Ring fault diameter	Subsidence ring fault	Remarks
	(cm)	(°)	(°)	(cm)	(cm)	(cm)	(cm)	(°)	(cm)	(cm)	
Doming and evacuation experiments with two cycles of resurgence and withdrawal											
Exp12Zykl1	5	0	28	20	7	0.5	22	20	18	0.6	HS PM
Exp12Zykl2	5	0	36	27	9	1	28	9	18	1.3	HS PM
Exp12Zykl3	5	0	30	30	11	1.5	28	3	19	2	PM
Exp13Zykl1	5	10	30	23	6	0.3	23	12	18	0.3 + 0.3	HS PM
Exp13Zykl2	5	10	30	26	8	1.4	24	8	19	1HS + 0.3	PM
Exp13Zykl3	5	10	35	28	10	1.5	24	7	19	2	PM
Exp14Zykl1	5	20	35-40	20	7	1.5	22	10	18	0.8	PM
Exp14Zykl2	5	20	40	24	11	1.5	24	6	19	1.8	PM
Exp14Zykl3	5	20	40	25	ca.12	1.5-2	24	3	19.5	2.3	PM
Exp15Zykl1	5	30	44	19	8	1.2	20.5	7	16	0.3	HS PM
Exp15Zykl2	5	30	45	20	10	1.5	21	6	17	0.3	PM
Exp15Zykl3	5	30	48	23	13	1.8	23	5	17	0.6	PM
Exp4Zykl1	7	10	30	22	7	0.5	24	15	17	0.5	HS
Exp4Zykl2	7	10	35	23	8	1	25	8	18	1	PM
Exp4Zykl3	7	10	40	26	n.d.	n.d.	27	5	20	1.2	PM
Exp5Zykl1	7	0	20	20	5	0.5	22	15	16	0.3	HS
Exp5Zykl2	7	0	30	26	7	1	24	5	17/19	0.7	PM
Exp5Zykl3	7	0	30	28	9	2	27	4	17.5	2	PM
Exp16Zykl1	9	0	27	21	7	1.8	22.5	19	14	0.6	Fig. 7
Exp16Zykl2	9	0	28	25	12	1.5	27	10	16	1.8	PM
Exp16Zykl3	9	0	28	30	15	1	29	6	20	2	PM
Exp17Zykl1	9	5	28	20.8	6.5	1.6	22	16	14.6	0.7	Fig. 7
Exp18Zykl1	9	10	30	19.8	6	2	23	14	14.6	0.5	Fig. 7
Exp19Zykl1	9	15	34	19.5	7.5	1.8	21	10	14.8	0.6	Fig. 7
Exp19Zykl2	9	15	35	22	9	1.3	25	7	15.5	0.9	PM
Exp19Zykl3	9	15	33	28	10	1	29	6	17.3	1.3	PM
Exp20Zykl1	9	20	35	19.5	7	2.2	20.5	9	15.3	0.6	Fig. 7
Exp21Zykl1	9	25	39	19.3	7.5	1.9	20.3	8.5	15.6	0.7	Fig. 7
Exp22Zykl1	9	30	44	18.5	8	2	20	7	16	0.6	Fig. 7
Exp22Zykl2	9	30	50	27	9	2.3	29	9	21	0.7	PM
Exp22Zykl3	9	30	37	30	12	2.5	29	6	22	1.2	PM
Exp2Zykl1	11	30	40	33	7	n.d.	34	8	17	0.8	
Exp2Zykl2	11	30	45	35	n.d.	n.d.	34	8	21	2.2	PM
Exp2Zykl3	11	30	50	34	n.d.	n.d.	34	8	23	2.5	PM
Exp1Zykl1	11.5	35	40	30	n.d.	n.d.	18	12	17	1.5	HS
Exp1Zykl2	11.5	35	60	36	n.d.	n.d.	29	5	21	4	PM
Exp1Zykl3	11.5	35	60	36	n.d.	n.d.	33	5	25	4	PM
Pure evacuation experiments											
[F] Exp23	5	0	n.d.	n.d.	n.d.	n.d.	24.3	n.d.	17.4	0.4	Fig. 4
[S] Exp24	5	0	n.d.	n.d.	n.d.	n.d.	22	n.d.	19	2	BL
[F] Exp27	7	0	n.d.	n.d.	n.d.	n.d.	23	n.d.	17.2	0.4	Fig. 4
[S] Exp28	7	0	n.d.	n.d.	n.d.	n.d.	22	n.d.	16.5	0.7	BL
[F] Exp30	9	0	n.d.	n.d.	n.d.	n.d.	20.5	n.d.	14	0.6	Fig. 4
[S] Exp31	9	0	n.d.	n.d.	n.d.	n.d.	20	n.d.	14	0.9	BL
[S] Exp33	11	0	n.d.	n.d.	n.d.	n.d.	18.5	n.d.	13	1	BL
[F] Exp34	11	0	n.d.	n.d.	n.d.	n.d.	17.8	n.d.	13.7	0.7	Fig. 4
[F] Exp36	13	0	n.d.	n.d.	n.d.	n.d.	14.5	n.d.	12.5	0.7	Fig. 4
[S] Exp37	13	0	n.d.	n.d.	n.d.	n.d.	15	n.d.	13.3	1.6 + 0.2	HS
[F] Exp38	15	0	n.d.	n.d.	n.d.	n.d.	12	n.d.	10	2	P
[S] Exp40	15	0	n.d.	n.d.	n.d.	n.d.	n.d.	n.d.	9.5	2	P

Table 1. *Selected experiments and measured geometric structures, for 16-cm balloon diameter. Column 1 is the model description and identifies the experiment (e.g. Exp5) and the cycle of resurgence (Zykl1-3). F Experiments in flour, S sand; if not specified each experiment was modelled twice using both materials average values. Columns 2-11 present the measured maximal distribution of structures. Column 12 summarises types of subsidence (HS horseshoe shaped; BL bench-like; P piston; PM piecemeal). n.d. Not defined*

Results

The results are summarised according to the three end-member mechanisms of pure doming (reservoir inflation), pure evacuation collapse (reservoir deflation), and recurring inflation and deflation. For each of those mechanisms, we checked the influence of the initial volcano morphology and gravitational forces. Additionally, the influence of different chamber depths was tested for each of these set-ups. Every experiment was reproduced and performed for both analogue materials.

Pure doming

A plateau surface was arranged in separate experimental set-ups at 5, 7, 9, 11, 13 and 15 cm above the balloon. Upon balloon inflation, the surface fractured forming radial cracks that propagated outwards from a central polygonal block (Fig. 2). The radial fractures propagated perpendicularly to the least principal compressive stress $\sigma 3$ and parallel to the maximum principal compressive stress $\sigma 1$, with displacements approximately normal to the fracture surface (mode-I fractures). Independent of the experimental geometries and analogue material, concentric reverse (thrust) faults formed subperpendicular to the opening radial cracks, resulting in a morphological "s-shaped" flank deformation (Fig. 2).

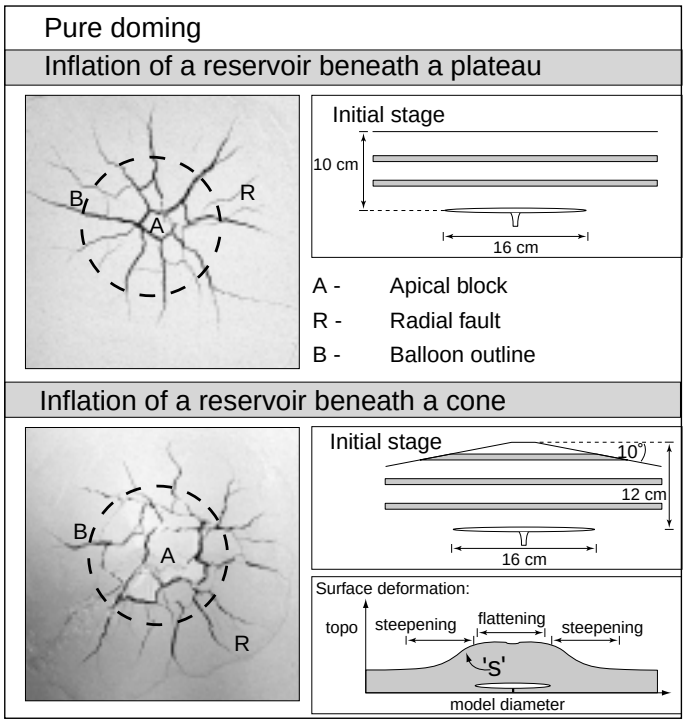

Fig. 2. *Photographs of doming experiments in flour taken from the top and sketch of initial experimental conditions. Inset lower right outlines the regions of morphological steepening and flattening (not to scale)*

The dip of these curved concentric faults decreased towards the periphery and within individual set-ups as a function of increasing chamber depth. The relative motion of the fracture combined extensional and shear displacements, propagating upwards. The

uplifted flanks also produced a flattening and subsequent polygonal apical graben structure (i.e. proto-caldera) in all doming experiments, similar to those described by Komuro (1987) and Marti et al. (1994). The apical graben was chiefly limited by steep, rotational normal faults. The depression widened by polygonal blocks that were detached from the oversteepened walls. Some apical grabens were defined by only one tilted and/or downward slumped angular block.

Experiments with deeper balloons resulted in larger areas of (a) tumescence, (b) apical graben and (c) radial cracks. Deeper situated reservoirs resulted moreover in a reduced domal uplift and a reduced apical graben subsidence.

For cone-shaped morphologies, doming produced a more heterogeneous radial fault pattern compared with the plateau-shaped morphology. This is most likely a function of the model construction, differing slightly from an ideally shaped cone.

Greater initial flank inclination (steepness) of the cone resulted in the surface-parallel stress being tensional at the apex of the edifice but compressive in its periphery (see Figs. 8, 9). The latter influenced the orientation of concentric reverse faults on the flanks, which became shallower with increasing flank inclination near the surface. The region of apical extension increases and the subsiding area was larger, compared with plateau-shaped experiments (Fig. 2). In dry sand experiments, flank oversteepening of the initial steep cones ($>20°$) produced grain-flow processes and occasionally outward-directed slides.

Pure evacuation collapse

In pure evacuation experiments, a balloon was inflated prior to its emplacement at the desired depth. The reservoir was then evacuated, simulating chamber deflation by, for example, magma withdrawal from a magma chamber, causing the chamber roof to subside. On evacuation, slight downsagging (<0.5 cm) was the initial surface expression, followed by failure along numerous discrete sub-circular concentric fractures on the surface (Fig. 3). Modelling different heights of the plateau showed the third dimension of these faults to be mostly outward dipping (i.e. "bell-shaped"; Fig. 3), corroborating previous studies (e.g. Marti et al. 1994; Roche et al. 2000). This set of curved faults propagated from the reservoir upwards, where the first underground faults were arranged sub-horizontally above the centre of the balloon, followed by steeper synthetic faults (main ring faults; Fig. 3). At the surface, these concentric faults defined an en echelon pattern, forming a circular arrangement around a central collapse basin. Wedge-shaped and crescentic blocks slumped and tilted from the outer undisturbed wall into the basin along a set of interconnected antithetic listric faults. Failure of hanging-wall blocks occurred, causing the caldera rim to propagate outwards (Fig. 3).

No radial cracks developed during the pure evacuation collapse experiments (cf. Marti et al. 1994). The central basin subsided largely as a piston but was repeatedly dissected to crescentic benches bound by two or three outward-dipping concentric faults reaching the surface (Fig. 3). This was more common in experiments with a shallow chamber (i.e. 5-8 cm).

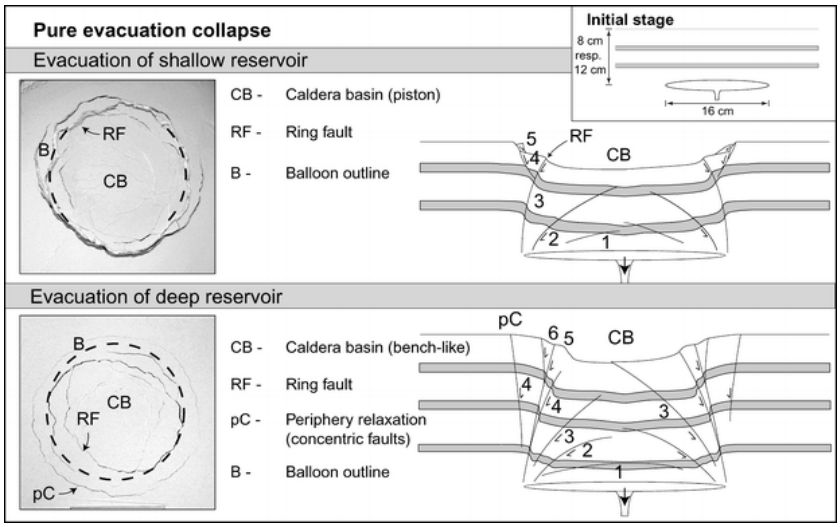

Fig. 3. *Pure evacuation collapse of an analogue magma chamber beneath an initial plateau surface. Photographs of flour experiments and schematic profiles from sectioned experiments show the structural development of a shallow and a deep magma chamber. Separate experiments near a glass pane allowed assignment of numbers, indicating the chronological order of the faults*

Some experiments developed a discrete circumferential zone of vertical to inward-dipping normal faults, with a total diameter larger than the simulated magma chamber, but lacking a significant dilation. As pointed out by Roche et al. (2000), these were triggered by outward-dipping reverse faults. Inward-tilted wedges formed that were defined by such antithetic periphery cracks and the outer ring fault(s) (Figs. 3, 4).

To evaluate the influence of the initial topography, the deflation experiments were performed beneath cones with an initial flank steepness of 10, 15, 20, 25 and 30°. With larger initial flank inclination, the central collapse basin was fractured in an increasingly chaotic manner. The position of concentric fractures was influenced by gravity load and gradually shifted outwards with increasing cone inclination. Increasing the chamber depth caused a systematic decrease of the near-surface diameters of the encircling concentric faults (Fig. 4).

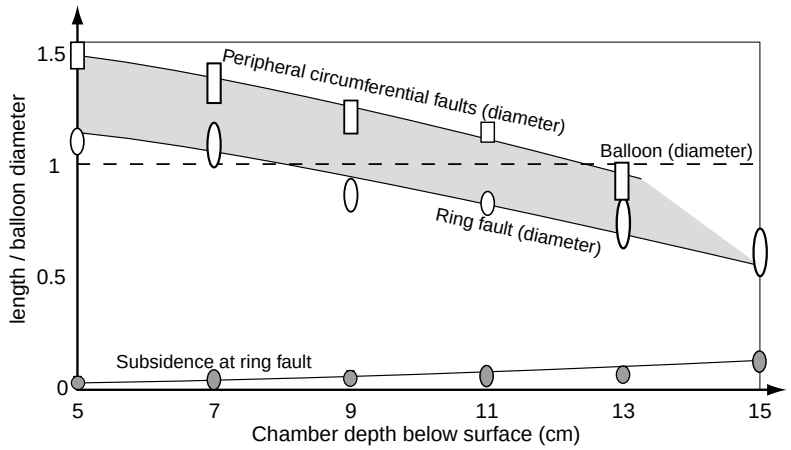

Fig. 4. *Plot for pure evacuation experiments beneath a plateau showing chamber depth vs length of the measured structures (ring fault diameter, ring fault subsidence, diameter of periphery circumferential faults, balloon diameter) as a function of the balloon diameter. Data points at variance due to analogue materials are shown as vertically elongated and were connected by a "best-fit" curve. Increasing chamber depth shows a slight increase of the ring fault subsidence rate, a decrease of the diameter of the major ring faults and a decrease of the peripheral circumferential faults. One centimetre in experiments corresponds to approximately 1 km in nature.*

Doming and collapse

Experiments were designed to simulate doming and subsequent chamber evacuation, focusing on the interaction of the resulting structures. Doming reproduced the tumescent fault arrangement, i.e. radial cracks and subordinate concentric reverse faults, followed by encircling or horseshoe-shaped faults which define an apical graben with a mean diameter approximately half of the reservoir diameter (see Fig. 7).

Subsequent evacuation resulted in a closure of the radial cracks, accompanied by two concentric domains: (a) a bell-shaped fracture system forming the major caldera basin (main ring fault); and (b) periphery en echelon faults with diverse dips. The outermost concentric peripheral faults formed outside the extent of the visible radial doming cracks, whereas the inner concentric caldera faults crosscut them (Figs. 5, 6). The interaction of reversal reactivated radial fractures and newly formed concentric collapse faults generated a heterogeneous polygonal intracaldera structure and non-coherent caldera subsidence in all cyclic experiments.

The maximum cumulative caldera subsidence was a combination of apical graben fault displacement plus ring-fault subsidence. Surprisingly, in plateau experiments with equivalent volumes of inflation and subsequent deflation, the ratio of apical subsidence versus caldera subsidence was approximately 1 (Table 1). The diameter of the caldera ring-fault was ca. 1.5 times larger than the apical graben diameter for shallow chamber depths and largely unaffected by the cone geometry (Fig. 7). With increasing chamber depth, however, this discrepancy shrunk.

On evacuation, during initial sagging of the structural dome, synthetic and antithetic fractures formed wedges in the outermost periphery (Figs. 5, 6). These concentric peripheral fractures rooted at depths near the reservoir(s) but 2-5 cm beyond the horizontal extent of these (Fig. 8). Their surface expression caused terraces as well as horst and graben structures, 2-4 cm in length. Concentric peripheral faults were most common and dilation was strongest on cone-shaped edifices. The formation of these concentric peripheral faults, together with crosscutting radial faults requires a structural interplay of doming and evacuation collapse.

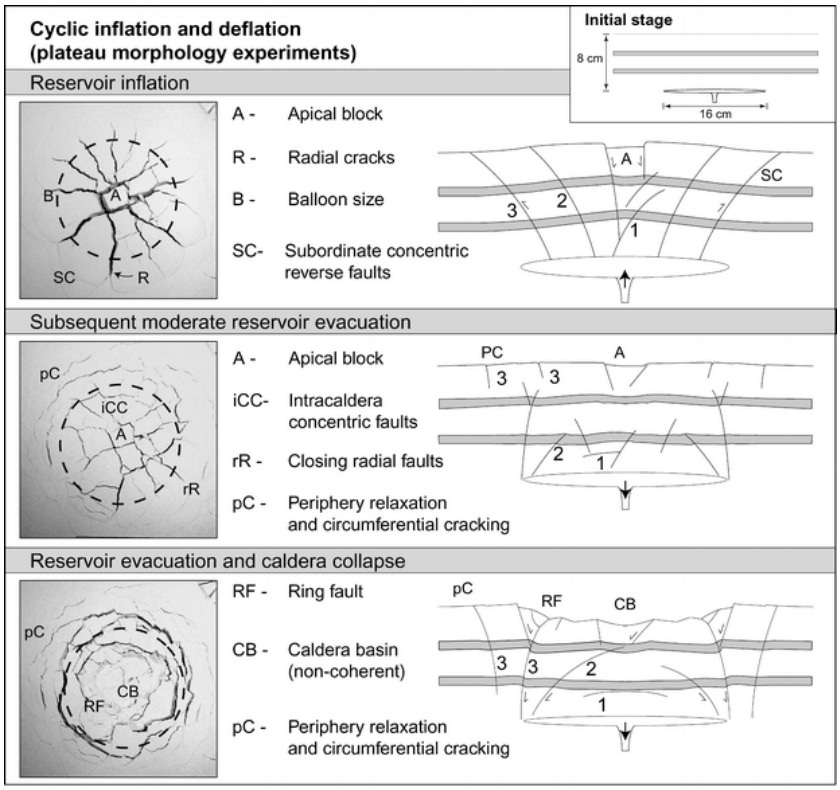

Fig. 5. *Photographs and schematic profiles of experiments showing the structural development for chamber inflation and subsequent evacuation beneath a plateau (flour). The numbers indicate the chronological order of the faults*

Since tumescence influenced a greater area at the surface than the bell-shaped ring faults, this structural incongruity resulted in gravitational flank relaxation during chamber evacuation and the formation of circumferential peripheral fractures on the outer flanks of the edifice.

Experiments with deeper balloons resulted in larger areas of (a) tumescence, (b) apical graben and (c) radial cracks. Deeper situated reservoirs resulted moreover in a reduced domal uplift and a reduced apical graben subsidence.

For cone-shaped morphologies, doming produced a more heterogeneous radial fault pattern compared with the plateau-shaped morphology. This is most likely a function of the model construction, differing slightly from an ideally shaped cone.

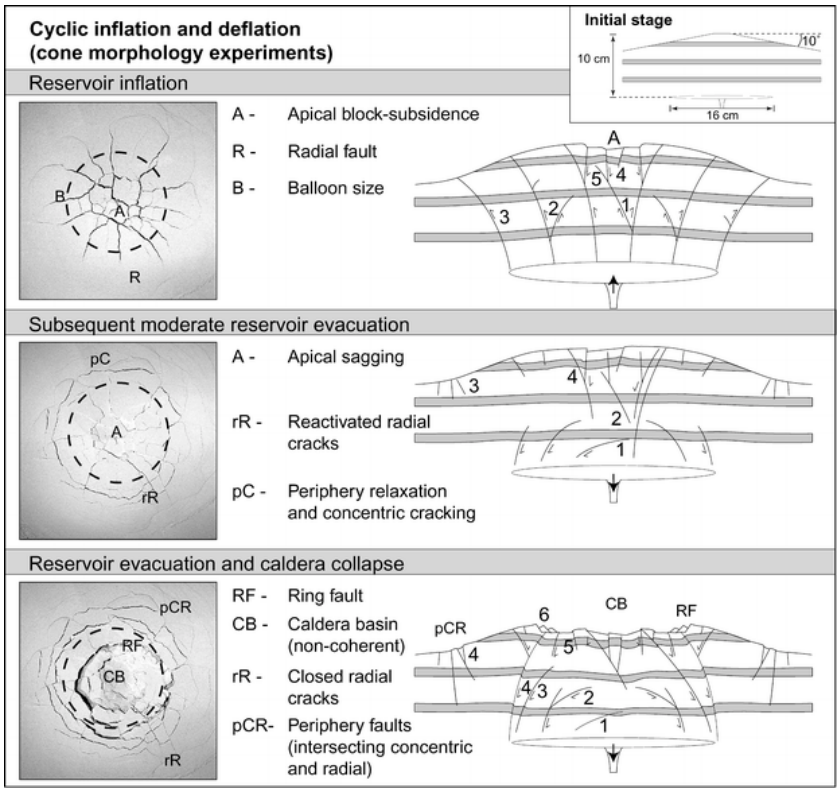

Fig. 6. *Photographs and schematic profiles of experiments (flour) with initial cone morphology, showing the structural development for chamber inflation and subsequent evacuation. The numbers indicate the chronological order of the faults*

During further cycles of doming and evacuation collapse, the outermost domed flanks remained as morphological highs (Fig. 8). Balloon resurgence in sand models formed supplementary faults to the fault patterns described above and incrementally destabilised the steepened and fractured flanks, which frequently collapsed and formed outward-directed slides. Such sliding sectors were bound and initiated by revived radial cracks and concentric peripheral faults. The occurrence and size of lateral failures is thought to be a function of the initial flank inclination, the quantity of radial fractures, and the position and depth of peripheral relaxation faults.

Summary and discussion

A variety of geometric models of caldera formation have been suggested, including the piston caldera (Anderson 1937; Williams 1941; Smith and Bailey 1968; Lipman 1997), the funnel-type caldera (Aramaki 1984; Yokoyama and Ohkawa 1986), the trap-door

(Steven and Lipman 1976) and downsag caldera (Walker 1984), and the non-coherent or chaotic-type caldera (Scandone 1990; Branney and Kokelaar 1994; Moore and Kokelaar 1998). In order to comprehend such complex caldera structures, simulation in analogue experiments was employed using the two end-member mechanisms of doming (Komuro 1987; Marti et al. 1994) and evacuation collapse (Roche et al. 2000), but also a combination of both mechanisms, i.e. the inflation and subsequent deflation of a reservoir.

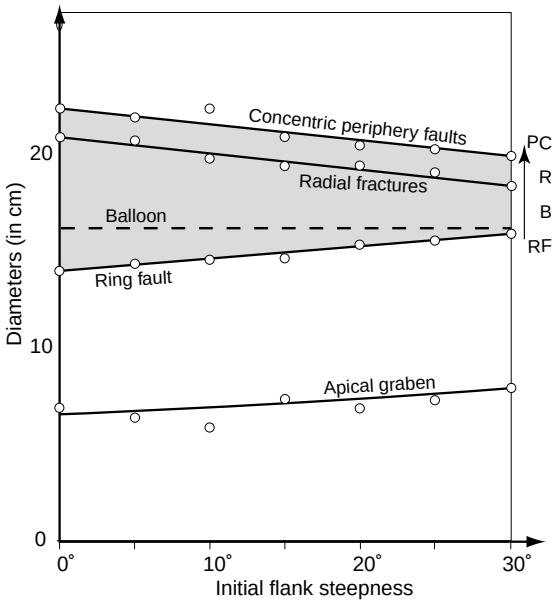

Fig. 7. *Plot of multi-stage flour experiments of cone morphology: increasing initial inclination of the flanks of the cones (0, 10, 15, 20, 25, 30°) vs measured diameter. The initial topography slightly influences the diameter of radial cracks (R), the apical graben and the ring fault (RF) diameter. During subsequent balloon deflation, the diameter of concentric peripheral faults (PC) decreases with increasing initial flank steepness. "Best-fit" curves, where the shaded area includes the relations of RF, B, R and PC. The balloon (B) was situated at a depth of 9 cm below the surface; 1 cm in experiments corresponds to approximately 1 km in nature*

Doming: During "dome-shaped" uplift, tensile stress is predominant at the centre of the dome, causing magma intrusion along normal faults, balanced by the overpressure of magma within the dyke. The propagation of dykes stops and they close when magma pressure has been reduced to a value equal to the stress across the dyke (McLeod and Tait 1999). Following the experimental observations, dykes are thought to propagate primarily in a radial mode during doming (Fig. 9A). A structural dome increases the edifice volume and results in steepening of the volcano flanks and a compressive stress regime in the caldera periphery. Extension is strongest in the apical region, resulting in subsidence of a graben. The experiments may provide an assessment of early apical subsidence in natural calderas, subsequently overprinted by ongoing caldera evolution (cf. Troll et al. 2000). Such apical graben subsidence, accomplished by slumping of large blocks into the expanding centre, may produce pressure jumps in the associated shallow magma reservoir and possibly trigger large-scale ash-flow eruptions (Gudmundsson 1998).

Evacuation collapse: Reduction of the pressure inside the analogue magma chamber causes a gravity-driven downward displacement of the chamber roof into the reservoir (Fig. 9B). Major ring faults develop that are outward dipping with a curved outline (cf. Marti et al. 1994; Roche et al. 2000). With decreasing depth, the influence of maximum

principal stress decreases so that the shear stress on the potential fault plane is sufficiently large to generate a shear fracture approaching this plane, leading to curved ring faults. In several experiments, subsidence was slightly delayed following balloon evacuation, suggesting that faults may remain active during and following magma chamber evacuation until their expression reaches the surface, implying a temporal hiatus within the edifice.

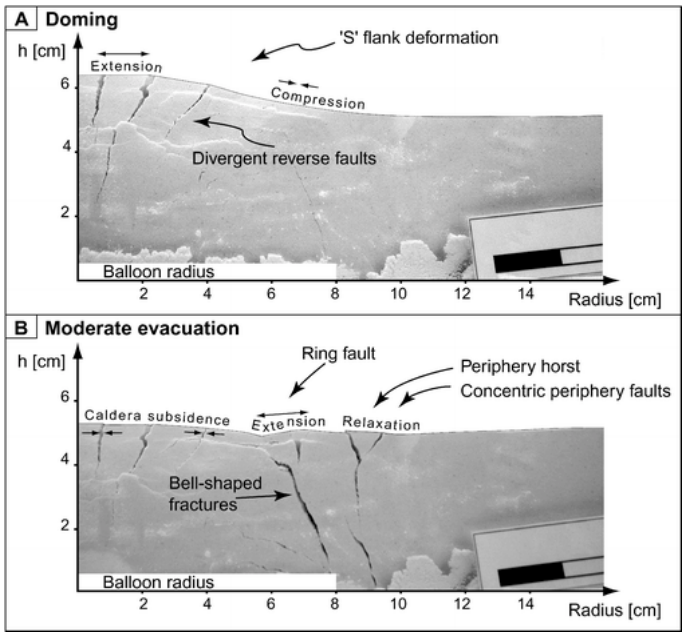

Fig. 8A, B. *Photographs of sections through the edifice illustrating doming and subsequent evacuation collapse. Deformation was simulated in flour adjacent to a pane of glass and photographed to record the fracture formation of* ***A*** *inflation causing tumescence and s-shaped flank deformation of an initial plateau surface, initiated by divergent reverse fractures. Note the flattening of the apical centre.* ***B*** *Subsequent deflation of ca. 50 % produces bell-shaped fractures and a contraction of the central material towards the shrinking magma reservoir, defining a caldera subsidence along a major ring fault. Relaxation of the flanks produced periphery faults and wedges, as well as horst and graben structures*

Combined doming and evacuation collapse: Initial reservoir inflation generates radial cracks and subordinate concentric reverse faults, causing flank deformation and an apical subsidence. Subsequent deflation of the reservoir generates caldera structures that overprint the previously domed edifice. When chamber evacuation is initiated, the area above the chamber sags, resulting in closure of the radial cracks. Subsequently, caldera ring faults and peripheral circumferential fractures form simultaneously. The location of the peripheral fractures may be several kilometres away from a caldera rim. As a consequence of the intersecting radial and concentric fault systems, the caldera floor fractures sequentially and subsides in a disjointed manner by reactivating radial structures and a set of newly formed bell-shaped faults. Erosion and inward slumping of megablocks is common, leading the caldera rim to propagate outwards (Lipman 1997; Roche et al. 2000). The structural network of intracaldera radial and concentric fractures is also present on the flanks of the edifice, where these form as a result of: (a) flank deformation and steepening; (b) radial fracture propagation during doming; and (c) circumferential faulting produced by flank relaxation upon chamber evacuation (Fig. 9). In this, three concentric fault domains are discriminated by the position, mechanism and chronology, i.e. the apical graben faults, the circumferential peripheral faults and the caldera ring

faults. In caldera volcanoes with several stages of doming and evacuation, the extent of radial faults and the diameter of concentric faults is thought to migrate outwards with each additional stage. In this case, the number of faults increases incrementally (Table 1), reducing the stability of the volcano flanks. Whether doming precedes reservoir evacuation, or resurgent doming succeeds pure evacuation collapse, has no effect on the general structural arrangement.

Effect of initial edifice geometry: The state of stress within a multicyclic caldera volcano is strongly controlled by the magma chamber(s), but is also influenced by gravitational near-surface stresses due to pre-existing topography. The effect of topography is most pronounced for the distribution and location as well as the orientation of the concentric fracture systems. The dip-line curvature of reverse doming faults enhances with steeper initial volcano flanks. In turn, if the magma chamber evacuates beneath a steep cone, the concentric peripheral fractures have a less pronounced tendency to form open faults. Moreover, the central collapse basin fractures in a more disorganised way (Fig. 6). For irregular edifice morphologies, the caldera floor is likely to be piecemeal, even in pure evacuation experiments, since fractures arrange less uniformly compared with symmetric volcano-morphology experiments (Table 1). For cone morphologies not directly centred above the chamber, the pattern of radial fractures is uniform only near the centre. Away from the centre, the radial fractures propagate parallel to the dip line of the slope. Chamber evacuation beneath a slope produces concentric fractures with non-uniform fault offset, resulting in a tilted caldera floor. The position of the chamber beneath the surface influences the geometric arrangement of the subsurface structures, confirming the emphasis placed on the roof aspect ratio by Roche et al. (2000). For shallow chambers, the distribution of concentric fractures reflects the chamber geometry. For larger chamber depths, however, this structural mirror becomes less pronounced.

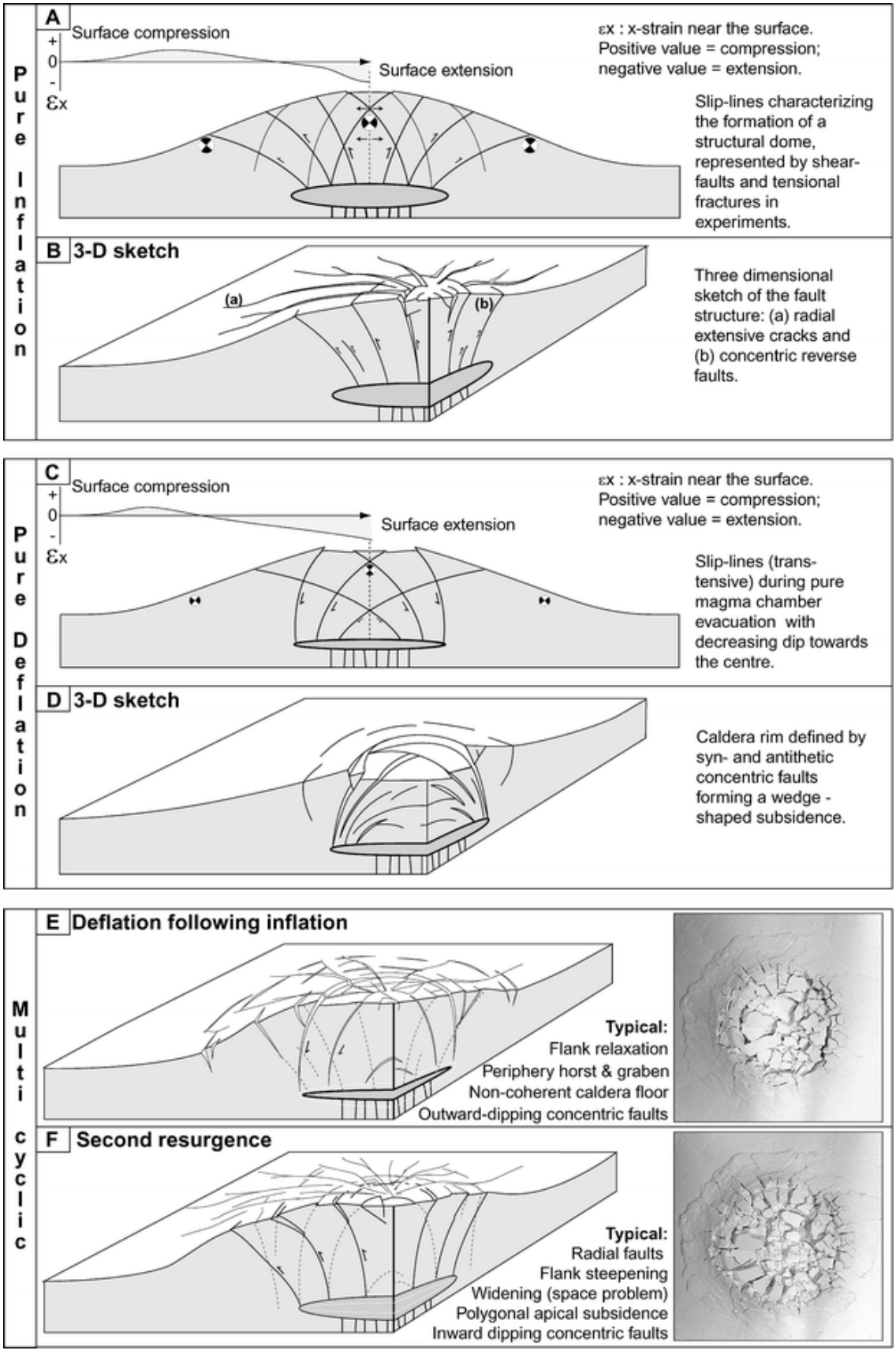

Fig. 9. *Three-dimensional reconstruction of characteristic structures formed during **A**, **B** pure inflation, **C**, **D** pure deflation and **E**, **F** multi-stage inflation and subsequent deflation*

Natural examples

The near-surface structural arrangements that result from magma chamber inflation, chamber evacuation, and repeated chamber withdrawal and replenishment stages, as seen in experiments, are recorded at several active and extinct volcanoes.

Tumescence: Examples of volcanic tumescence are provided by recent ground deformation measurements at, for example, Long Valley Caldera (Simons et al. 2000) and Campi Flegrei, Italy (Usai et al. 2000), illustrating amounts of resurgent doming of 2-4 cm $year^{-1}$, the latter example with a maximum annual uplift of ca. 40 cm $year^{-1}$ in the early 1970s. The reconstruction of large-scale dome-shaped uplift induced by chamber inflation in the Aizu and Motojuku district of NW Japan showed circular shapes of 20-60 km in diameter, with amounts of domal uplift prior to caldera collapse of the order of 500-1000 m (Fujita et al. 1970; Komuro et al. 1984). In the Tertiary Rum Igneous Complex, Scotland, doming resulted in a tremendous basement uplift of approximately 1000-1500 m (Emeleus 1997; Troll et al. 2000). This wide range of recorded tumescence rates in natural volcanoes is well recorded in our doming experiments, where maximum uplift rates translate to several 100 m in nature.

The patterns of eruptive fissures on the Galapagos island volcanoes include radial fissures and dike swarms, and are thought to be related to dome-shaped uplift triggered by magma chamber inflation (McBirney and Williams 1969; Simkin and Howard 1970). On the island of Fernandina, doming caused annular dyking in the extensional apical region contemporaneous with radial dyke intrusion on the flanks of the volcano (Chadwick and Dieterich 1995; Rowland 1996). This is in agreement with the fracture arrangement observed in ourdoming experiments. This lateral and vertical expansion of the edifice causes "general expansion all around the volcano" (Walker 1999), putting the centre into tension, subsequently relived by normal fault caldera collapse (Gudmundsson et al. 1997).

Evacuation collapse: In turn, deflation of the magma chamber coupled with caldera collapse caused concentric faults to form at Darwin Caldera, Albemarle Island (McBirney and Williams 1969). An arcuate, flat-topped bench along the southern wall defines the caldera collapse basin, indicating that the engulfment of the caldera took place by at least two caldera ring faults forming two crescent plateaus. This compares well with the bench-like caldera floors observed in our pure evacuation set-ups.

The islands of Miyakejima and Sakurajima, Japan, are stratovolcanoes that erupted historically along radial fissures, thought to be associated with an expanding magma chamber (Ode 1957; Walker 1999). Numerous earthquakes have occurred beneath Miyakejima since 26 June 2000, with hypocentres initially beneath the island, moving westward (unpublished data of the Volcano Research Center, Earthquake Research Institute, University of Tokyo). Since 10 August 2000, intermittent phreatic eruptions

have occurred on the summit, following roof collapse forming a small caldera 1.6 km across with a fault displacement of 450 m. The depression continued subsiding, accompanied by earthquake swarms and tilt changes. The amount of material erupted during the phreatic phase was < 0.02 km^3 (before 10 August), contrasting with a subsidence volume of 0.45 km^3 inside the newly formed caldera. The cause of this was magma chamber deflation caused by drain back of magma that intruded laterally, implying that the eruption was induced by the collapse of the roof into an evacuated reservoir (Nakada and Fujii 2000). This also suggests that the process of caldera subsidence may be delayed by several weeks following evacuation, which compares well with the "time gap" observed in several of our experiments. Moreover, during subsidence of the Miyakejima caldera, concentric faults formed crescentic terraces separating the caldera basin, whereas inward-falling crescentic megablocks widened the caldera rim and disguised the direct ring fault arrangement. Deflation in our experimental chamber caused an initial apical sagging and tilting of the flanks, until a delayed bench-like collapse of the caldera floor occurred. Tilting of the Miyakejima flanks displayed relaxation; however, the formation of peripheral fractures and horst and graben structures is, as yet, not well constrained.

Multi-stage caldera activity: Caldera resurgence that cause uplift of the caldera floor has been reported repeatedly, and several structural mechanisms including uplift of separate blocks, trap-door uplift or coherent caldera floor uplift have been suggested in the literature (Lipman 1997). A space problem can arise when the resurgent block is structured by, for example, outward-dipping faults, as reported on Ischia caldera, Italy (Tibaldi and Vezzoli 1998). Our experiments show that bell-shaped outward-dipping faults are prone to become reactivated on resurgence, so that the caldera periphery is forced to uplift, and radial and concentric structures expand and dilate outwards. Similar mechanisms were suggested based on seismic data from Rabaul Caldera (Mori and McKee 1987; Jones and Stewart 1997).

On Gran Canaria (Canary Archipelago), caldera periphery faults and dyke-swarms surround the multi-stage Miocene Tejeda Caldera and are ordered in radial and concentric arrangement around the subaerial shield volcano (Schmincke 1967, 1968). At a distance of ~ 7 km from the ca. 20-km-wide central caldera, horst and graben structures are bound by radial faults and en-echelon-like concentric faults with normal and reverse sense. The latter are growth faults that formed during multicyclic ~ 20 ignimbrite eruptions (Schmincke 1994). The peripheral concentric and radial network of growth faults and dyke swarms reflects multi-cyclicity of the caldera that is consistent with the ignimbrite record and sheds light on mechanisms of "doming and collapse".

On Olympus Mons, caldera periphery terraces are located at a distance of 50% of the volcano's radius from the caldera centre and are thought to be genetically related to magma chamber pulsation and the development of the large 100-km-wide central

caldera basin (Thomas et al. 1990). On the edifice flanks, the position and explicitness of the peripheral terraces was controlled by chamber depth and initial morphology to form thrust faults, and genetically resembles the circumferential outer periphery belt produced in our multi-stage experiments.

Conclusion

The arrangement and distribution of peripheral caldera fractures is linked to the mechanism(s) by which calderas form. These mechanisms include the following:

- Magma chamber inflation results in radial fractures and dyke injection, and an expansion of the flanks (doming; Fig. 9A, B). In the apical region, these structures are crosscut by chiefly concentric or horseshoe-shaped faults forming a polygonal apical graben (i.e. proto-caldera). Inward tilting and slumping of angular megablocks is common.
- Pure evacuation collapse: Curved outward-dipping concentric faults encircle a collapsed caldera-basin including sharply defined ring faults (Figs. 9C, D). Additional characteristics are inward-slumped crescentic megablocks, growth faults plus the absence of widespread radial structures.
- Multi-stage caldera volcanoes are recognised by a network of intersecting radial and concentric structures (dykes and faults) in the central caldera basin and the caldera's periphery (Fig. 9E, F). Moreover, peripheral relaxation during evacuation forms circumferential en echelon faults in normal and reverse sense and horst and graben structures in-between. These may be present several kilometres away from the caldera rim on the volcano flanks and could prompt major flank collapses.

The occurrence of peripheral circumferential faults crosscutting and crosscut by radial dykes or fractures requires at least one large incidence of doming or resurgence and one event of evacuation collapse. Based on the present experiments, a peripheral crosscutting radial and circumferential fault system suggests that caldera subsidence was necessarily non-coherent following a doming or resurgence event. This may illuminate the structural history of calderas that are covered by substantial caldera infill and/or where the intracaldera setting is obscured by later intrusions.

Acknowledgements: The authors thank H.-U. Schmincke and M. Hort for discussions and critical reading of previous versions of the manuscript. We are grateful to R. Seyfried for remarks and N. Urbanski for assistance with experimental equipment. We thank P. Lipman and J. Stix for helpful comments, and A. Gudmundsson and O. Roche for stimulating reviews. Thanks go to VRC-ERI (Tokyo) for outstanding presentation of material related to the recent Mijakejima eruptions on the Web. Financial support was provided

by the Deutsche Forschungsgemeinschaft (grants Schm 250/77-1 and Schm 250/72-1) to H.-U. Schmincke and a grant of the Studienstiftung des deutschen Volkes to VRT.

References

Anderson EM (1937) Cone sheets and ring dykes; the dynamical explanation. Bull Volcanol 1:35-40

Aramaki S (1984) Formation of the Aira caldera, southern Kyushu, ~22,000 years ago. J Geophys Res 89:8485-8501

Branney MJ (1995) Downsag and extension at calderas. New perspectives on collapse geometries from ice-melt, mining, and volcanic subsidence. Bull Volcanol 57:303-318

Branney MJ, Kokelaar P (1994) Rheomorphism and soft-state deformation of tuffs induced by volcanotectonic faulting at a piecemeal caldera, English Lake District. Bull Geol Soc Am 106:507-530

Byerlee J (1978) Friction of rocks. Pure Appl Geophys 116:615-626

Chadwick WW, Dieterich JH (1995) Mechanical modeling of circumferential and radial dyke intrusion on Galapagos volcanoes. J Volcanol Geotherm Res 66:37-52

Cobbold PR, Castro L (1999) Fluid pressure and effective stress in sandbox models. Tectonophysics 301:1-19

Druitt TH, Sparks RSJ (1984) On the formation of calderas during ignimbrite eruptions. Nature 310:679-681

Emeleus CH (1997) Geology of Rum and the adjacent islands. Mem British Geol Surv Scotland, Sheet 60

Fujita Y, Kawakita T, Arai T (1970) Tectonogenesis in the formative process of the Motojuku Green Tuff beds. Assoc Geol Collabor Japan 16:81-95

Glicken H, Janda RJ, Voight B (1980) Catastrophic landslide/ debris avalanche of May 18, 1980, Mount St. Helens volcano. EOS Trans Am Geophys Union 61:1135

Gudmundsson A (1988) Formation of collapse calderas. Geology 16:808-810

Gudmundsson A (1998) Formation and development of normal-fault calderas and the initiation of large explosive eruptions. Bull Volcanol 60:160-170

Gudmundsson A, Marti J, Turon E (1997) Stress fields generating ring faults in volcanoes. Geophys Res Lett 24:1559-1562

Hoshino K, Koide H, Inami K, Iwamura S, Mitsui S (1972) Mechanical properties of Japanese Tertiary sedimentary rocks under high confining pressures. Geol Surv Japan 244:1-200

Hubbert M (1937) Theory of scale models as applied to the study of geologic structures. Geol Soc Am Bull 48:1459-1520

Hubbert M (1951) Mechanical basis for certain familiar geologic structures. Geol Soc Am Bull 62:355-372

Jones RH, Stewart RC (1997) A method for determining significant structures in a cloud of earthquakes. J Geophys Res 102:8245-8254

Komuro H (1987) Experiments on cauldron formation: a polygonal cauldron and ring fractures. J Volcanol Geotherm Res 31:139-149

Komuro H, Fujita Y, Kodama K (1984) Numerical and experimental models on the formation mechanism of collapse basins during the Green Tuff orogenesis of Japan. Bull Volcanol 47:649-666

Krantz RW (1991) Normal fault geometry and fault reactivation in tectonic inversion experiments. Geol Soc Spec Publ 56:219-229

Lipman PW (1997) Subsidence of ash-flow calderas: relation to caldera size and chamber geometry. Bull Volcanol 59:198-218

Mandl G (1988) Mechanics of tectonic faulting; models and basic concepts. Elsevier, Amsterdam

Marti J, Ablay GJ, Redshaw LT, Sparks RSJ (1994) Experimental studies of collapse calderas. J Geol Soc London 151:919-929

Marti J, Folch A, Neri A, Macedonio G (2000) Pressure evolution during explosive caldera-forming eruptions. Earth Planet Sci Lett 175:275-287

McBirney AR, Williams H (1969) Geology and petrology of the Galapagos Islands. Geol Soc Am Mem 118:1-197

McLeod P, Tait S (1999) The growth of dykes from magma chambers. J Volcanol Geotherm Res 92: 231-246

Moore I, Kokelaar P (1998) Tectonically controlled piecemeal caldera collapse: a case study of Glen Coe volcano, Scotland. Geol Soc Am Bull 110:1448-1466

Mori J, McKee CO (1987) Outward-dipping ring-fault structure at Rabaul Caldera as shown by earthquake locations. Science 235:193-197

Nakada S, Fujii T (2000) Sequence and interpretation of Caldera-Forming Event at Miyakejima Volcano, Japan. EOS Trans Am Geophys Union 81:1258

Newhall C, Dzurisin D (1988) Historical unrest at large calderas of the world. US Geol Surv Bull 1855:1-1108

Ode H (1957) Mechanical analysis of the dyke pattern of the Spanish Peaks area, Colorado. Geol Soc Am Bull 68:567-576

Odonne F, Menard I, Massonnat GJ, Rolando JP (1999) Abnormal reverse faulting above a depleting reservoir. Geology 27:111-114

Prucha JJ (1965) Deformation of Silurian salt in Cayuga Rock Salt Company Mine, Myers, New York. EOS Trans Am Geophys Union 46:163

Ramberg H (1981) Deformation structures in theory and experiments. Geol Soc Sweden, 131 pp

Roche O, Druitt T, Merle O (2000) Experimental study of caldera formation. J Geophys Res 105:395-416

Rowland SK (1996) Slopes, lava flow volumes, and vent distributions on Volcano Fernandino, Galapagos Islands. J Geophys Res 101:23657-23672

Sanford A (1959) Analytical and experimental study of simple geological structures. Geol Soc Am Bull 42:19-52

Scandone R (1990) Chaotic collapse of calderas. J Volcanol Geotherm Res 42:285-302

Schmincke H-U (1967) Cone sheet swarm, resurgence of Tejeda Caldera, and the early geologic history of Gran Canaria. Bull Volcanol 31:153-162

Schmincke H-U (1968) Faulting versus erosion and the reconstruction of the mid-Miocene shield volcano of Gran Canaria. Geol Mitt 8:23-50

Schmincke H-U (1969) Ignimbrite sequence on Gran Canaria. Bull Volcanol 33:1199-1219

Schmincke H-U (1976) The geology of the Canary Islands. In: Kunkel G (ed) Ecology and biogeography of the Canary Islands. Junk, Holland, pp 76-184

Schmincke H-U (1994) Geological field guide of Gran Canaria. Part I and II. Pluto Press, Kiel, pp 1-64

Schultz RA (1996) Relative scale and the strength and deformability of rock masses. J Struct Geol 18:1139-1149

Simkin T, Howard KA (1970) Caldera collapse in the Galapagos Islands, 1968. Science 169:429-437

Simons M, Fialko Y, Rivera L, Chapin E, Hensley S, Rosen PA, Shaffer S, Webb FH, Langbein J (2000) Analysis of geodetic measurements of crustal deformation at Long Valley Caldera. EOS Trans Am Geophys Union 81:1322

Smith R, Bailey R (1968) Resurgent cauldrons. Geol Soc Am Mem 116:83-104

Steven TA, Lipman PW (1976) Calderas of the San Juan volcanic field, southwestern Colorado. US Geol Surv Prof Pap 958:1-35

Swanson DA (1982) Magma supply rate at Kilauea volcano 1952-1971. Science 175:169-170

Thomas PJ, Squyres SW, Carr MH (1990) Flank tectonics of Martian volcanoes. J Geophys Res 95:14345-14355

Tibaldi A, Vezzoli L (1998) The space problem of caldera resurgence: an example from Ischia Island, Italy. Geol Rundsch 87:53-66

Troll VR, Emeleus CH, Donaldson CH (2000) Caldera formation in the Rum Igneous Centre, Scotland. Bull Volcanol 62:301-317

Usai S, Sansosti E, Lanari R, Tesauro M, Fornaro G, Berardino P, Lundgren P (2000) Deformation time series analysis and modeling surface deformation observed with SAR interferometry at Campi Flegreicaldera. EOS Trans Am Geophys Union 81:1322

Walker GPL (1984) Downsag calderas, ring faults, caldera sizes, and incremental caldera growth. J Geophys Res 89:8407-8416

Walker GPL (1999) Volcanic rift zones and their intrusion swarms. J Volcanol Geotherm Res 94:21-34

Williams H (1941) Calderas and their origin. Univ Calif Berkeley Publ Geol Sci 25:239-346

Williams H, McBirney A (1979) Volcanology. Freeman, Cooper and Co., San Francisco

Wisser E (1927) Oxidation subsidence at Bisbee, Arizona. Econ Geol Bull 22:761-790

Ye S, Rihm R, Danobeitia J, Canales J, Gallart J (1999) A crustal transect through the northern and northeastern part of the volcanic edifice of Gran Canaria. J Geodyn 28:3-26

Yokoyama I, Ohkawa S (1986) Subsurface structure of Aira caldera and its vicinity in southern Kyushu, Japan. J Volcanol Geotherm Res 30:253-282

Part I: Volcano flank instability by caldera formation

Chapter 2

Cyclic caldera collapse

Cyclic caldera collapse: Piston or piecemeal subsidence? Field and experimental evidence

Valentin Troll, Thomas R. Walter and Hans-Ulrich Schmincke

Abt. Vulkanologie & Petrologie, GEOMAR, Wischhofstrasse 1-3, 24148 Kiel, Germany

Abstract. Many multicycle caldera volcanoes display a complex extracaldera fault system genetically linked to caldera evolution. On Gran Canaria (Canary Islands), the Miocene Tejeda caldera was filled by ignimbrites and epiclastic sediments and intruded by syenites and a major cone-sheet swarm, obscuring intracaldera structural relations. Extracaldera radial and circumferential faults and dikes are well exposed. We used field data and experiments scaled to the island of Gran Canaria to clarify the poorly understood structural, temporal, and genetic relationship of peripheral faults to the central caldera. The experimental set-up comprises a cone of medium-grained sand in which a rubber balloon was repeatedly inflated and deflated. Balloon inflation resulted in updoming and a dominantly radial fault pattern, whereas balloon deflation caused piecemeal caldera collapse and a concentric peripheral fault arrangement on the edifice flanks. A complex interplay of repeated inflation and deflation cycles of the experimental magma chamber is found to explain the peripheral fault system of the Tejeda caldera on Gran Canaria and offers insight into the structure of the caldera floor and the mechanisms acting in multicycle caldera volcanoes.

Keywords: multicycle caldera volcanoes, analogue experiments, Tejeda caldera, Gran Canaria.

Introduction

Calderas probably form by decompression of a shallow-level magma chamber, followed by roof collapse into the evacuating reservoir (Smith and Bailey, 1968; Druitt and Sparks, 1984; Lipman, 1997). Different styles of gravitational subsidence suggested include piston collapse, noncoherent (piecemeal) collapse, downsag, and funnel collapse (Lipman, 1997). Experimental and theoretical studies show that the structural evolution and the subsidence mechanisms of an individual caldera depend on the initial structure of the volcano, the presence and/or absence of regional tectonic influence, the size, depth, and shape of the underlying magma chamber, and the eruptive magnitude and intensity of the pressure variation within the magma chamber (Komuro, 1987; Gudmundsson, 1988; Marti et al., 1994, 2000; Roche et al., 2000; Acocella et al., 2000; Walter and Troll, 2001). Two main collapse mechanisms have been proposed; piecemeal collapse and piston cylinder subsidence (Lipman, 1997), the former being thought to be much less important than the latter. Here we demonstrate that extracaldera structural relationships

on Gran Canaria and analogue modeling argue for piecemeal evolution of multicyclic calderas to be more common than previously thought. The type of evidence assembled overcomes the common difficulty in distinguishing between different structural processes because many young calderas are filled by thick ignimbrite sequences and/or are obscured by postcaldera intrusions.

On Gran Canaria (Canary Islands), a major Miocene multicycle caldera is filled with ignimbrites and sediments, but displays a complex extracaldera (peripheral) structural system of radial and concentric dikes and faults (Schmincke, 1976). This type of peripheral structure is a common phenomenon in multicycle caldera systems (e.g., Varnes, 1963; Smith and Bailey, 1968; Gardeweg and Ramirez, 1987; Newhall and Dzurisin, 1988; Henry and Price, 1989; Nappi et al., 1991), but its origin and relationship to the ring fault and intracaldera structure remain poorly understood. In order to evaluate the structural implications of fault systems peripheral to calderas, we combine field evidence on Gran Canaria with scaled analogue experiments simulating a multicycle caldera volcano. A comparison of the fault and dike distribution of the Tejeda caldera with the experimental results helps us to understand the origin of the Tejeda caldera and its peripheral fault structure. The results are applicable to caldera periphery fault systems of multicycle calderas elsewhere.

Field observations

A well-exposed outer caldera margin on Gran Canaria (Fig. 1) separates the Miocene basaltic shield lavas overlain by felsic extracaldera ignimbrites from intracaldera ignimbrites, sediments, and intrusives (Schmincke and Swanson, 1966; Schmincke, 1967). The caldera formed as a result of more than 20 trachytic to rhyolitic ignimbrites between 14 and 13.2 Ma (Mogan Group) and many trachyphonolitic ignimbrites and lava flows between 13.2 and 8.5 Ma (Fataga Group) (Schmincke, 1976; Bogaard and Schmincke, 1998). Correlation of intracaldera ignimbrites with the extracaldera ignimbrite succession suggests at least 1 km subsidence of the caldera basin (Schmincke, 1967). The caldera fill was intruded by syenites and a cone-sheet swarm of more than 500 trachytic to phonolitic sheets, emplaced between 12.3 and 7.3 Ma, representing late resurgence of the Tejeda caldera (Schirnick et al., 1999). Due to lack of exposed caldera basement and the obscured nature of the intracaldera structural relations, information on the caldera-forming mechanism(s) is best preserved at the caldera margin and the extracaldera periphery fault system.

The topographic caldera margin dips 50°–80° inward, whereas shield basalts and the ignimbrite succession dip gently toward the sea. Tuffs and sediments that fill the caldera pinch out against the steep caldera margin. An upsection decrease in the dip of depositional bedding indicates progressive filling of the caldera. At deeper levels the caldera

margin increasingly steepens, reaching vertical orientation in the deeply dissected erosional valley of El Risco in the northwest of the island. Here, but at a higher stratigraphic level, the caldera margin shallows to an inward dip of only 40°–50°, suggesting a curved caldera margin, progressively shallowing toward the former land surface. Whether the observed caldera margin represents only the outer erosional limit of the caldera basin or is actually a fault remains speculative. However, the curvature of the contact may suggest a gradation from an erosional margin higher up the contact to a fault origin at depth.

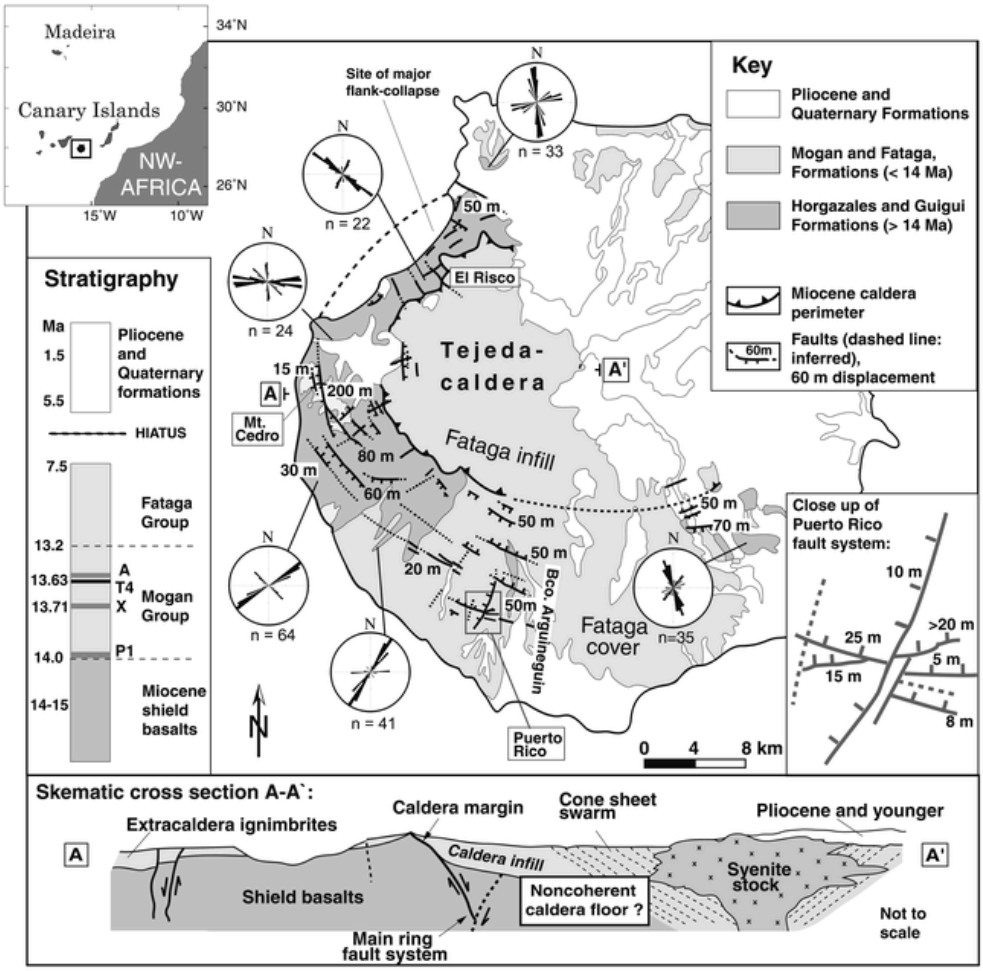

Figure 1. *Map of Gran Canaria showing caldera and peripheral fault distribution. Equal-area pole plots (axial with class interval of 5°, n = number of data) represent dike orientations at given locality with radial and concentric trends throughout caldera periphery. Inset lower left shows major stratigraphic units of Gran Canaria. Lower right inset is closeup of Puerto Rico fault system showing intersecting radial and concentric faults of several generations. Bottom inset is schematic cross-section through Gran Canaria (A–A).*

Several generations of radial and concentric faults outside the caldera margin can be correlated to several episodes of volcanic activity. Radial dikes comprise pre-ignimbrite Miocene shield basalts, early Mogan rhyolites, and Fataga alkalic basalts and phonolites.

Radial dikes and faults occur from the caldera margin to the island coast and crosscut, and are crosscut by, concentric caldera rim–parallel faults. The concentric faults form a complex system of local horst and graben structures to 10 km outside the caldera margin (Fig. 1).

For example, the concentric Montaña Cedro fault zone in the southwest of the island, ~5 km from the caldera margin, shows a relative downthrow of the outer flank of the island, defining a large horst between the fault zone and the caldera rim. Particular marker ignimbrites, such as ignimbrite A, show substantial thickening to the west of the fault (A ≥ 25 m), compared to the eastern, more proximal side to the caldera, where A is ≤10 m thick but vertically displaced by ~200 m. Stratigraphic units below ignimbrite A, however, show a reverse thickness relationship on either side of the fault; e.g., ignimbrite X is ~60 m thick on the eastern side, but ~20 m thick on the western side of the fault and displaced by only ~90 m. The fault zone is strongly brecciate and filled by Mogan-type basalt, rhyolite, and trachyte, plus Fataga phonolite fragments dragged into the fault. The fault was thus active during several eruptive episodes. This repeated fault activity differs from that of a simple growth fault, and is realistically only accomplished by multiple reactivation of the fault with opposing senses of displacement.

Many additional examples of complex, caldera margin-parallel faults displace the post-shield ignimbrite succession in the south of the island. In Arguineguin valley, ~3-6 km from the caldera margin, subparallel concentric faults define horst and graben structures of several hundred meters to 2 km in width. These uplifted and subsided blocks displace the lower units of the ignimbrite succession but leave upper units increasingly undisturbed, thus representing a system of repeatedly reactivated syncaldera faults.

The interplay of radial and concentric faults is well preserved, e.g., in Puerto Rico erosional valley, where a local concentric graben is intersected by a radial fault zone, producing a mosaic of smaller blocks. Within the graben, ignimbrite A is ≥30 m thick and shows its full sequence of 7 flow units. Beyond the graben, A is ≤10 m thick and the lower flow units are missing. There, along the radial fault, displacement of ignimbrite X shows a downthrow of ~15 m to the west. The overlying basalt flow T4 (that underlies A) is ~5 m thick on the downthrown side, but reaches ~15 m thickness on the uplifted eastern side of the radial fault. This implies several reactivations of radial and concentric faults to accumulate lava and ignimbrite within local grabens, some of which became uplifted blocks with extreme thicknesses of individual units. Evidence for multiple reactivation of once- formed syncaldera radial and concentric fault zones is therefore overwhelming in the periphery of the Gran Canaria caldera.

Experiments

The experimental set-up consists of a basement and cone of medium-grained sand, between which a latex balloon was placed. The balloon was connected with a pipe system to an external water reservoir; water input simulated magma chamber inflation and caused tumescence, while water withdrawal, and simulated chamber evacuation, led to subsidence of the chamber roof. Experiments obey the principle of similarity (see Komuro, 1987; Roche et al., 2000). The ratios of physical parameters (X) are determined by $X^* = X_{Model}/ X_{Nature}$. The geometric proportions of the model were scaled to Gran Canaria Island, where a shallow ellipsoidal magma reservoir is postulated at 6–7 km depth with a diameter of ~17 km (Freundt and Schmincke, 1995; Ye et al., 1999; Krastel and Schmincke, 2001). Our scaling factor was $X^* = 10^{-5}$, so that 1 cm in the model corresponds to ~1 km in nature (Table 1). The slope of the cone was initially 10° with a flattened apex and a total height of the set-up of 14–16 cm.

Crustal rocks and sand are Coulomb materials with a shear stress (τ) that depends on the material's cohesion (c), the normal stress (σ_n), and the angle of internal friction (ϕ), with $\tau = c + \sigma_n \tan \phi$. The granular sand used had a mean grain diameter of 300 μm, a density of $\rho_{Model} = 1300$ kgm^{-3}, and an angle of internal friction of $\phi_{Model} = 33°$, permitting simulation of brittle behavior of natural rocks (Hubbert, 1951), with $\rho_{Nature} = 2700$ kgm^{-3}, $\phi_{Nature} = 25°–40°$ and $g_{Nature, Model} = 10$ ms^{-2}. The stress ratio (σ^*) is defined by the ratios of the length (L^*), the gravity acceleration (g^*), and the density (ρ^*), with $\phi^* = \rho^* g^* L^* = 5 \times 10^{-6}$ Pa. Natural rocks cover a range of cohesive strength from 5×10^7 Pa to 10^6 Pa. The lower cohesion resembles strength values on larger scales and/or in fractured materials that contain cohesion-reducing discontinuities (see Roche et al., 2000). From the stress ratio σ^* that equals C^* follows a required cohesion for the analogue material of $C_{Model} = C^* \times C_{Nature} = 5$ Pa; a stress approximation using low cohesive sand was, therefore, suitable.

Cohesion in sand depends on its compaction, so that stressed and faulted sand has a lowered cohesion, allowing faults to become reactivated (Krantz, 1991). Limitations of the set-up, however, include the tensile strength of the granular material, timing, gravity acceleration, and the size and shape of the chosen latex balloon. The latter is considered merely as an approximation, because the dimensions of natural reservoirs commonly remain speculative. Moreover, an inflated latex balloon with known shape produces on evacuation artificially reduced fault displacement near the balloon membrane. This is because fault propagation and sinking of roof blocks into the reservoir is hindered by the balloon membrane. In our experiments, balloon inflation raised the summit by 1–2 cm and steepened the flank by ~10°. This inflation rate may somewhat overestimate the effects of a single natural inflation event. However, natural caldera volcanoes with domal uplift of 1000 m and more are known (Komuro, 1987; Troll et al., 2000). The fault

pattern produced did not depend on the rate of doming, only the displacement and length of the faults diverged.

Experimental results

During balloon inflation, open radial cracks formed and propagated divergently from the center outward, reaching a length of ~12 cm (Fig. 2; Table 1). Fracturing decreased from the free surface downward, as seen in experiments next to a glass pane. Simultaneously, the summit region extended laterally, producing polygonal concentric cracks that limited an apical graben. The formation of the apical graben included inward tilting and sagging of 1–3 cm blocks with normal fault subsidence of as much as 1 cm. The graben interior was strongly dissected by radial faults (Komuro, 1987). A small set of reverse concentric (inward dipping) faults formed on the flanks of the dome, with a relative uplift of the material closer to the center.

Subsequently, we deflated the balloon, causing synchronous surface sagging of the central region of the dome, followed by a slightly delayed caldera collapse. Within a radius of 8 cm, a set of vertical to steeply outward dipping ring faults formed, with as much as 0.6 cm fault displacement, resulting in noncoherent caldera-floor subsidence that was controlled by intersecting preexisting radial faults and newly formed concentric faults. The most significant vertical displacement was at the ring faults. At depth, coherence of the subsided roof increased due to reduced fault displacement closer to the balloon membrane, preventing fault propagation into the reservoir. Outside the caldera, the flanks tilted inward followed by formation of a concentric fault pattern spanning the entire central caldera basin in en echelon fashion with a radius of 12.5–13 cm (Fig. 2). These faults were vertical to outward dipping and intersected the preexisting radial doming structures on the flanks. Local horst and graben structures with blocks of 2–4 cm formed between concentric en echelon faults in the periphery and at the intersection of crosscutting radial and concentric faults in both the periphery and in the caldera.

Scaled Parameters (1:100 000)	Experiment (after cycle 1)	Experiment (after cycle 2)	Gran Canaria (multicyclic)
Magma chamber diameter	17 cm	17 cm	~17 km
Magma chamber depth	6 cm	6 cm	~6 km
Angle of internal friction	40°	40 °	35°–45°
Radial crack or dike diameter	24 cm	28 cm	~32 km
Ring fault diameter	16 cm	20 cm	18–20 km
Ring fault subsidence	0.6 cm	1 cm	>1 km
Concentric periphery faults (maximum diameter)	25 cm	29 cm	~30 km
Periphery horst/graben blocks	2–4 cm	2–4 cm	1–4 km
Apical graben blocks	1–3 cm	2 cm	?
Apical graben subsidence	0.7 cm	0.8 cm	?

Table 1. *Geometric relations of experiments versus Gran Canaria*

Further cycles of inflation and deflation produced only subordinate new fractures but dominantly reused the pre-existing faults in normal and reverse sense. These multicyclic experiments caused a widening of the central caldera basin by inward slumps from the steep ring fault and increased the radius of radial cracks on repeated doming. Horst and graben structures in the periphery also became reactivated and individual blocks were frequently uplifted during one stage of a cycle to become subsided grabens in another stage of the same cycle.

A circular collapse basin with only circular ring faults, lacking radial faults (piston cylinder), was only observed in some pure chamber evacuation experiments, i.e., without any precollapse or postcollapse tumescence (Marti et al., 1994; Roche et al., 2000). Peripheral horst and graben structures, in turn, were not produced during pure chamber evacuation runs.

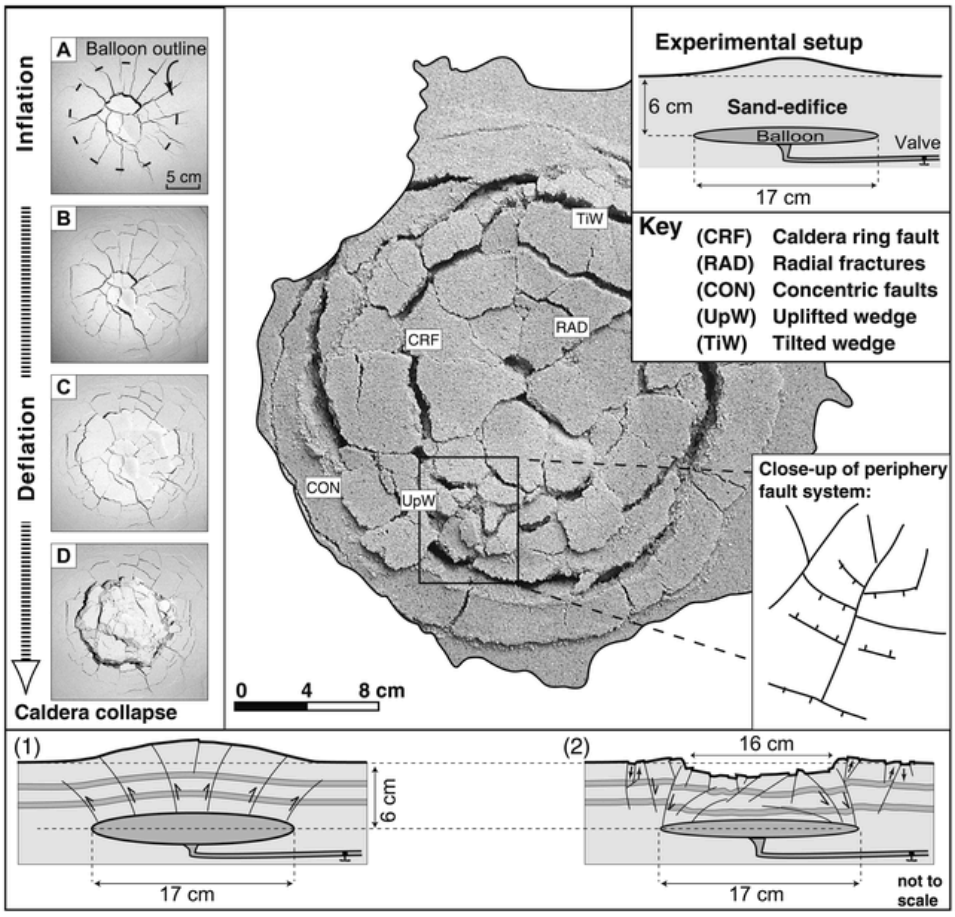

Figure 2. *Experimental set-up and results. Inset top right shows initial experimental construction prior to chamber inflation. Inset left shows photographs taken from above experimental set-up after* ***A*** *inflation,* ***B***, ***C*** *subsequent moderate deflation, and* ***D*** *evacuation of ~75% of balloon volume. Center: Photograph of surface deformation after cyclic inflation and deflation, projected onto outlines of Gran Canaria. Inset lower right: Close-up of complex fault interplay in periphery of produced caldera structure. Bottom inset: Cross sections of characteristic structures that form on balloon inflation* ***1*** *and subsequent balloon evacuation* ***2***

Discussion

On Gran Canaria, radial and concentric caldera periphery faults were active during multicycle ignimbrite eruptions and corresponding caldera evolution. The concentric periphery fault zone is not a single sharply defined circular fault; rather, it forms a set of steeply dipping fault segments including horst and graben structures and large concentric horst structures between the concentric periphery zone and the caldera margin (Fig. 1). Reactivation of radial faults, episodic radial dike emplacement, and reactivation of concentric horst and graben structures was common and produced repeated differential uplift or subsidence of individual blocks according to the local stress pattern. Field observations on Gran Canaria are consistent with our experimental results, and the comparison of nature and experiment strongly resembles a series of structural features and proportions (Table 1).

The similarities between Gran Canaria and the scaled experiments suggest that the floor of the Tejeda caldera and the lower caldera infill are controlled by radial faults that crosscut, and are crosscut by, concentric faults. However, they are now largely covered by younger deposits and obscured by intrusives. The inference of intracaldera crosscutting radial and concentric fractures on Gran Canaria is consistent with observations by Schirnick (1996), who found crosscutting radial and concentric dikes of Mogan age in a deeply eroded valley that cuts into the intracaldera succession. The existence of crosscutting radial and concentric faults and dikes in the caldera periphery, in the intracaldera succession, and in the experiments, strongly implies that multicycle calderas, such as Tejeda caldera on Gran Canaria, are unlikely to have undergone simple piston-type collapse. We suggest discrete block subsidence (i.e., piecemeal) to be the major subsidence mechanism in such long- lived caldera systems. Combining experimental and field observations, we infer that the periphery of calderas reveals important information on the mechanisms of caldera formation and the structure of the underlying caldera floor.

Acknowledgements: We thank B. Wenskowski and M. Sumita for help in the field, N. Urbanski for cooperation in the experimental set-up, J. Stix, P. Lipman, R. Seyfried, L. Schwarzkopf, C. Schirnick, and S. Krastel for discussion, and O. Roche and an anonymous referee for constructive criticism. Grants from the Studienstiftung des Deutschen Volkes to Troll and from the Deutsche Forschungsgemeinschaft to Schmincke (Schm-250/72-1 and Schm-250/77-1) are gratefully acknowledged.

References

Acocella, V., F. Cifelli, and R. Funiciello. 2000, Analogue models of collapse calderas and resurgent domes: Journal of Volcanology and Geothermal Research. 104,81–96.

Bogaard, P., and H.-U. Schmincke. 1998, Chronostratigraphy of Gran Canaria, in Weaver P.P.E., et al., Proceedings of the Ocean Drilling Program, Scientific results, Volume 157: College Station, Texas, Ocean Drilling Program, p. 127–140.

Druitt, D.H., and R.S.J. Sparks. 1984, On the formation of calderas during ignimbrite eruptions: Nature. 310,679–681.

Freundt, A., and H.-U. Schmincke. 1995, Petrogenesis of rhyolite-trachyte-basalt composite ignimbrite P1, Gran Canaria, Canary Islands: Journal of Geophysical Research. 100,455–474.

Gardeweg, M., and C.F. Ramirez. 1987, La Pacana caldera and Atana Ignimbrite—A major ash flow and resurgent caldera complex in the Andes of northern Chile: Bulletin of Volcanology. 49,547–566.

Gudmundsson, A. 1988, Formation of collapse calderas: Geology. 16,808–810.

Henry, C., and J. Price. 1989, The Christmas Mountains caldera complex, Trans-Pecos Texas: Bulletin of Volcanology. 52,97–112.

Hubbert, M. 1951, Mechanical basis for certain familiar geologic structures: Geological Society of America Bulletin. 62,355–372.

Komuro, H. 1987, Experiments on cauldron formation: A polygonal cauldron and ring fractures: Journal of Volcanology and Geothermal Research. 31,139–149.

Krantz, R.W. 1991, Normal fault geometry and fault reactivation in tectonic inversion experiments, in Roberts et al., eds., The geometry of normal faults: Geological Society [London] Special Publication 56, p. 219–229.

Krastel, S., and H.-U. Schmincke. 2001, Crustal structure of northern Gran Canaria deduced from active seismic tomography: Journal of Volcanology and Geothermal Research (in press).

Lipman, P.W. 1997, Subsidence of ash-flow calderas: Relation to caldera size and chamber geometry: Bulletin of Volcanology. 59,198–218.

Marti, J., G.J. Ablay, L.T. Redshaw, and R.S.J. Sparks. 1994, Experimental studies of collapse calderas: Geological Society [London] Journal. 151,919–929.

Marti, J., A. Folch, A. Neri, and G. Macedonio. 2000, Pressure evolution during explosive caldera-forming eruptions: Earth and Planetary Science Letters. 175,275–287.

Nappi, G., A. Renzulli, and P. Santi. 1991, Evidence of incremental growth in the Vulsinian calderas (central Italy): Journal of Volcanology and Geothermal Research. 47,13–31.

Newhall, C., and D. Dzurisin. 1988, Historical unrest at large calderas of the world: U.S. Geological Survey Bulletin. 1855,1–1108.

Roche, O., T. Druitt, and O. Merle. 2000, Experimental study of caldera formation: Journal of Geophysical Research. 105,395–416.

Schirnick, C. 1996, Formation of an intracaldera cone sheet dike swarm (Tejeda caldera, Gran Canaria) [Ph.D. thesis]: Kiel, Christian- Albrechts-Universität Kiel, p. 204.

Schirnick, C., P. Bogaard, and H.-U. Schmincke. 1999, Cone sheet formation and intrusive growth of an ocean island—The Miocene Tejeda complex on Gran Canaria, Canary Islands: Geology. 27,207–210. [ABSTRACT]

Schmincke, H.-U. 1967, Cone sheet swarm, resurgence of Tejeda caldera, and the early geologic history of Gran Canaria: Bulletin of Volcanology. 31,153–162.

Schmincke, H.-U. 1976, The geology of the Canary Islands, in Kunkel, G., ed., Ecology and biogeography in the Canary Islands: The Hague, Netherlands, Junk B.V., p. 67–184.

Schmincke, H.-U., and D.A. Swanson. 1966, Eine alte Caldera auf Gran Canaria: Neues Jahrbuch für Geologie und Paläontologie. 5,260–269.

Smith, R., and R. Bailey. 1968, Resurgent cauldrons, in Studies in volcanology: A memoir in honor of Howel Williams: Geological Society of America Memoir 116, p. 83–104.

Troll, V.R., C.H. Emeleus, and C.H. Donaldson. 2000, Caldera formation in the Rum central igneous complex, Scotland: Bulletin of Volcanology. 62,301–317.

Varnes, D. 1963, Geology and ore deposits of the South Silverton mining area, San Juan County, Colorado: U.S. Geological Survey Professional Paper 378-A, p. 1–56.

Walter, T.R., and V.R. Troll. 2001, Formation of caldera periphery faults, an experimental study: Bulletin of Volcanology. 63,191–203.

Ye, S., R. Rihm, J. Dañobeitia, J. Canales, and J. Gallart. 1999, A crustal transect through the northern and northeastern part of the volcanic edifice of Gran Canaria: Journal of Geodynamics. 28,3–26.

Part I: Volcano flank instability by caldera formation

Chapter 3

Mirrors of shallow magma reservoirs

Collapse calderas – mirrors of shallow magma reservoirs

Thomas R. Walter [1], Valentin Troll[1,2], Falk Amelung[3], Ralf Seyfried[1]

[1] GEOMAR, Dept. of Volcanology, Wischhofstrasse 1-3, D- 4148 Kiel, Germany
[2] Dept. of Geology, University of Dublin, Trinity College, Dublin 2, Ireland
[3] HIGP/SOEST, University of Hawaii, 2525 Correa Rd, Honolulu, HI 96822, USA

Abstract. Determining size and structure of a magma reservoir is a fundamental problem in understanding volcanoes. Analogue experiments on the origin of collapse calderas provide new insights into the formation of caldera volcanoes. Large calderas are associated with large magma reservoirs, whereas the diameter of a caldera decreases systematically with depth of the magma reservoir. We propose an empirical relationship between these fundamental parameters and infer reservoir diameters for caldera volcanoes, such as in the Canary Islands, Rabaul, Galapagos and for Olympus Mons on Mars.

Keywords: magma reservoir size, collapse caldera, volcano deformation, Rabaul, Canary Islands, Galapagos

Introduction

Magma reservoirs form in the Earth's crust when molten rock accumulates by a combination of buoyancy-driven magma movement, friction and crystallization (Marsh 2000). Such reservoirs are the major sites of magma evolution, their dynamic processes control the mechanisms of volcanic eruptions. The volume and location of magma that rests beneath a volcano is unknown for most volcanic systems, since evaluating the dimensions of magma reservoirs is a difficult task. Geophysical measurements allow locating zones of earthquakes and velocity contrasts in the crust, frequently interpreted as migrating and partially molten material, as well as the depth of reservoirs based on deformation studies. Robust data on the reservoir size are only available for a handful of active magma systems.

Volume increase of a shallow magma reservoir results in a structural dome (Komuro et al. 1984). Surface deformation data allow only poor resolution, however, on the actual size and shape of the magma reservoir. Most such data are well explained by a point dilation model (Mogi source). In turn, volume decrease of a shallow reservoir causes subsidence and collapse of the overburden roof; the surface expression is a caldera, structurally defined by outward dipping ring faults (Lipman 1997; Walter and Troll 2001). As shown in Figure 1, such faults are reverse faults, somewhat smaller in diameter than the source reservoir (Anderson 1937). At the surface, inward-directed landslides plus shallow normal faults widen the morphological caldera basin (Lipman 1984).

Calderas have a variety of surface geometries, generally increasing in diameter with the size of the edifice and eruptive volumes, providing information about the diameter of the magma reservoir (Wood 1984; Lipman 1997). Here, we use scaled analogue experiments to find out how a caldera diameter relates to the diameter of the underlying magma reservoir and to the depth of the reservoir below the surface.

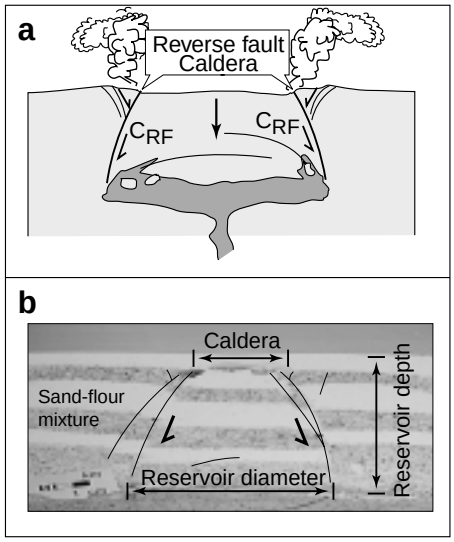

Figure 1: *Schematic illustration of caldera formation with respect to magma chamber evacuation.*

a. *Drainage of the magma reservoir causes roof subsidence into the magma chamber. Displacement is of a maximum along caldera reverse faults (C_{RF}). The topographic caldera size increases due to inward-directed landslides.* ***b*** *Cross section through experimentally produced caldera.*

Caldera formation experiments

We simulated the formation of a collapse caldera by placing an oblate air-filled rubber balloon into a tank filled by a mixture of dry sand and flour. In separate experiments, we used two different sand/flour mixtures as analogue materials to approximate the wide spectrum of natural rocks. The sand-flour mixture has material properties such that 1 cm in the experiments translates to about 1 km in nature (the scaling procedure is given in Table 1).

On reservoir evacuation, the roof material above the reservoir subsided into the void and displacement occurred along bell-shaped faults. The voids propagated sequentially to the surface, resulting in the formation of near-surface ring faults. We interpret coherent subsidence of the sand surface along these faults as analogous to the formation of collapse calderas. Accordingly, the surface diameter of the collapse caldera is defined herein as the diameter of the outward dipping ring faults along which the main subsidence occurs.

The balloons used had the shape of an oblate rotational ellipsoid with a height-to-width aspect ratio of ~ 0.25. Aspect ratios of natural magma reservoirs, as inferred from eroded plutons, range between 0.5 and 0.05 (Marsh 2000). First, we used a balloon with a given diameter, varied its depth and measured the resulting caldera diameters. Then, we

repeated this set of experiments using balloons with different diameters. The measured caldera diameters are shown in Fig. 2 as a function of reservoir depth and the balloon diameters. Increasing the depth and decreasing the diameter of the balloon results in smaller calderas. For very shallow balloons, the caldera diameter approaches the balloon diameter. For balloon depth smaller than half the balloon diameter, the diameter of the caldera decreases approximately linearly with the depth of the balloon. All the experimental results can be explained by a quadratic equation of the form

$$d_R = \frac{Z_R}{2k} + \sqrt{\frac{Z_R^{\,2}}{4k^2} + d_C^{\,2}},$$

where d_R is the reservoir diameter, Z_R is the reservoir depth, d_C is the caldera diameter.

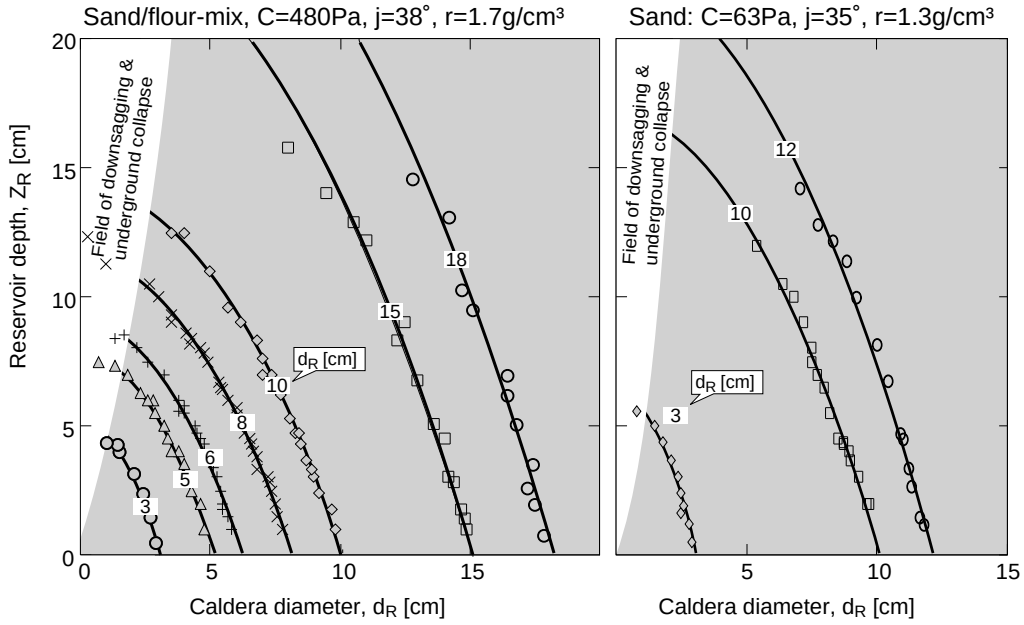

Figure 2: *Experimental results and derived relationship between reservoir size, reservoir depth and caldera diameter. Curved lines show the diameter of the reservoir d_R as a function of caldera diameter d_C and reservoir depth Z_R. Due to analogue material properties, massive crystalline (left) and weak/fractured environments (right) were simulated. In experiments we calculated k values of 1.63 for tough (cohesive sand/flour mixture) and 1.98 for weaker materials (low cohesive sand). The variation as a function of material properties becomes insignificant for very shallow reservoirs.*

The dimensionless coefficient *k* describes the mechanical behavior of the material used. *k* increases with the materials' friction coefficient and decreases with cohesion. In analogy to natural systems, *k* yields about 1.5 for materials with high cohesion and high angle of internal friction, and >2.0 for fractured rocks with lower cohesion and lower angle of internal friction (Table 1). All experiments fit this relationship with a correlation coefficient *(R)* of $R>0.97$. The value of *k* becomes significant for reservoirs at great depth (Fig. 2).

Reservoirs that are situated at very great depth compared to their size (roof aspect ratio >2) formed in many experiments no clear caldera collapse; the ring faults did not propagate to the surface, so that we observed merely a slight surface flexure, termed herein as the *field of downsagging*.

	L	g	ρ	φ	C
	(m)	(ms^{-2})	(kg/m^3)	(°)	(Pa)
Rock	10^3	9.8	2700	25-40	10^6 - 5X10^7
Sand	10^{-2}	9.8	1700	35	63 -
Sand/Flour	10^{-2}	9.8	1300	38	- 480
X_{model}/X_{nature}	$RL = 10^{-5} = \alpha$	Rg = 1	$R\rho \sim 0.5$	$R\varphi \sim 1$	$R_C \sim \alpha$

Table 1. *Experimental scaling. For affinity (Hubbert 1937; Sanford 1959), the length (1:100,000) and material behaviour must be scaled to natural values (Handin 1966; Schultz 1996). Required analogue materials must hence be weaker than rock, by a factor $\alpha = 10^{-5}$. The sand–flour mixtures used show a linear relation of shear stress and normal stress by the Coulomb criterion of brittle failure (for $-\sigma < 10^5$ Pa). All lengths L were scaled by the factor α, the friction coefficient $\mu = \tan\varphi$ is invariant. By using $R_X = X_{model}/X_{nature}$, scaling ratios of the physical values X were obtained (R_L, Rg, $R\varphi$, $R\rho$, R_C) (Roche et al. 2000). The stress ratio $5x10^{-6}$ Pa is defined by R_L x Rg x $R\varphi$. The used sand-flour mix therefore simulates high rock cohesion, while the low-cohesive sand approximates lower natural values. 1 cm in experiments therefore translates to ~1 km in nature. Since an influence in viscosity is negligible, time scaling is not required. Also, the effect of elastic force in such large deformations is insignificant (Komuro et al. 1984). [Length is L, gravity acc. g, density ρ, angle of internal friction φ, cohesion C].*

Comparison with natural calderas

To test whether our experimental results can be applied to natural calderas we compared known reservoir sizes with predictions made by our experiments. The calderas of Gran Canaria (Canary Islands), and of Rabaul (Papua New Guinea) are among the very few caldera examples in the world for which the geometry of the underlying magma reservoir is relatively well constrained. Since many natural calderas and reservoirs are elliptically shaped due to external (tectonic) stress fields we consider equivalent diameters in this study (a diameter equivalent is the corresponding diameter of a circle with the same area as the initial ellipse).

The Tejeda caldera on Gran Canaria (Fig. 3) is a large Miocene central caldera (width between 18 km and 20 km) that formed during episodic explosive eruptions of one of the worlds most voluminous pyroclastic sequences on ocean islands (Schmincke 1976; Troll et al. 2002). Geochemical data suggest that the magma reservoirs associated with these eruptions were located at a depth of 6-7 km (Freundt and Schmincke 1995). Also in this level, seismic reflection data reveal a lens-shaped anomaly of just over 20 km diameter and 6 km height, interpreted as the solidified parts of the Miocene magma reservoir (Krastel and Schmincke 2002). The height-to-width aspect ratio is accordingly 0.3, similar

to the balloon rotational ellipsoid shape used. For a caldera with a diameter equivalent $d_C = 19$ km and a reservoir depth $Z_R = 6.5$ km, our experiments predict a reservoir diameter equivalent $d_R = 21$ km (Fig. 3), consistent with the size of the seismic anomaly. The volume of the plutonic reservoir complex within Gran Canaria is hence > 1400 km³.

Rabaul Caldera is a nested caldera complex with an overall width of 8 to 14 km. During the latest historic caldera-forming event 1400 years ago more than 11 km³ of magma were erupted (Walker et al. 1981; Saunders 2001). Volcanic activity continues to the present. Eruptions since 1994 occur along the caldera bounding ring-faults. Seismicity over the past 30 years defines an elliptic 5 to 9 km tremor area that formed by migrating magma and faulting (Saunders 2001). Below ~ 4 km depth the seismic events lessen, which has been interpreted as the nearby top of the magma reservoir (Mori and McKee 1987). Our experiments predict a reservoir diameter equivalent of 8 km (Fig. 3), also consistent with the seismically inferred reservoir.

Discussion

We modelled piston-like caldera collapse, and introduced a mathematical linkage of the three interconnecting parameters caldera diameter, reservoir depth and reservoir diameter. This relationship can also be used to infer the presence and size of the magma reservoir for other caldera volcanoes.

Implications for natural calderas

We now discuss the implications of the experimental results for the Las Cañadas basin, Tenerife (Canary Islands). The origin of this elliptical depression with a diameter of 10 km and 16 km is debated. In one hypothesis it is a nested collapse caldera (Marti et al. 1994). In another hypothesis the depression formed by a giant north-directed landslide into the sea; the southern scarp is the landslide headwall (Araña et al. 1989; Carracedo 1994; Watts and Masson 2001). Geochemical studies revealed that during the evolution of the Las Cañadas basin, a small migrating reservoir was located between 3 and 7 km beneath the present caldera floor (Araña et al. 1989; Ablay et al. 1995). Seismic data indicate a small recent magma reservoir with a remnant diameter of 4 km at 4 km depth (Banda et al. 1981). If Las Cañadas is a single collapse caldera, our experiments require a huge magma reservoir with a diameter equivalent of 14 km (Fig. 3). Such a reservoir, however, is neither evident nor supported by any studies of the structure, geochronology and stratigraphy (Ancochea et al. 1999). If Las Cañadas is a nested caldera made up by 3 smaller collapse calderas each with ~ 7 km in diameter that formed at different times (Marti et al. 1994), our experiments show the need of a (migrating) reservoir with 8.4 km diameter in 4 km depth – a size that is again not supported by geophysical data. This

suggests that the large size of the Las Cañadas caldera may not be a pure collapse caldera and substantial landslides were involved in the basin formation.

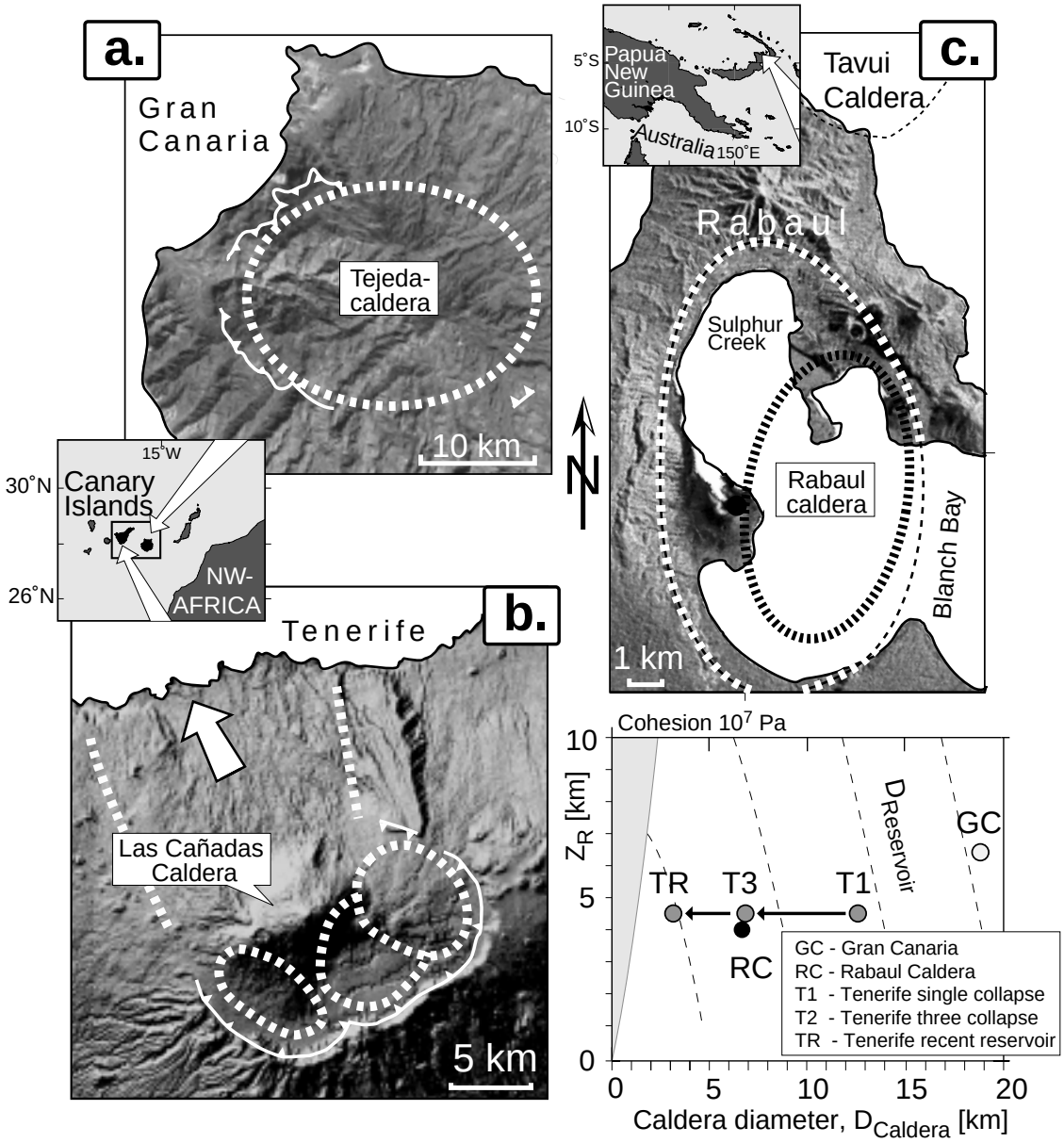

Figure 3: *Caldera examples. Analogue experiments transferred to kilometre scale with application to* ***a.*** *Gran Canaria (GC),* ***b.*** *Tenerife (TF), and* ***c.*** *Rabaul Caldera. In maps, dotted circles show assumed collapse basin outlines. The diameter of the Gran Canaria magma reservoir d_R is ~21 km. To match the recent 4 km reservoir size that is located ca. 4 km beneath the Las Cañadas basin on Tenerife, a resulting caldera should be no larger than 3 or 4 km across. Moreover, three nested 8 km-wide calderas require a reservoir of at least 8 km in ~4 km depth (TF-3). Apparently a huge landslide formed parts of the caldera rim, making up for this deficiency. For Rabaul Caldera the reservoir is ellipsoid shaped (6-10.5 km). Geometric relations are shown for tough crustal rocks, so that the magma chamber diameters of GC, TF and RC are minimum values. Image source: Spaceborne Imaging Radar-C and X-Band Synthetic Aperture Radar (SIR-C/X-SAR).*

Olympus Mons on the planet Mars, the largest known volcano, is a shield volcano measuring >620 km in diameter and a height of >25 km. It is about 100 times larger than Mauna Loa on Earth. Olympus Mons is located near the equator on the Tharsis Plateau, bordered by a steep peripheral escarpment. Huge central craters resemble the calderas found on shield volcanoes on Earth. The nested caldera in the center is in total ~90 x 60 km wide, made of multiple (at least 6) circular collapse craters created by different collapse events (Fig. 4). Circular fractures and possibly ring dikes define the oldest and largest collapse caldera basin, which has a structural diameter equivalent of about 50 km; the morphological basin eroded and enlarged, giving now a diameter of 65 km. The reservoir depth was estimated to be shallower than 16 km (Zuber and Mouginis-Mark 1992). Our experiments suggest for a reservoir depth of between 10 and 16 km a reservoir diameter equivalent of 52 km to 54 km.

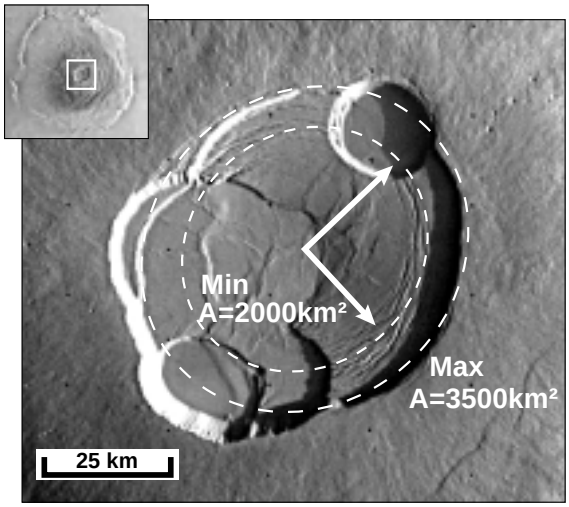

Figure 4: *Olympus Mons Caldera, Mars.*
Mosaic of Olympus Mons (insert) and close up of the nested summit caldera complex. The large central caldera floor is defined by ring structures (ring dikes and/or ring faults), giving a size of the structural bounded caldera floor of ~1900 km². Erosion, normal faulting and smaller collapse events widened the caldera basin to >3500 km². The magma reservoir was of an equivalent diameter of 54 km if located in 16 km depth. Image source: Viking orbiter images, available online.

The morphologic caldera diameters of the basaltic Galapagos volcanic shields of Isabela and Fernandina range from 3 to 8 km diameter. The caldera of Fernandina volcano collapsed by 300 m in 1968 (Simkin and Howard, 1970). A recent study based on 1992-1998 Interferometric Synthetic Aperture Radar data (InSAR) showed that all but one of the volcanoes are actively inflating due to accumulation of magma in central reservoirs beneath the calderas (Amelung et al., 2000). Interpretation of the InSAR data using point (Mogi) and sill sources suggest reservoirs at depths of 2 km, 3 km, and 5 km for the volcanoes Sierra Negra, Darwin and Cerro Azul, respectively. The calderas are nearly circular, suggesting that the external stress field had only little influence during the formation of the caldera. The morphological diameters of the calderas d_R of these volcanoes are 8 km, 5.5 km, and 3.7 km. Our experimental results predict diameters of 8.6 km, 6.4 km, and 5.3 km. However, due to erosion and normal fault caldera widening, the structural diameters of the Galapagos ring faults are probably somewhat smaller. In

analogy to this dilemma, Lipman (1984, 1997) indicated for calderas of western North America the structural caldera diameter (reverse faults) to be about 40 to 80% of the topographic caldera wall. Also experimental data demonstrated that the ring fault diameter is ~50 to 90% the outer depression diameter, the discrepancy augments with the reservoir depth (Walter and Troll 2001, Acocella et al. 2001). For the Galapagos volcanoes the accurate reverse fault position is vague, but we can approximate the structural collapse caldera diameter by using ~70% of the topographic caldera expression. Then, the ring fault diameters are smaller, being 5.6 km, 3.9 km and 2.6 km, in same order. The inferred diameters for the Sierra Negra reservoir is hence 6.2 km, the Darwin reservoir is 4.9 km, and Cerro Azul 4.3 km. As an important fact, we now know that the reservoir of Sierra Negra is significantly larger than the reservoirs of Darwin and Cerro Azul; a result that may affect petrological and dynamical studies, as well.

Limitations: For complement understanding of the experiments, we should be conscious of the central simplifications of the analogue models. Mechanical and geometrical constraints are unavoidable in any types of modeling, thus we have to make assumptions on the materials behavior, neglect the elasticity of the crustal rocks, and use a membrane-limited reservoir. The reservoir membrane did not allow to simulate a gradual transient from reservoir to crust, but allows precise control on the reservoir geometries.

The influence of external stress fields such as due to the topography of the volcano (Walter and Troll 2001), due to magmatic underplating (Gudmundsson 1998), and regional tectonic background stresses (Moore and Kokelaar 1998) was neglected in these experiments. For many volcanic complexes and ocean islands these assumptions may be justified and the experiments therefore provide a first-order estimate on the size of the underlying magma reservoirs.

Conclusion

Monitoring surface deformation at active calderas using satellite data (InSAR, GPS) provides an estimate on the depth of the magmatic source (cf. Amelung et al. 2000). The analogue experiments discussed above provide a means to estimate the diameter of such a reservoir. The effortless use of our experimentally derived geometric relationship of a caldera diameter, its associated reservoir diameter beneath, and the reservoir depth, provides novel information about the structural evolution of a volcano. This information is crucial for the long-term forecasting of volcanic eruption because it provides a handle of the pressure increase in the reservoir associated with magma intrusion. It can further be used to estimate a) the dimension and variability of reservoir sizes, b) to provide preliminary and comparative information for seismic measurements, c) to offer important bounds for petrological studies on magma chamber dynamism, or d) allows assessing whether a basin was formed by vertical or lateral sector collapse.

Acknowledgements: The authors thank O. Roche, J. Gardner, H.-U. Schmincke, and T. Hansteen for discussion and critical comments on earlier versions of the manuscript. Financial support was provided by the Deutsche Forschungsgemeinschaft by grants Schm 250/77-1/2 to H.-U. Schmincke and a grant from the Studienstiftung des deutschen Volkes to VRT.

References

Ablay, G.F., J. Martí, and R.S.J. Sparks, The 2ka subplinian eruption of Montaña Blanca, Tenerife, *Bull. Volcanol., 57*, 332-355, 1995.

Amelung, F., S. Jónsson, H. Zebker, and P. Segall, Widespread uplift and ‚trapdoor' faulting on Galápagos volcanoes observed with radar interferometry, *Nature, 407*, 993-996, 2000.

Ancochea, E., M.J. Huertas, J.M. Cantagrel, J. Coello, J.M. Fúster, N. Arnaud, and E. Ibarrola, Evolution of the Cañadas edifice and its implications for the origin of the Cañadas caldera (Tenerife, Canary Islands), *J. Volcanol. Geotherm. Res., 88*, 177-199, 1999.

Anderson, E.M., Cone sheets and ring dykes; the dynamical explanation, *Bull. Volcanol., 1*, 35-40, 1937.

Araña, V., F. Barberi, and G. Ferrara, The complex volcanism of Teide-Pico Viejo (in Spanish), *in Los Volcanes y la Caldera del Parque Nacional del Teide (Tenerife, Islas Canarias)*, edited by V. Araña, and J. Coello, pp. 101-126, ICONA, Madrid, 1989.

Banda, E., J.J. Dañobeitia, E. Suriñach, and J. Ansorge, Features of crustal structure under the Canary Islands, *Earth Planet. Sci. Lett., 55*, 11-24, 1981.

Carracedo, J.C., The Canary Islands: an example of structural control on the growth of large oceanic-island volcanoes, *J. Volcanol. Geotherm. Res., 60*, 225-241, 1994.

Freundt, A., and H.-U. Schmincke, Petrogenesis of rhyolite-trachyte-basalt composite ignimbrite P1, Gran Canaria, Canary Islands, *J. Geophys. Res., 100*, 455-474, 1995.

Gudmundsson, A., Formation and development of normal-fault calderas and the initiation of large explosive eruptions, *Bull. Volcanol., 60*, 160-170, 1998.

Handin, J., Strength and ductility, in *Handbook of Physical Constants*, edited by S.P.J. Clarck, Geol. Soc. Am., 223-289, 1966.

Hubbert, M.K., Theory of scale models as applied to the study of geologic structures, *Bull. Geol. Soc. Am., 48*, 1459-1520, 1937.

Komuro, H., Y. Fujita, and K. Kodama, Numerical and experimental models on the formation mechanism of collapse basins during the Green Tuff Orogenesis of Japan, *Bull. Volcanol., 47*, 649-666, 1984.

Krastel, S., and H.-U. Schmincke, Crustal structure of northern Gran Canaria deduced from active seismic tomography, *J. Geophys. Res. (in the press)*, 2002.

Lipman, P.W., The roots of ash flow calderas in western North America: windows into the tops of granitic plutons, *J. Geophys. Res., 89*, 8801-8841, 1984.

Lipman, P.W., Subsidence of ash-flow calderas: relation to caldera size and magma-chamber geometry, *Bull. Volcanol., 59*, 198-218, 1997.

Marsh, B.D., Magma Chambers, in *Encyclopædia of Volcanoes*, edited by H. Sigurdsson, pp. 191-206, Academic Press, San Diego, 2000.

Marti, J., J. Mitjavila, and V. Araña, Stratigraphy, structure and geochronology of the Las Cañadas caldera (Tenerife, Canary Islands), *Geol. Mag., 131*, 715-727, 1994.

Moore, I., and P. Kokelaar, Tectonically controlled piecemeal caldera subsidence: a case study from the Glen Coe volcano, Scotland, *Geol. Soc. Am. Bull., 110*, 1448, 1998.

Mori, J., and C. McKee, Outward-dipping ring fault structures at Rabaul caldera as shown by earthquake locations, *Science, 235*, 193-195, 1987.

Roche, O., T. Druitt, and O. Merle, Experimental study of caldera formation, *J. Geophys. Res., 105*, 395-416, 2000.

Sanford, A.L., Analytical and experimental study of simple geologic structures, *Bull. Geol. Soc. Am., 70*, 19-52, 1959.

Saunders, S.J., The shallow plumbing system of Rabaul caldera: a partially intruded ring fault? *Bull. Volcanol., 63*, 406-420, 2001.

Schmincke, H.-U., The geology of the Canary Islands, in *Ecology and Biogeography in the Canary Islands*, edited by G. Kunkel, pp. 67-184, The Hague, Netherlands, 1976.

Schultz, R.A., Relative scale and the strength and deformability of rock masses, *J. Struct. Geol., 18*, 1139-1149, 1996.

Simkin, T., and K.A. Howard, Caldera collapse in the Galapagos Islands, 1968, *Science, 169*, 429-437, 1970.

Troll, V.R., T.R. Walter, and H.-U. Schmincke, Cyclic caldera collapse: Piston or piecemeal subsidence? Field and experimental evidence, *Geology, 30*, 135-138, 2002.

Walter, T.R., and V.R. Troll, Formation of caldera periphery faults: an experimental study, *Bull. Volcanol., 63*, 191-203, 2001.

Watts, A.B., and D.G. Masson, New sonar evidence for recent catastrophic collapses of the north flank of Tenerife, Canary Islands, *Bull. Volcanol., 63*, 8-19, 2001.

Walker, G.P.L., R.F. Heming, T.J. Sprod, and H.R. Walker, Latest major eruptions of Rabaul volcano, *Geol. Surv. Papua New Guinea Mem., 10*, 181-193, 1981.

Wood, C.A., Calderas: A Planetary Perspective, *J. Geophys. Res., 89*, 8391-8406, 1984.

Zuber, M.T., and P.J. Mouginis-Mark, Caldera subsidence and magma chamber depth of the Olympus Mons Volcano, Mars, *J. Geophys. Res., 97*, 18,295-18,307, 1992.

Part II: Volcano flank instability by caldera formation

Chapter 4

Recurrent flank collapse in Teno

Rifting, recurrent landsliding and Miocene structural reorganization in Teno, NW-Tenerife (Canary Islands)

Thomas R. Walter and Hans-Ulrich Schmincke
Abt. Vulkanologie & Petrologie, GEOMAR, Wischhofstrasse 1-3, 24148 Kiel, Germany

Abstract. We studied mechanisms of structural destabilization of ocean island flanks by considering the linkage between volcano construction and volcano destruction, exemplified by the composite Teno shield volcano on Tenerife (Canary Islands). During growth, Tenerife episodically experienced giant landslides, genetically associated with rifting and preferentially located between two arms of a three-armed rift system. The deeply eroded late Miocene Teno massif allows insights into the rifting processes, the failure mechanisms and related structures. The semicircular geometry of paleo-scarps and fracture systems, breccia deposits and the local dike swarm reconfigurations delineate two landslide scarp regions. Following an earlier collapse of the older *Los Gigantes Formation* to the north, the rocks around the scarp became fractured and intruded by dikes. Substantial lava infill and enduring dike emplacement increased the load on the weak scarp and forced the flank to creep again, finally resulting in the collapse of the younger *Carrizales Formation*. Once more, the changing stress field caused deformation of the nearby rocks, a fracture belt formed around the scarp and dikes intruded into new (concentric) directions. The outline, size and direction of the second failed flank of Teno very much resembles the first collapse. We suggest structural clues concerning mechanisms of recurrent volcano flank failure, verifying the concept that volcano flanks that have failed are prone to collapse again with similar dimensions.

Keywords: Flank instability, dike reconfiguration, recurrent sector collapse, Canary Islands, volcano spreading

Introduction

Volcanic islands are structurally unstable and thus susceptible to seaward-directed mass wasting. The lateral collapse of huge sectors of a volcano can by highly destructive, manifested in debris avalanches, volcanic explosions and tsunamis. Despite the hazard-potential of volcanoes, the structural mechanisms relating the size, frequency and direction of giant landslides are poorly understood.

Volcanoes are predisposed to spread outward due to their topographic load and their intrusive complexes that tend to decouple the stress field (Fiske and Jackson 1972; Borgia 1994). Intrusions frequently form rift zones, defined by parallel swarms of (feeder) dikes and topographic ridges of aligned vents, which are prominent structural features of

ocean-island volcanoes (Stillman 1987; Walker 1992). The lateral collapse of volcanic edifices is commonly structurally linked to those rift zones (Siebert 1984).

To reconstruct the volcano-tectonic paleo-stress field controlling the emplacement of a dike-swarm, detailed studies of dike arrangements are required. The direction of a propagating dike typically tends to be perpendicular to the minimum principal compressive stress, allowing to study the paleo-stress relations within a volcanic edifice at time of dike emplacement (Anderson 1937). Structural field data have been used in the past to study the tectonic evolution of the Canary Islands (Schmincke 1968; Féraud et al. 1985; Stillman 1987; Barrera et al. 1989; Carracedo 1994, 1996; Martí et al. 1997; Marinoni and Gudmundsson 2000). Some rift zones formed during the entire evolution of a volcanic island, some extending over 50 km from a nucleus (Fig. 1). These rift zones initiated most commonly during the shield-building stage of an island and –once established– imply the location of unstable volcano sectors. On La Palma, an unstable flank is sited normal to a major north–south rift zone (Day et al. 1999). Failures of El Hierro and Tenerife often bisect the angles formed by two structural axes of persistent diking, whereas magmatic activity concentrated along three structural axes, forming morphological ridges and triangular elongated edifices (Navarro and Farrujia 1989; Carracedo 1994, 1996). The collapse of huge volcanic sectors into the sea produced additional serrate shorelines (Carracedo 1994; Krastel et al. 2001).

Here, we report the results of detailed field studies, focusing on the late Miocene basaltic shield of Teno (northwestern Tenerife), with an attempt to infer the paleo-stress that constrained the brittle deformation and several dike arrangements. Deep erosion of the Teno volcano has revealed a relationship between dike emplacement and major sector collapses. The data analysis of ~800 measured dikes and fractures allowed to estimate a local paleo-stress field, significantly influenced by near-surface effects. We describe the substantial intrusive activity focused on the Teno rift zones, and the modification of dike traces linked to recurrent collapses of volcano sectors.

The aim of this study is to better understand the mechanisms of volcano deformation and flank destabilization, sector collapse and the structural aspects acting together. This study may help to focus dedicated studies on volcanic edifices that are in-between two sector collapse events.

Volcano-tectonic evolution of Tenerife

Tenerife is the highest island of the Canaries and centrally located in the Archipelago. The oldest subaerial rocks of Tenerife are those of three separate basaltic shield volcanoes on the corners of the island, composed mainly of alkali basalts, basanite, ankaramite and minor phonolite and trachyte, emplaced between 12 and 3.3 Ma (Ancochea et al. 1990; Thirlwall et al. 2000). These Miocene series crop out at the

eroded volcanic massifs Roque del Conde, Anaga and Teno (Fig. 1). Mainly basaltic and phonolitic eruptions formed the huge Las Cañadas edifice, starting around 3.5 Ma ago (Ancochea et al. 1990; Martí et al. 1997). The volcano-tectonic evolution of this pivotal edifice was dominated by rifting, concentrated in three rift arms that diverge from the Las Cañadas center to the northeast, to the northwest and to the south (Ancochea et al. 1990; Carracedo 1994).

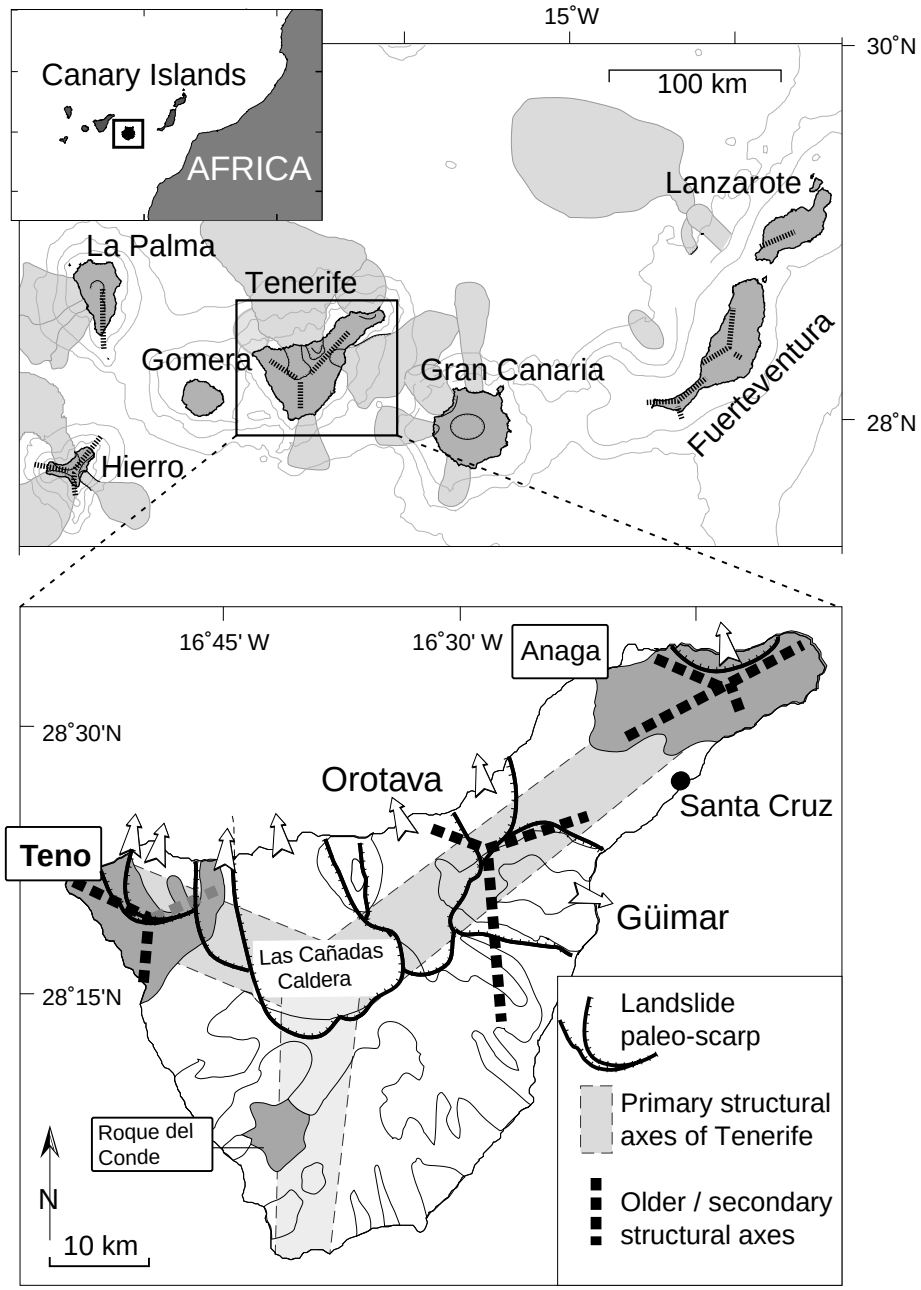

Figure 1: *Location of the Canary Islands and structural axes of rift zones (after Féraud et al. 1985, Carracedo 1996). Areal distribution of submarine debris avalanche, debris flow and slump deposits after Krastel et al. (2001). Enlarged inset showing Tenerife with inferred structural axes and sites of lateral failures (after Navarro and Farrujia (1989), Carracedo (1994), and own work). Shaded areas represent the Miocene shield volcanoes of Anaga, Roque del Conde, and Teno.*

The internal structural design of Tenerife was earlier inferred from gravity data, also showing density zones in triaxial geometry (McFarlane and Ridley 1968). However, the existence of an active southern rift zone is questioned by some workers (cf. Marti et al. 1996). The main structural axis of Tenerife during its Pliocene and Pleistocene evolution is the southwest-northeast ridge (Cordillera Dorsal) between the Las Cañadas volcano and the Anaga massif, dominated by basaltic lavas and scoria cones. The major rifts of Tenerife overlap with shorter, secondary structural axes (Fig. 1), probably defining separate volcanic centers (Navarro and Farrujia 1989; Navarro and Coello 1989), but flank collapses destroyed large parts of such centers, forming the scarps e.g. of Güimar and La Orotava. At least six north-directed flank collapses have been documented (Ancochea et al. 1990; Cantagrel et al. 1999; Hürlimann et al. 1999; Ablay and Hürlimann 2000; Watts and Masson 2001), generating submarine landslide deposits that cover several thousands of square-kilometers north of Tenerife (Teide Group 1997; Watts and Masson 2001). The most recent giant landslide formed when the upper part of the Las Cañadas edifice failed ~0.18 Ma ago north of the present scarp of the "Las Cañadas Caldera" (Navarro and Coello 1989; Ancochea et al. 1990; Watts and Masson 2001), interpreted by some authors as mainly due to vertical caldera collapse (Martí et al. 1997). A giant explosion formed when the active magmatic/hydrothermal system of the Las Cañadas volcano was decapitated, leaving an extremely widespread blast deposit on Tenerife (Schmincke et al. 1999). The morphological Las Cañadas depression was subsequently filled by the Teide-Pico Viejo complex that towers 3718 m high.

The episodes of volcano growth were periodically interrupted by unstable flanks that failed seawards – a process that affected already late Miocene paleo-Tenerife. Numerous dike swarms and fracture sets form structural unconformities in the Teno complex that preserve a complex record of volcano deformation. A paleo-stress reconstruction of the Miocene massifs Teno and Anaga, based on dikes and fault planes, revealed extensional tectonics without traces of major compression, inferring three major tectonic episodes for Tenerife: 1) a pre-intrusive dip-slip fault extension trending NE-SW; 2) an extension trending WNW-ESE with oblique to strike-slip faulting; and 3) a strong late/post-intrusive extension trending NE-SW (Marinoni and Gudmundsson 2000). Local influences on these deformational episodes related to sector collapses were, however, not considered. The origin of the reorientation of the stress field principal axes was not established; it may include island-size gravitational effects due to island growth.

The structure of Teno

The Teno massif in NW-Tenerife is strongly eroded, with deep seaward-trending canyons (*barrancos*). The maximum elevation of ridges more than 1300 m asl alternates with 500 m deep barrancos, frequently with >200 m high vertical cliffs that allow detailed

structural analyses.

Neglecting minor post-Miocene volcanic and sedimentary deposits, the Teno composite shield is largely underlain by aa and pahoehoe basalt lavas erupted between 7.4 and 5.0 Ma, belonging to the 'Old Basaltic Series' of Tenerife (Ancochea et al. 1990). New geochronologic data indicate a very rapid history of Teno in Messinian age, forming the vast bulk of the massif in a time interval between 6.4-6.0 Ma (Thirlwall et al. 2000; v.d. Bogaard unpublished).

The Teno composite shield (see Table 1) is here reconstructed using unconformity-bounded stratigraphic units. An angular unconformity defines two sub-series for Teno, termed 'lower sequence' and 'upper sequence' by Ancochea et al. (1990). We identified two irregular unconformities marked by individual polymict debris deposits, separating three major evolutionary stages of Teno. We here name the three series based on well-exposed localities *Los Gigantes Formation (LGF)*, *Carrizales Formation (CF)* and *El Palmar Formation (EPF)*.

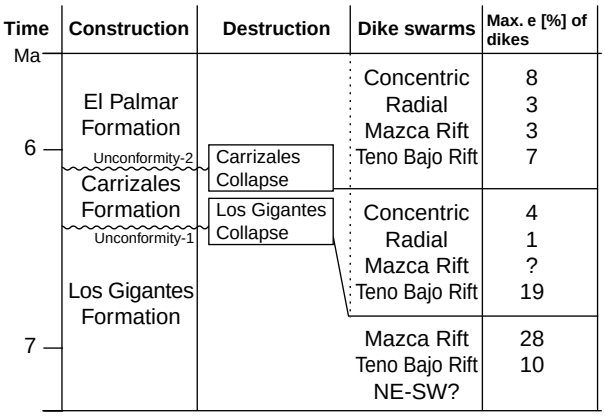

Table 1: *Structural evolution of Teno. The three major stages of Teno are unconformity-bounded. Note the changing quantity of dikes before, and after, a sector collapse event. The intrusive activity along the rift zones decreased, while concentric dike directions sequentially increased. The maximum extensional strain e [%] measured by dikes was computed for 100 m profile units.*

The *Los Gigantes Formation* largely forms the deeply eroded cliff of Los Gigantes south of Teno Bajo in southwestern Teno (Fig. 3) by a sequence of predominantly basaltic, <1 m thick lava flows, that are frequently clastic and dip up to 40° to the western shoreline. Reddish scoria deposits and local unconformities are common. Phonolites occur in the top of the formation such as the up to 80 m thick glassy phonolitic agglutinate with discontinuous basaltic spatter lenses, at 700 m asl southeast of the village of Mazca. Most of the Los Gigantes Formation is formed by steeply inclined pahoehoe flows and is covered unconformably by sub-horizontal lavas of the *Carrizales Formation*. The unconformity separating these two formations represents the trace of a ~ 6 Ma old landslide, and is marked by the presence of a polymict breccia (Cantagrel et al. 1999). The lava flows of the *Carrizales Formation* are mostly 1-2 m thick and are characteristically rich in fresh olivine and pyroxene, forming picritic lava flows (e.g. near the village of Los Carrizales). In addition, the Carrizales Formation clearly differs from the underly-

ing lavas in showing fewer dikes and scoria cones. A second angular unconformity separates the Carrizales Formation from the overlying *El Palmar Formation* (Fig. 2). The El Palmar Formation consists of generally horizontal basaltic and minor phonolitic and trachytic flows. The eroded formation is still >700 m thick with an age at its top of ~5.0 Ma (Ancochea et al. 1990).

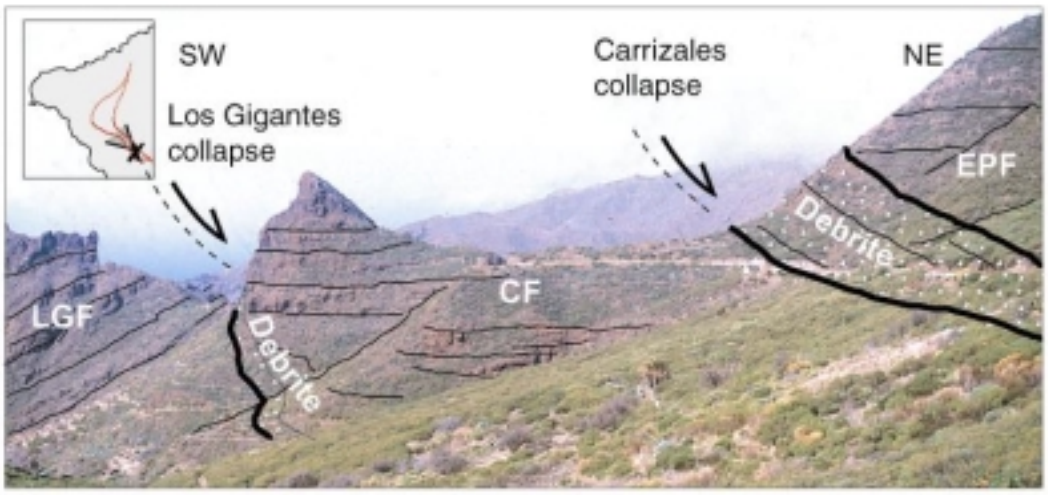

Figure 2: *Photographs of Teno unconformities. On the left, steeply seaward-dipping Los Gigantes Formation (LGF) is unconformably overlain by the sub-horizontal Carrizales Formation (CF). About 300 m eastward, a second debrite outlines the Carrizales collapse scarp, overlain by the El Palmar Formation (EPF). Photo is taken from Cruz de Gilda to the northwest (view inset).*

Both unconformities are overlain by polymict debrites defining abrupt scarps, which enclose horseshoe-shaped areas similar in size and open towards the NNE. Moreover, the dip and strike of the unconformities is generally very similar. We analyzed numerous fractures that characterize the volcano deformation and the linked flank instability. Dikes emplaced following flank failure intruded along new directions. Named by the formation that failed, the first Teno sector collapse is called the *Los Gigantes collapse*, the second collapse *Carrizales collapse*. The arrangements of dikes and fractures are tentatively grouped into pre- and postcollapse swarms (Table 1). Analyzing the fractures, we distinguish between faults with a measurable displacement >5 cm, and fractures with smaller displacements. Most fractures in Teno, however, are joint sets without obvious mismatch. The structural arrangement of dikes and displacing fractures was studied in detail along 9 profiles (Fig. 3d) and statistically analyzed in stereographic projections.

Los Gigantes collapse

The western unconformity is marked by two facies, strongly altered scoria/lapilli deposits and an overlying heterolithological debrite, both inclined 30-40° to the north-northeast

(e.g. 1 km south of Los Carrizales). The yellowish-brown scoria/lapilli deposit is up to 1 m thick and contains about 15% of mainly basalt clasts up to 10 cm. The altered matrix is rich in pyroxene (15-25%) and olivine (10-20%), glassy at the base and very heterogeneous (crystalline / vesicular / glass). Fragmentation of clasts and minerals, and the vesicularity and high amount of glass (up to ~50%) indicate explosive eruptions and very rapid cooling. The overlying debrite is 4 to 8 m thick and dips toward the valley of El Palmar in the north-northeast. The outline of this polymict debrite defines in part a horseshoe-shaped amphitheater (Fig. 3). Clasts reach decimeters in size and are mostly basaltic, the ten largest clasts in a 10-m² area ranging from 0.12 m to 0.33 m.

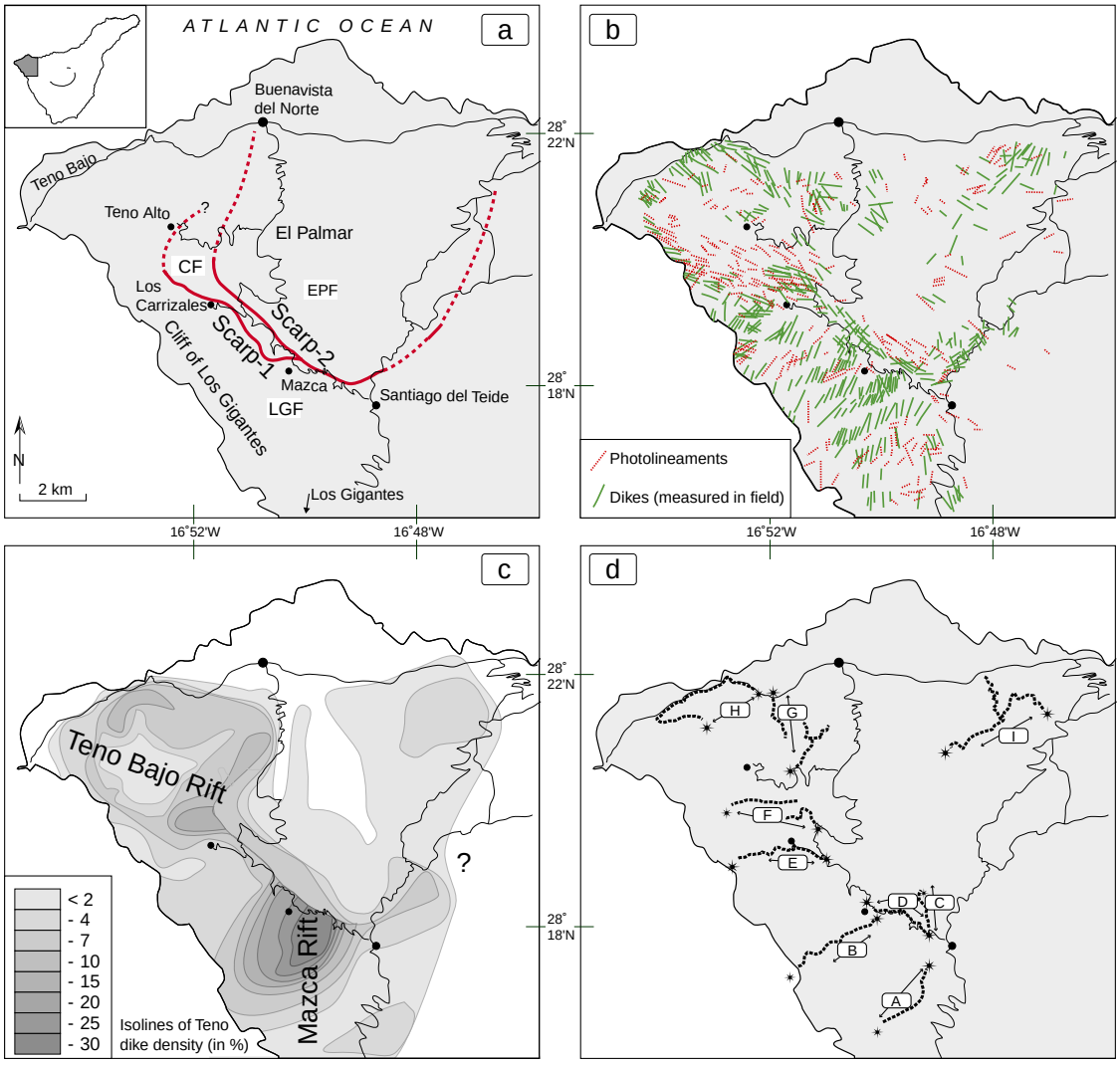

Figure 3: *Maps of Teno with* ***a*** *outline of the paleo-scarps,* ***b*** *summarizing dike orientations as measured in the field (solid lines) and studied in aerial photographs (dashed lines),* ***c*** *isolines of dike density, calculated for a 0.5 km grid,* ***d*** *locations of 9 profiles (A-I) studied in detail.*

The underlying Los Gigantes Formation lavas close to the unconformity are fractured. The fractures decrease in quantity and offset with increasing distance from the uncon-

formity. The orientation of the fractures is diffuse close to the breccia. Independent of displacement rates, the direction of the fractures is mainly scarp-parallel at a distance of 50 m west of the unconformity. East–west directed fractures are also common, dipping 60° to 90°. In contrast, the dip of widespread scarp-parallel fractures is generally less inclined (50-80°), with dip lines toward and away from the unconformity. Scarp-parallel faults have minor dip-slip fault offsets (< 1 m) and form synthetic and antithetic faults and small horst and graben structures.

Thin picritic lava flows above the debrite contain up to 70 modal % mafic phenocrysts, representing the younger Carrizales Formation and replenishment of the landslide scarp. The unconformity (scoria/lapilli and debrite deposits), as well as overlying basalt flows of the Carrizales Formation, are brittle deformed by at least one younger volcano-tectonic episode that produced shear zones and slickensides (Fig. 6). Several clasts of the debrite are broken and shear zones of the overlying Carrizales lavas indicate shear sense 'top toward the northeast'. Normal faulting was thus accomplished near this discordance after the formation of the scarp and after substantial reloading, indicating a further stage of northeast–southwest extension, with the hanging wall being located again on the northeast side.

Carrizales collapse

The scarp-replenishment lavas (Carrizales Formation) end unconformably at a second debrite (Fig. 2). The Carrizales debrite resembles the Los Gigantes debrite, being deposited in several episodes into a scarp. The thicknesses of the breccia unit reach about 35 m near Mazca and 20 m near Santiago del Teide. Clast sizes reach more than 1.5 m. Beside basaltic clasts, numerous clasts are rich in mafic phenocrysts (> 30% Ol + Px) similar to the picritic flows of the Carrizales Formation. The diameter of the ten largest clasts on a 100-m² area is about 0.4 m on average. At elevations of 600-700 m (next to Mazca), the debrite dips about 35° to northeast. The unconformity is traceable for more than 7 km, encircling a second horseshoe-shaped amphitheater with an enclosed area of ~ 50 km². At deeper levels, the Carrizales debrite is largely concordant to the older one and locally has eroded into it. The horizontal distance between the bases of both unconformities varies, but reaches more than 1 km north of Carrizales. Assuming a mean parallel dip of both unconformities of 35° slightly flattening to the northeast, and a horizontal distance of 1 km, the thickness of the Carrizales Formation would originally have exceeded ~ 700 m.

Close to the unconformity beneath the El Palmar Formation, the Carrizales Formation lavas are strongly crashed; abundant small-scale fracture-sets disrupt the older lavas and dikes. About 50 m west of the unconformity, joint sets without obvious mismatch show average joint spacing on a 10 m transect of ~ 0.04 m (Fig. 4a). Younger dikes and sills

intruded erratically, mainly parallel to the main fracture direction surrounding the scarp. Several dikes are largely un-fractured apart from cooling joints, thus younger than the main fracture event and clearly re-used the structural zones of weaknesses. More than 200 m west of the unconformity, fracture spacing increases and the strike and dip arrangement becomes less chaotic (Fig. 4b). The number of joints decreases significantly and average joint spacing is about 0.35 m. Steeply 60 to 90° dipping faults show generally displacements of only some centimeters and include polished surfaces. Normal faults can rarely be traced for more than 50 m. Some normal faults show offsets of several meters, defining horst and graben structures and/or large blocks (e.g. east of Los Carrizales) of occasionally >1000-m³ that slumped to the north and east. The direction of extension causing this brittle deformation was northeast-southwest.

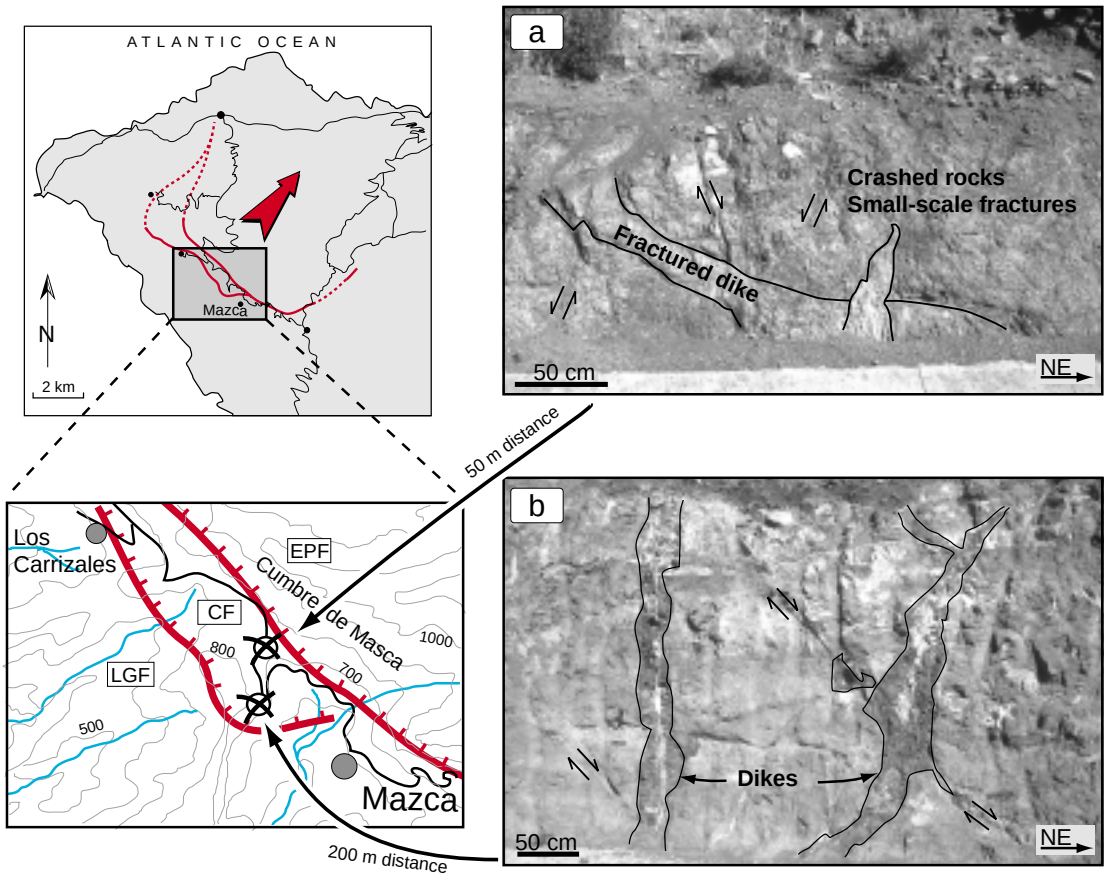

Figure 4: *Photographs of fracture belt near Los Carrizales,* ***a*** *at 50 m distance and* ***b*** *at 200 m distance from the unconformity. The fracture spacing decreases with decreasing distance to the Carrizales collapse amphitheater.*

Teno rift zones

Teno was subjected to intense rifting before and after the northern sector failed. Before the edifice collapsed, at least two rift-arms converged, defining an eruptive focus cen-

tered about 2 km north-northeast of the present village of Mazca (Fig. 3b). Away from the rift zones, dikes decrease in quantity and tend to intersect and crosscut dikes of the adjacent rift zone. The rift zones define two structural axes, showing: 1) a general north–south trend of dikes south of Mazca, with up to one third of the rock volume being intrusive, and 2) a northwest–southeast trend toward Teno Bajo. A vague third southwest–northeast dike trend is largely covered and/or poorly developed (Fig. 3b,c). Both collapses of the northern sector of Teno wiped out the nucleus of the rift system, as well as large parts of the rift-axes (Fig. 3).

To estimate the dilation due to dike emplacement (see Marinoni 2001), we measured the thickness T of a dike, the azimuth α of the computed dilation, and the strike of the dike β, giving the absolute dilation D by $D = T\sin(\alpha - \beta)$. For estimating the dilation of several dikes, the cumulative dilation was computed by the change in length (∂L) of a profile unit. This allows extensional strain computation $e = \partial L / L$, expressed as a percentage change in length. All measured orientations were corrected by the magnetic declination values, using the GEOMAG routine (USGS) based on the current International Geomagnetic Reference Field (IGRF).

Below, we describe both main rifting trends with an attempt to separate arrangements of structures (dikes, fractures) that formed due to sector collapse mechanism.

1) The Mazca Rift Zone: north–south trending dikes are mostly basaltic and frequently picritic, generally 0.6-0.8 m thick and show very constant orientations, especially in the southern sector (profile A). The dike quantity slightly increases with depth in this dike swarm and towards the inner north–south axis. In 100 m traverses, the large quantity of dikes illustrates extensional strain of more than $e = 25$ %, computed for an area south of Mazca (Fig. 3c). Profile B shows slightly diverging orientations of dikes close to the sea, here trending more NNE-SSW. Most dikes near the shoreline of Barranco de Mazca (western profile B) are vertical (Fig. 6), but some (14 dikes) dip towards the sea with 50-70°. Significant post-intrusive fracturing is not obvious in the western part of the rift zone. Profiles B and D in total (mean dike thickness $T' = 0.7$ m) show a horizontal east–west extension normal to the rifting axis of $\partial L_B + \partial L_D = 125$ m. These profiles, however, only resemble the western part of the north–south Mazca rift. Thus, an extension exceeding 200 m is more likely for the entire Mazca rift zone.

Both landslide-related unconformities are accompanied by an immediate change in dike quantity and orientation. The dike quantity of the Mazca Rift Zone abruptly decreases from a maximum e of 28 % in the Los Gigantes Formation to at most 3 % within the El Palmar Formation (Fig. 3c). The intrusive activity of the Mazca Rift Zone into the intermediate Carrizales Formation is difficult to determine, since this sequence is largely missing due to landsliding. Following the Carrizales sector collapse, two additional trends of dikes and fractures formed concurrently to the moderately ongoing north–south

dike intrusion. Near the Carrizales unconformity, one of these new trends is sub-parallel to the scarp (Profiles C-F). Profile C comprises 90 measurements of dikes (18) and fractures (72), showing trends to N015° and to N110° (Fig. 5). In profile C, the Mazca rift axis no longer prevails in the El Palmar Formation. The bulk intrusive activity of the Mazca Rift Zone was thus earlier than the Carrizales collapse.

The number of fractures increases significantly toward this unconformity in profiles C, D, E, and F. The mean fracture directions are N110° (profile C), N30° and N175° (profile D), N130° (profile E) and N170° (profile F). Profile D west of the unconformity along the road cut between 'Mazca' and 'Degollada de Cherfe' also shows a general north–south (N170°) dike arrangement of the Mazca Rift Zone. In total, a locally bimodal arrangement is shown by the structural data near the unconformities (Profiles C-D, Fig. 5), moreover, thin sills (< 30cm) are common along profile D (Fig. 6). Due to the systematic variance of fractures near an unconformity, the brittle deformation is likely related to sector failure rather than to rifting. Marinoni and Gudmundsson (2000) analyzed the same road cut (our profile D) and also found a general northeast–southwest extension. Moreover, dikes younger than the majority of Mazca Rift dikes have orientations very much resembling those of the fractures (Fig. 5). The post-Carrizales collapse maximum horizontal extensional strain measured by concentric dikes was only 5 % near Mazca.

The north–south dikes maintain their vertical dip away from the main intrusive axis of the Mazca rift zone, but decrease in quantity and crosscut, and are crosscut by, dikes of the accompanying northwest–southeast rift. In the Los Gigantes formation, profile E summarizes the data in the distal part of two main rift zones of Teno, with intersecting trends of the (here minor developed) Mazca rift and the northwest–southeast directed dikes.

2) Teno Bajo Rift Zone: This northwest–southeast trend dissects the succession by hundreds of dikes, presumably jointly responsible for the northwest-elongated morphological shape of Teno. The basaltic dikes are generally thinner than 1 m, whereas more evolved trachyandesitic to phonolitic dikes (mostly outcropping near the northern shoreline) reach more than 6 m, multiple dikes more than 12 m in width. The dike direction did not change significantly following the Los Gigantes collapse. However, broad outcrops of the Teno Bajo Rift Zone are limited to northwestern Teno Alto and to the area north of the village Los Carrizales. They have since became covered or obscured by younger volcanic episodes. Both unconformities result in a sudden discontinuity of the northwest–southeast dike quantity. Intrusion was continuing, with pronounced dike emplacement in the Carrizales Formation (Fig. 7).

Following the Carrizales collapse and the El Palmar Formation, intruding dikes crosscut the pre-collapse dikes of the Teno Bajo Rift Zone at an acute angle. These reconfigured dikes may imply that the structural axis rotated slightly (10-30°) after sector collapse(s) (Fig. 7). Profile F summarizes trends of dikes oriented generally N125°. From the sum of

96 dikes, 71 dikes with an average $T = 0.8$ m show a northeast–southwest extension of about $\partial L = 57$ m. An extensional strain for 21 scarp-circumscribing dikes that intruded the Carrizales Formation of $\partial L = 25$ m in direction ENE-WSW is computed. The El Palmar Formation is intruded by only a small number of northwest–southeast dikes of the Teno Bajo Rift Zone (profile F). Hence, the activity of the Teno Bajo Rift decreased in this region, whereas the amount of concentric dike trends increases (Fig. 7). Concentric dikes are slightly curved and/or arranged in an en-echelon fashion close to the weakened unconformity. Towards the northern shoreline, the quantity of dikes that circumscribes the scarp of the sector-collapses decreases (compare profile G), while the N130° Teno Bajo Rift trend prevails (profile H). Moreover, dikes in the large valley of El Palmar are also generally oriented comparable to the Teno Bajo Rift Zone, suggesting an extension directed northeast–southwest, there still existing after the bulk of the El Palmar Formation had been emplaced.

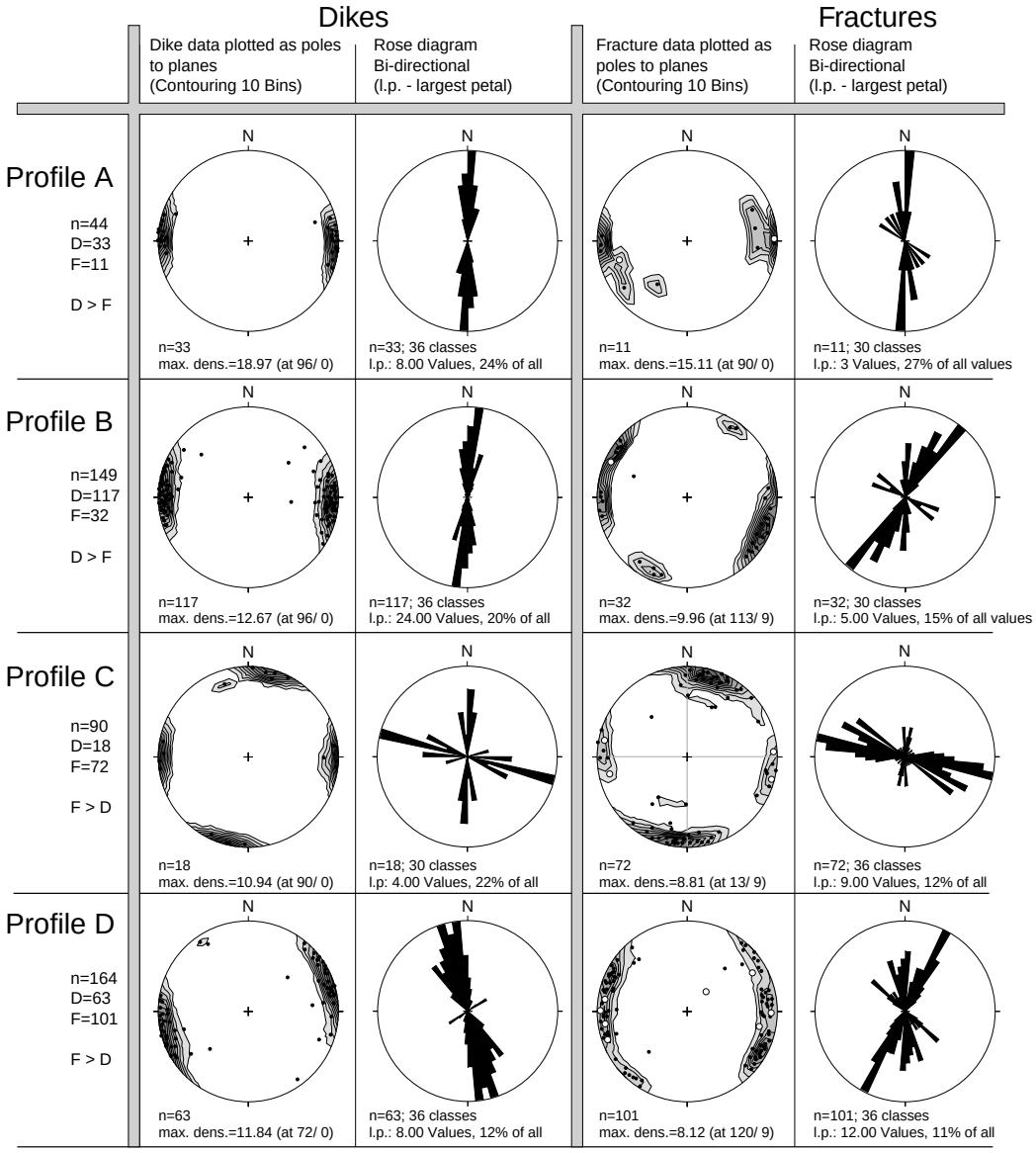

Figure 5 *(this page and previous page): Schmidt's projections, rose and contour diagrams for dikes and fractures in 9 profiles through Teno massif indicated as A - I (see Fig. 3 d). n= number of measurements, D=dikes, F=faults (white circles) and fractures (black dots).*

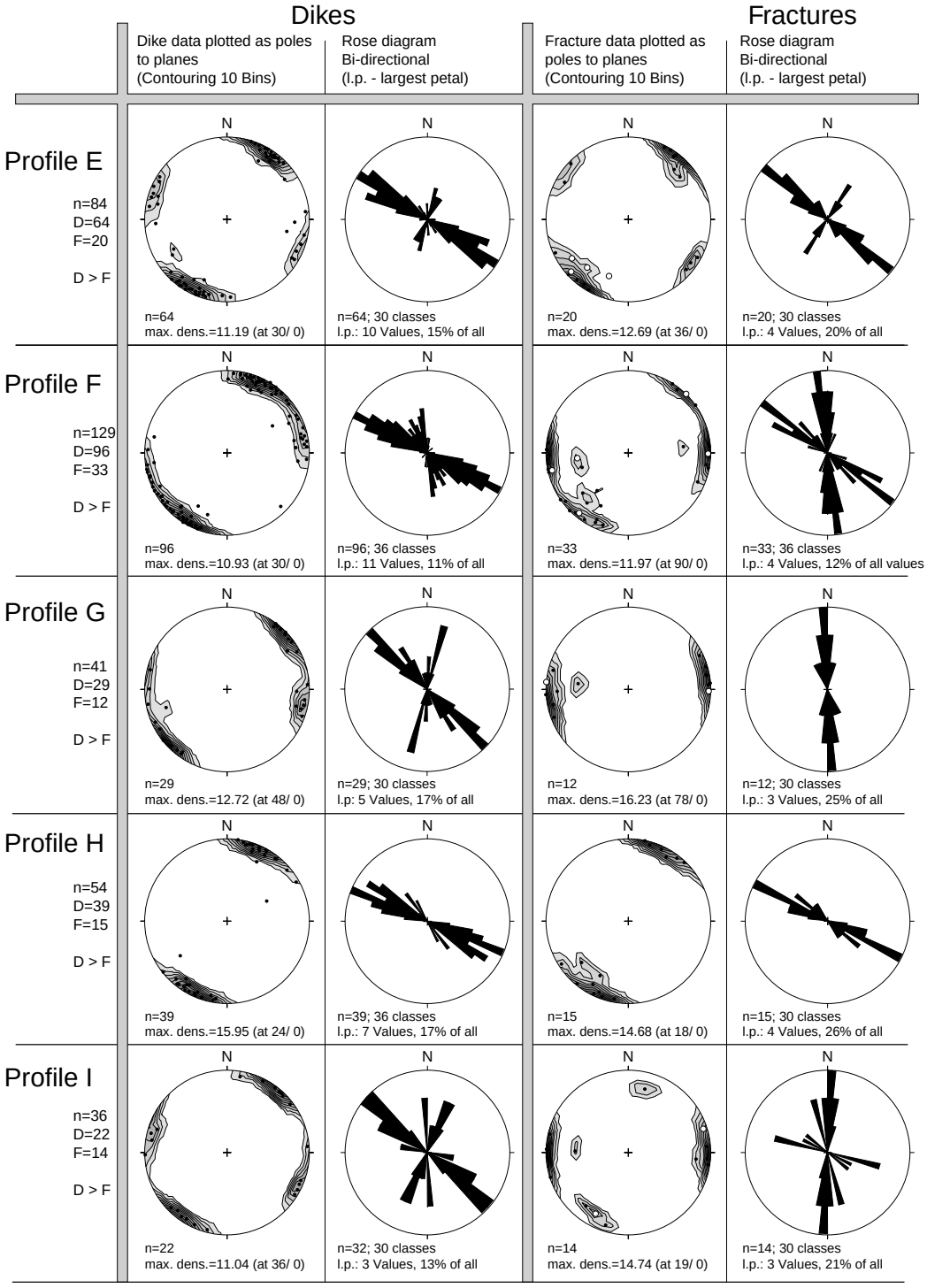

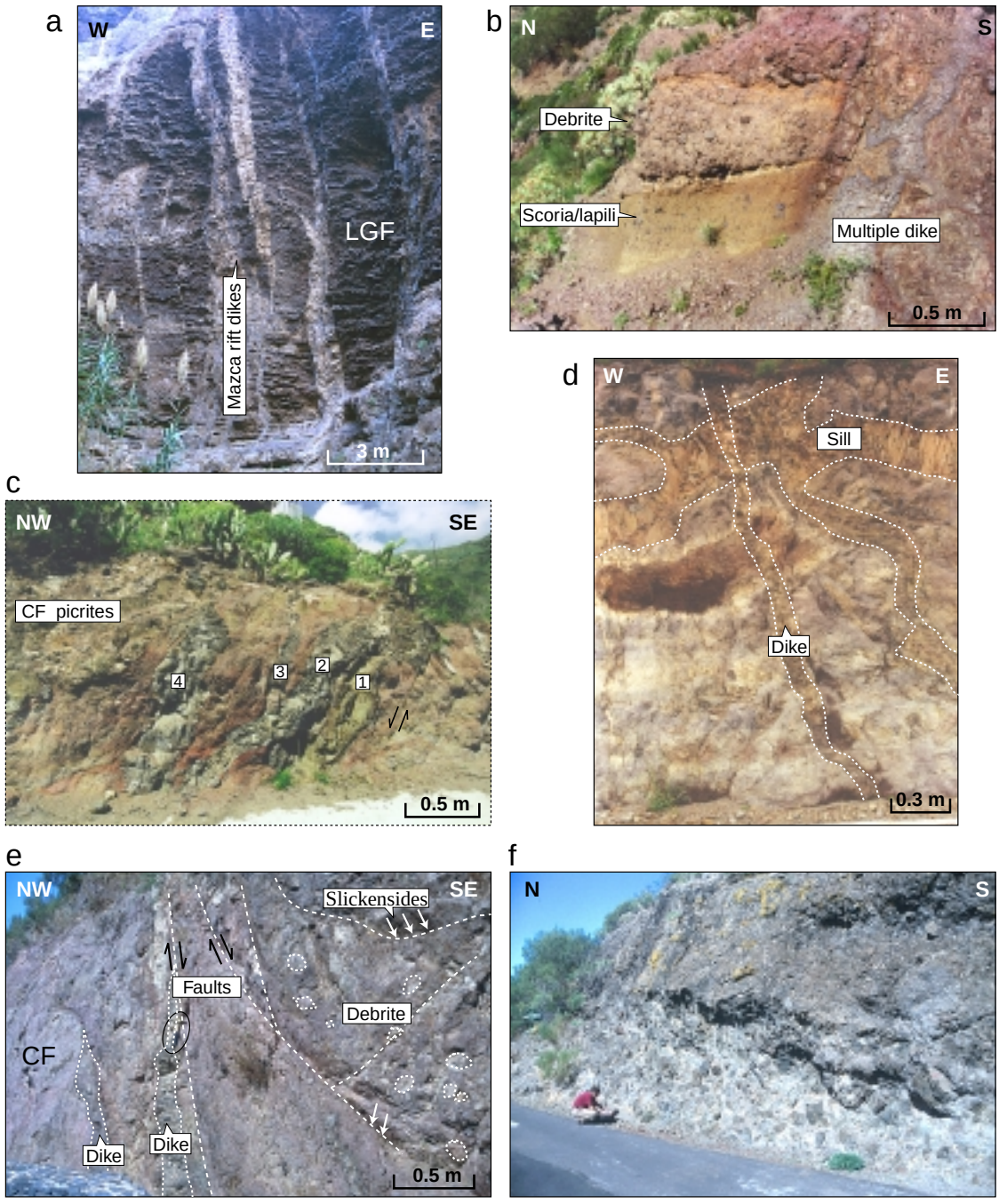

Fig. 6: ***a*** *Dark, very thin discontinuous pahoehoe lavas of the Los Gigantes Formation cut by light-colored dikes (Valley of Mazca, 220m asl.).* ***b*** *Debrite and scoria/lapilli deposits, defining the Los Gigantes collapse unconformity, intruded by dikes (0.5 km south of the village of Los Carrizales).* ***c*** *Picrites of the Carrizales Formation cut by four dikes of the Mazca rift zone. Locality along road profile D.* ***d*** *Dikes grading into columnar sills cut by younger dike in Carrizales Formation. Along road Mazca–Los Carrizales.* ***e*** *Fault zone displacing Carrizales debrites down to the NE (sector creep). Locality is east of Los Carrizales.* ***f*** *Debrites of Carrizales scarp, 30° dip to NE. Outcrop 0.5 km north of Mazca. [Los Gigantes Formation = LGF, Carrizales Formation = CF].*

The fracture belt(s)

The spacing of fractures along individual profiles is generally inhomogeneous. Most profiles radially away from landslide unconformities show a decrease in fracture quantity. A characteristic 100 m traverse unit of profile A could not reveal significant fracturing. In contrast, a 100 m unit of profile C, D, or eastern profile B exposes displacing fracture quantities ranging on average from 20 (B) to 50 (C) fractures. Profile-parallel fractures may have been underestimated, however.

Since fracturing within the rift zones is negligible at distance from the scarps, rifting as a main cause for fracturing seems unlikely (profile A and profile H). Moreover, fracturing increases with decreasing distance from the unconformities and thus reflects the large structural influence of the unstable northern flank of Teno. In close-up, the fracture quantity increases from west toward the first unconformity (Los Gigantes collapse), then slightly decreases, and strongly increases again towards the second unconformity formed by the Carrizales collapse. In the El Palmar Formation, fracture spacing is large again. Sorting out the trends of the rift zones, the orientation of the fractures of Profiles B, C, D, E, F and G show two main trends: concentric and diffuse-radial relative to the unconformity(-ies). This fracture belt with *bimodal* orientations resembles those non-rift-trends of dikes near the unconformities.

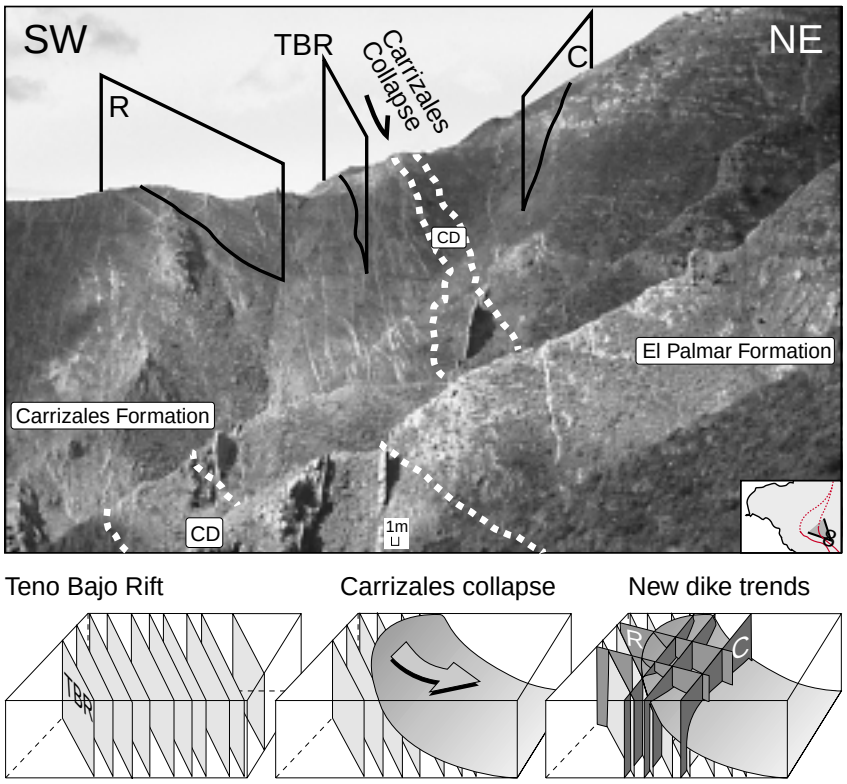

Figure 7: *Photograph taken from 'La Tabaiba' to the northwest (view insert), showing Carrizales– and El Palmar Formation, separated by Carrizales debrites (CD). Dike swarm of the Teno Bajo Rift (TBR) is clearly cut-off at the unconformity. Younger dikes intruded concentrically (C) and, to a lesser degree, radially (R) into the El Palmar Formation. The debrite of the older Los Gigantes collapse crops out ~1 km west of CD.*

Discussion

Volcano sector collapse associated with rift zone-bounded flanks is one of the most common destructive events during the evolution of volcanic oceanic islands (Siebert 1984). Giant landslides in the Canary Islands are thought to be triggered by accumulative tensional stresses, which include long-lasting stresses resulting from the progressive edifice growth/construction, cumulative stresses by dike intrusions, plus ephemeral stresses such as local seismicity (Carracedo 1994).

In Teno, a Miocene composite shield volcano in northwestern Tenerife, three successive formations are separated by landslide unconformities, indicating episodically alternating constructive and destructive evolutionary stages. The rapidity of these constructive and destructive events is remarkable, including at least two giant landslides and subsequent huge scar replenishments, all probably within less than 0.5 Ma (age data of Thirlwall et al. 2000; v.d. Bogaard, unpublished data). The northern and southern regions of Teno were under different extensional stress fields, being east–west in southern and northeast–southwest in central and northern Teno. There is no evidence for regional tectonic influences to have affected the entire Teno shield. The tensional stresses are constrained by two main rift zones; a (minor) third northeast–southwest rift zone may have been active as a local tension consequence of the compression induced by dilation of the two main rift zones. Dike emplacement rates along the rift zones decreased with time, showing the main tensional stress to have acted prior the recurrent lateral collapse.

The establishment and orientation of a fractured belt flanking the sector collapse-related paleo-scarps on Teno shows no structural relationship to preceding rift zone positions and dike directions. Such fracture zones may be the combined result of localized fault zones with a set of associated shear fractures formed by a progressive creeping sector, followed by rapid decompression of initially underlying parts during sector collapse. Along the profiles, the quantity of faults and fractures opposed to the quantity of dikes varies strongly and thus allows defining the site of maximum brittle deformation (profiles C, D) to have been located between the villages of Mazca and Los Carrizales. Here, moreover, numerous thin sills intruded into the Carrizales Formation beneath the unconformity (Fig. 6). Some sills are strongly fractured, others not, indicating intrusive activity prior and subsequent to the Carrizales collapse, possibly further weakening or lubricating the décollement.

The Carrizales Formation lavas, in particular, are increasingly fractured with decreasing distance to the second unconformity. The concentric and subordinate radial structural systems delineating the scarp are in part similar to configurations known from structural doming. In the landslide case of Teno, however, the concentric trend clearly prevails. Such a horseshoe-shaped structural pattern of dikes and fractures provides a clue to the hidden unstable flank and/or paleo-scarp location. In northeastern and northwestern

Teno, the Los Gigantes and Carrizales sector collapse scarps are largely covered or eroded by smaller landslides and thus difficult to define. However, some of the dike and fracture trends are apparently semi-concentric, suggesting the continuation of the obscured unconformities to be located nearby (Figs. 3 and 5). Based on the structural pattern around the rim of ancient headwalls in Teno, we suggest that if dikes and fractures on volcano flanks do not fit the general tectonic and/or rift zone pattern, the nearby site of an ancient sector collapse or creeping flank should be considered.

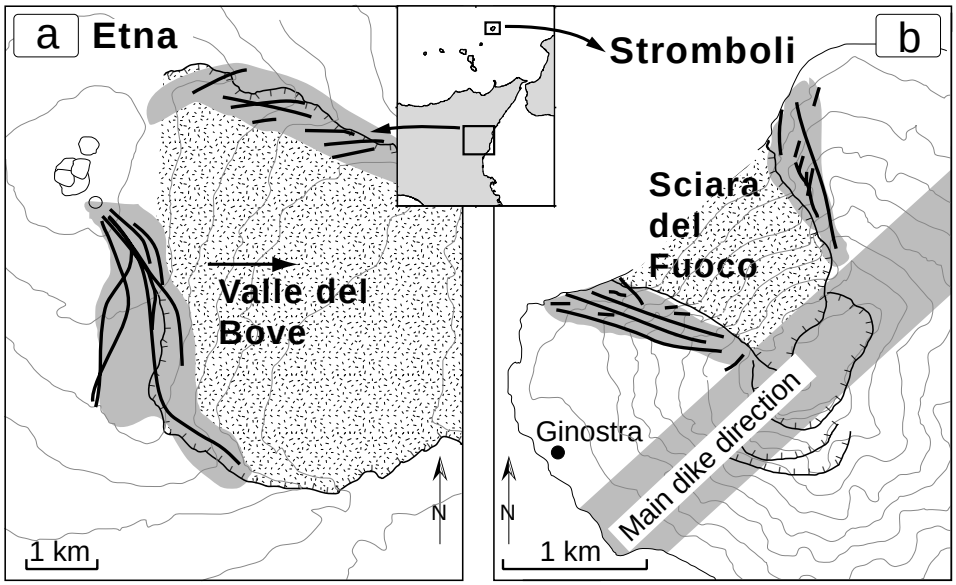

Figure 8: ***a*** *Map showing the traces of dikes emplaced on the upper southeastern flank of Etna between 1978 and 1991 as inferred from deformation measurements. Modified after Ferrari et al. (1991) and McGuire et al. (1997).* ***b*** *The Sciara del Fuoco depression is related to multiple sector collapses (after Tibaldi 2001). Dike swarms of Neostromboli material on both sides of the Sciara indicate that zones of weakness already developed during that period, probably heralding the collapse.*

Fiske and Jackson (1972) showed that the orientation and evolution of a dike swarm depends upon near-surface stress fields; hence stress field changes due to volcano flank instability may adjust their orientation. This relationship has been demonstrated for the lateral failure of Valle del Bove on Etna (McGuire et al. 1990) and Sciara del Fuoco on Stromboli (Tibaldi 2001), illustrating dike re-orientation, with the overall elongation of the swarm approximately following the rim of the headwall (Fig. 8). In Teno, new dike directions were established close to the unconformities, indicating a local change of the paleo-stress field at the time of dike emplacement. Recurrent sector collapse events at Stromboli Volcano took place whenever the scarp-replenishing sequence reached an almost similar height and volume (Tibaldi 2001). In Teno, the outline of the first collapse largely encircles the younger scarp in plan view; thus the first collapse was the largest, a structural relationship similar to that on Stromboli (Tibaldi 2001). When the accumulat-

ing mass of scarp-replenishments reaches a critical threshold, the edifice could collapse solely under its own load (cf. Voight and Elsworth 1997). Presumably, the intensely fractured zone surrounding the paleo-scarp in Teno underlies the former décollement also at depth, and mechanically influenced the edifice stability when reloaded by younger formations. A similar zone of weakness could have been involved in recurrent sector failures of Stromboli. The semi-concentric dike orientations in Teno reflect an extensional stress close to the scarps, most pronounced after infill/replenishment of the depression (Fig. 9). The semi-concentric dike orientation indicates lateral creeping of the replenishing sequence. The most vulnerable surface for this detachment is assumed to be the destabilized and fractured neighborhood of the earlier sector collapse footwall. Moreover, the influence of the weak zone in Teno may have become amplified by alteration, resulting in a reduction in confined and unconfined rock strength, cohesion, friction, and unit weight (Hürlimann et al. 1999; Watters et al. 2000). The concentric direction of younger dikes may thus well be a response of recurrent sector creep, and -once established- increases the stress acting on the encircled flank.

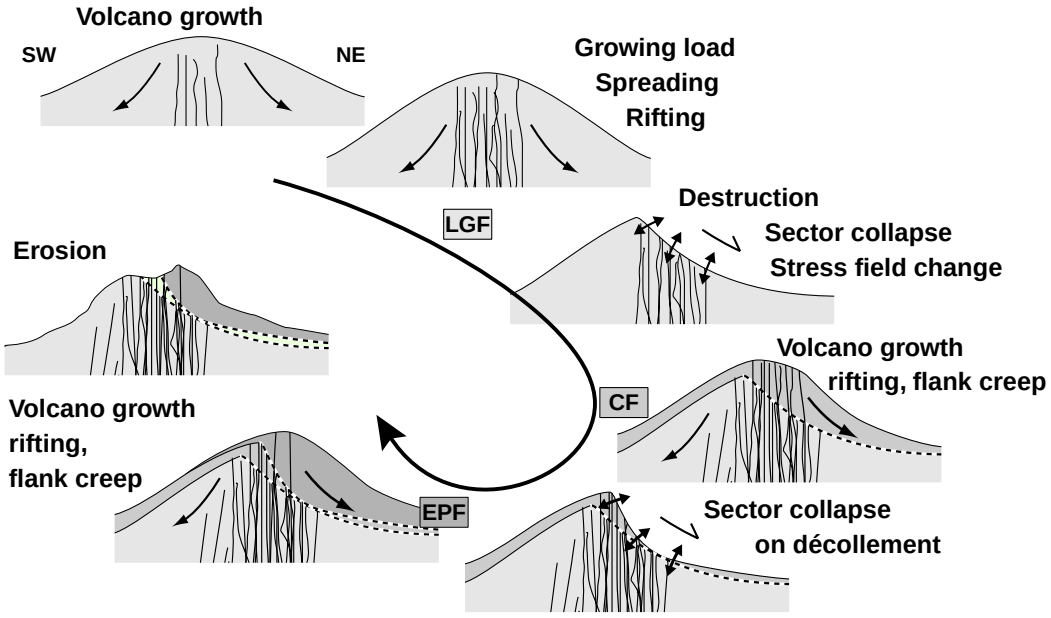

Figure 9: *Cycle of volcano construction and destruction. The growing load of the volcano causes gravitational spreading, expansion and focuses rifting. When the stability threshold is exceeded, the flank fails and collapses into the sea. This mass wasting is often accompanied by a change in stress field orientation, decompression of the magmatic system and explosion. Subsequent scarp-replenishment emplaced on top of the earlier debrites and the structurally weakened footwall. The increasing load gradually enhances flank creep and dike reorientation. The stability is again surpassed and recurrent sector collapse occurs, recycling the former décollement vicinity. This cycle may be repeated several times, or stops if magmatic activity and loading decline. [Los Gigantes Formation = LGF, Carrizales Formation = CF, El Palmar Formation = EPF].*

The Carrizales collapse scarp was replenished by lavas of the El Palmar Formation that reached a thickness of > 700 m. Although this replenishment was voluminous, it did not fail in a third giant NNW-directed flank collapse. Our dike data imply that the highest eruption rates occurred prior to the Carrizales collapse. The northwestern flank of the El Palmar Formation was initially creeping, and then intrusive activity (and also eruptions?) largely stopped. Conceivably, the load was not sufficiently high to cause failure, while intrusions and accompanied pressure variances could no more lubricate the weak zone beneath. The subaerial structure of the Teno edifice was henceforth principally stable, the stability being enhanced by a decrease in eruption rates.

However, the destructive history of a volcanic island may include three, four (e.g. Stromboli) or possibly more recurrent sector failures along the same direction, if high eruption and intrusion rates continue (Fig. 9).

Conclusion

Geometrically similar giant landslides took place in the northern part of the Miocene Teno shield volcano complex on Tenerife, defining three unconformity-bounded formations (LGF, CF, EPF). Two main rift zones indicate generally contemporaneous extension being northeast–southwest in northern and east–west in southern Teno, most of those dikes emplaced prior to the Carrizales flank failure.

Recurrent landslide mass transfer caused intense fracturing in the normal fault footwall, shown as a girdle of fractures that delineates the landslide scarp. Subsequently, younger lavas of the replenishment phase were largely positioned on a structurally weak plane. The volcano sector situated on such a potential décollement is most susceptible to become the site of future flank collapses or flank creep. Recurrent episodes of volcano construction and destruction are escorted by a change of the direction of dikes in Teno, reorganizing from narrow rift zones to semi-concentric dike arrangements encircling the paleo-scarps. The recurrent volcano landslides largely changed the structural configuration and thus the subsequent evolution of the volcano.

Acknowledgements: We thank Pepe Navarro for discussions and introducing us into the geological magnificence of Tenerife. Thanks to A. Belousov for comments and suggestions in field. This paper benefited from very constructive reviews of L. Marinoni, A. Gudmundsson and C. Stillman. The paper is part of the Ph.D. thesis of TRW. This project was supported by the Deutsche Forschungsgemeinschaft (DFG grant Schm 250/77-1), the graduate school "Dynamics of Global Cycles" (DFG grant Schm 250-49) and the Land Schleswig Holstein.

References

Ablay GJ, Hürlimann M (2000) Evolution of north flank of Tenerife by recurrent giant landslide processes. J Volcanol Geotherm Res 103: 135-159.

Ancochea E, Fúster JM, Ibarrola E, Cendrero A, Coello J, Hernan F, Cantagrel JM, Jamond C (1990) Volcanic evolution of the island of Tenerife (Canary Islands) in the light of new K-Ar data. J Volcanol Geotherm Res 44: 231-249.

Anderson EM (1937) Cone sheets and ring dykes; the dynamical explanation. Bull Volcanol 1: 35-40.

Barrera JL, Gomez JA, Bellido F (1989) Mapa geológico de España, E. 1:25000. IGME, Madrid.

Borgia A (1994) Dynamic basis of volcanic spreading. J Geophys Res 99: 17,791-17,804.

Cantagrel JM, Arnaud NO, Ancochea E, Fúster JM, Huertas MJ (1999) Repeated debris avalanches on Tenerife and genesis of Las Cañadas caldera wall (Canary Islands). Geology 27: 739-742.

Carracedo JC (1994) The Canary Islands: An example of structural control on the growth of large oceanic-island volcanoes. J Volcanol Geotherm Res 60: 225-241.

Carracedo JC (1996) Morphological and structural evolution of the western Canary Islands: hotspot induced three-armed rifts or regional tectonic trends? J Volcanol Geotherm Res 72: 151-162.

Day SJ, Carracedo JC, Guillou H, Gravestock P (1999) Recent structural evolution of the Cumbre Vieja volcano, La Palma, Canary Islands: volcanic rift zone reconfiguration as a precursor to volcano flank instability? J Volcanol Geotherm Res 94: 135-167.

Féraud G, Giannerini G, Campredon R, Stillman CJ (1985) Geochronology of some Canarian dyke swarms. Contribution to the volcano-tectonic evolution of the archipelago. J Volcanol Geotherm Res 25: 29-52.

Ferrari L, Garduño V-H, Neri M (1991) I dicchi della Valle del Bove, Etna: un metodo per stimare le dilatazioni di un apparato vulcanico. Mem Soc Geol It 47: 495-508.

Fiske RS, Jackson ED (1972) Orientation and growth of Hawaiian volcanic rifts: the effect of regional structure and gravitational stress. Proc R Soc London 329: 299-320.

Hürlimann M, Ledema A, Martí J (1999) Conditions favouring catastrophic landslides on Tenerife (Canary Islands). Terra Nova 11: 106-111.

Krastel S, Schmincke H-U, Jacobs CL, Rihm R, La Bas TP, Alibés B (2001) Submarine landslides around the Canary Islands. J Geophys Res 106: 3977-3997.

Marinoni LB (2001) Crustal extension from exposed sheet intrusions: review and method proposal. J Volcanol Geotherm Res 107: 27-46.

Marinoni LB, Gudmundsson A (2000) Dykes, faults and palaeostresses in the Teno and Anaga massifs of Tenerife (Canary Islands). J Volcanol Geotherm Res 103: 83-103.

Martí J, Hürlimann M, Ablay GJ, Gudmundsson A (1997) Vertical and lateral collapses on Tenerife (Canary Islands) and other volcanic ocean islands. Geology 25: 879-882.

McFarlane DJ, Ridley WI (1968) An interpretation of gravity data for Tenerife, Canary Islands. Earth Planet Sci Lett 4: 481-486.

McGuire WJ, Pullen AD, Saunders SJ (1990) Recent dyke-induced large-scale block movement at Mount Etna and potential slope failure. Nature 343: 357-359.

McGuire WJ, Stewart IS, Saunders SJ (1997) Intra-volcanic rifting at Mount Etna in the context of regional tectonics. Acta Vulcanol 9: 147-156.

Navarro JM, Coello J (1989) Depressions originated by landslide processes in Tenerife. ESF Meeting on Canarian Volcanism 159-152.

Navarro JM, Farrujia I (1989) Plan Hidrológico Insular de Tenerife. Zonificación hidrogeológía, aspectos geológicos e hidrogeológicos. Cabildo Insular de Tenerife 145 pp.

Rodríguez-Losada J A, Martinez-Frias J, Bustillo M A, Delgado A, Hernandez-Pacheco, A & de la Fuente Krauss J V (2000) The hydrothermally alterated ankaramite basalts of Punta Poyata (Tenerife, Canary Islands). J Volcanol Geotherm Res 103: 367-376.

Schmincke H-U (1968) Faulting versus erosion and the reconstruction of the mid-Miocene shield volcano of Gran Canaria. Geol Mitt 8: 23-50.

Schmincke H-U, Navarro JM, Sumita M (1999) A giant blast associated with flank collapse of the Cañadas Volcano (Tenerife, Canary Islands) 0.18 M.y. ago. EUG 10, Terra Nostra - J Conf Abs 4: 753.

Siebert L (1984) Large volcanic debris avalanches: characteristics of source areas, deposits and associated eruptions. J Volcanol Geotherm Res 22: 163-197.

Stillman CJ (1987) A Canary Islands dyke swarm: implications for the formation of oceanic islands by extensional fissural volcanism. In: Halls HC, Fahrig WJ (eds), Mafic Dyke Swarms. Geol Assoc Canada Spec Pap 34: 243-255.

Teide Group (1997) Morphometric interpretation of the northwest and southeast slopes of Tenerife, Canary Islands. J Geophys Res 102: 487-498.

Thirlwall MF, Singer BS, Marriner GF (2000) 39Ar-40Ar ages and geochemistry of the basaltic shield stage of Tenerife, Canary Islands, Spain. J Volcanol Geotherm Res 103: 247-297.

Tibaldi A (2001) Multiple sector collapses at Stromboli Volcano, Italy: How they work. Bull Volcanol 63: 112-125.

Voight B, Elsworth D (1997) Failure of volcano slopes. Geotechnique 47: 1-31.

Watters RJ, Zimbelman DR, Bowman SD, Crowley JK (2000) Rock mass strength assessment and significance to edifice stability, Mount Rainier and Mount Hood, Cascade Range volcanoes. Pure Appl Geophys 157: 957-976.

Watts AB, Masson DG (2001) New sonar evidence for recent catastrophic collapses of the north flank of Tenerife, Canary Islands. Bull Volcanol 63: 8-19.

Walker GPL (1992) Coherent intrusion complexes in large basaltic volcanoes - a new structural model. J Volcanol Geotherm Res 50: 41-54.

Part II: Volcano flank instability and dike intrusions

Chapter 5

Rift architecture in volcanoes

Rift architecture in volcanoes: from single rift to triaxial rifts

T.R. Walter, V.R. Troll, A. Belousov & H.-U. Schmincke
GEOMAR, Dept. of Volcanology, Wischhofstrasse 1-3, D- 4148 Kiel, Germany

Abstract. Creeping flanks of ocean island volcanoes are generally thought to be triggered and accompanied by dike intrusion within axial rift zones. The relationship between flank-creeping and intrusive rift formation remains poorly understood, however. In Anaga, the northeastern, deeply eroded shield volcano of Tenerife (Canary Islands), we identified three stages of rift-migration. A single rift zone dominated the early growth of the edifice. Later faulting resulted in creep of the northern flank and dike reorientation. A curved biaxial dike-swarm, located around the northern creeping sector, developed gradually, and a still younger third rift-arm formed to the south. All three axes nucleate in a somewhat diffuse center. To better understand the mechanisms of dike intrusions and dike reconfiguration with respect to creeping sectors of an edifice, we carried out physical models using ridges of gelatin and colored water injected from below. The gelatin ridge was positioned partially on a lubricated sector and was thus allowed to locally creep due to its own gravitational load. Injection of the fluid caused fractures to propagate in various directions, relative to (1) the geometric position of the creeping flank, (2) the edifice morphology, (3) the center of injection and its eccentricity relative to the gelatin edifice. We suggest that the structure of a single rift volcano (e.g. Anaga) reconfigures to a biaxial or triaxial rift when one sector starts to creep. The location of flank failure is, therefore, situated between these intrusive axes, as dilation of the basal detachment surface is at a maximum in-between.

Introduction

Dikes breach most volcanic edifices and feed fissure-eruptions when reaching the surface. Dikes commonly group in swarms that characterize the morphological and structural evolution of many volcanoes. Their formation and configuration, however, is still a matter of debate. Magmatic dikes that commonly intrude along rift zones dominate the endogenic growth of a volcano. Only a fraction of the total number of dikes ever reaches the surface (cf. Gudmundsson et al. 1999). Their cumulative quantity is reflected in the sites of eruptions, the consistency of magmatic activity and the morphology of the volcanoes of the Canary Archipelago (Carracedo 1994). Zones of highly concentrated

dikes may cause local subsidence (Walker 1992) and facilitate or even trigger volcano collapse.

The progress of rifting: persistence or feebleness?

Many volcanoes are structurally dominated by rift zones, which may contain one, two, three or more structural axes, which may be curved or straight, possibly controlled by loading/morphological effects (Fiske and Jackson 1972). Fiske and Jackson proposed that a ridge-like topography of the rift zones is a principal factor in geometrically organizing dike intrusions. They simulated the stress field of a volcanic ridge by triangular prismatic ridges of gelatin, into which colored water was injected to form fractures that propagated mainly laterally parallel to the ridge axes (along-strike). Fiske and Jackson (1972) described the load of the ridge, to cause horizontal expansion and vertical sagging normal to the ridge elongation. This implied that the typical topography of rift zones once established causes ongoing and focused dike intrusion parallel to the ridge elongation. Recalculation of these results by Dieterich (1988) suggested that additional processes act on the more gentle slopes of natural ridges and control their across-strike slopes. According to Dieterich, continued deep-reaching faulting predominant with rifting permits dike intrusion and rift persistence in balance with hydrostatic push due to dike emplacement. Volcanic rift zones probably have a critical slope to which a ridge would evolve naturally (Fialko and Rubin 1999). Driven by its gravity, ridge-spreading could produce extensional structures in the summit region and compression at its base (Borgia et al. 1992). The presence of a low-viscosity layer within the substratum is responsible for flow away from the excess load and causes spreading (Merle and Borgia 1996). For rift zones that form nucleated structural axes, pore fluid pressures and earthquakes may accompany dike intrusions and facilitate fault slip of huge "theoretical sectors" (Iverson 1995, Elsworth and Voight 1995, 1996), leading to lateral sector collapses inbetween the rift zones. Such faulting allows future dikes to propagate along the rift axis. Shallow gravity slides or normal flank faulting, in contrast, do not favor persistent rifting (Dieterich 1988).

Since deep basal detachment planes and lubricants are present irregularly beneath the slopes of a volcanic ridge, the fault planes we consider are locally limited in width, relative to the length of the ridge. For morphological ridges where lateral creep influences only parts of the ridge flanks, we studied the stress regime and thus the arrangement of propagating dikes that differ from the dominant morphological and long-lasting along-strike direction. We focus on rift zone reconfigurations with respect to a gravitationally destabilized flank that creeps on a basal detachment surface. We present field evidence for various episodes of rifting on Anaga (Tenerife), combined with physical modeling, to better understand the complexity of diking and volcano loading in relation to the creeping of a volcano flank.

Geological setting of Anaga (Tenerife)

Dike swarms are numerous on the Canary Islands (Staudigel and Schmincke 1984, Féraud et al. 1985, Anguita and Hernan 1986, Stillman 1987, Carracedo 1994, Marinoni and Gudmundsson 2000). Rift zones define persistent structural trends of intrusive and extrusive activity, as described for five of the seven Canary Islands. Tenerife, the largest (2060 km²) and highest (3718 masl) island of the Canarian archipelago, is located ca. 300 km off the Northwest African coast. Three old shield volcanoes are situated in the three corners of Tenerife (Anaga, Teno, Roque del Conde), each representing an independent edifice with its own volcanic history (Ancochea et al. 1990). The subsequent evolution of Tenerife was structurally and morphologically characterized by a major three-armed rift system. Fractures and rift zones on Tenerife are generally arranged in symmetrical triple-patterns with angles of ca. 120° inbetween, thought to be the result of the least-effort response to vertical upward loading (cf. Luongo et al. 1991, Carracedo 1994).

Lateral failures took place repeatedly during the subaerial evolution of Tenerife; at least 5 large landslide events wiped off large parts of the island within the last 2 Ma, generally located between two structural axes of the major triaxial rift system on Tenerife (Carracedo 1994). In addition, three secondary triaxial rift zones are present on Tenerife, characterized by thousands of exposed dikes in the deeply eroded Miocene shields of Teno and Anaga (Abdel-Monem et al. 1972, Féraud et al. 1985, Ancochea et al. 1990, Walter and Schmincke 2001). The basalts of the Miocene shields were termed collectively "Old Basaltic Series" (Fúster et al. 1968), erroneously implying a correlation between the old shield stages of Tenerife. Because the shields of Tenerife formed separately, we here use the term "Anaga Shield" series ("AS") for the easternmost complex shield edifice.

The formation of Anaga began in late Miocene at about 5.7 Ma and practically terminated in the Pliocene at around 3.3 Ma (Ancochea et al. 1990), but K-Ar geochronology could be ambiguous due to moderate to strong alteration of the rocks (Rodríguez-Losada et al. 2000, Thirlwall et al. 2000). New data by Thirlwall et al. (2000) define a polygenetic evolution of the Anaga massif, with basanitic activity around 8 Ma, alkali basalt around 5.8 Ma and, again, basanitic activity at ca. 4.2 Ma ago. The stratigraphy of Anaga is based on two (poorly defined) unconformities (Carracedo 1975), dated by Ancochea et al. (1990) at ca. 4 and 7 Ma, which allow to differentiate up to three sub-series: a) The arcuate Taganana area refers to a zone considered to be part of the "Lower Anaga Shield" (LAS) and outcrops in a structural window, concave to the North, with a radius of 10 to 14 km (Araña et al. 1979, Ancochea et al. 1990, Rodríguez-Losada et al. 2000). b) The Middle AS formed by basaltic and phonolitic rocks, inclined towards the sea and strongly eroded. c) The Upper AS, morphologically different from the older units, is made of

subhorizontally capping basalt flows. All these sub-series are traversed by many dikes that form rift zones, with diverse characteristics and trends.

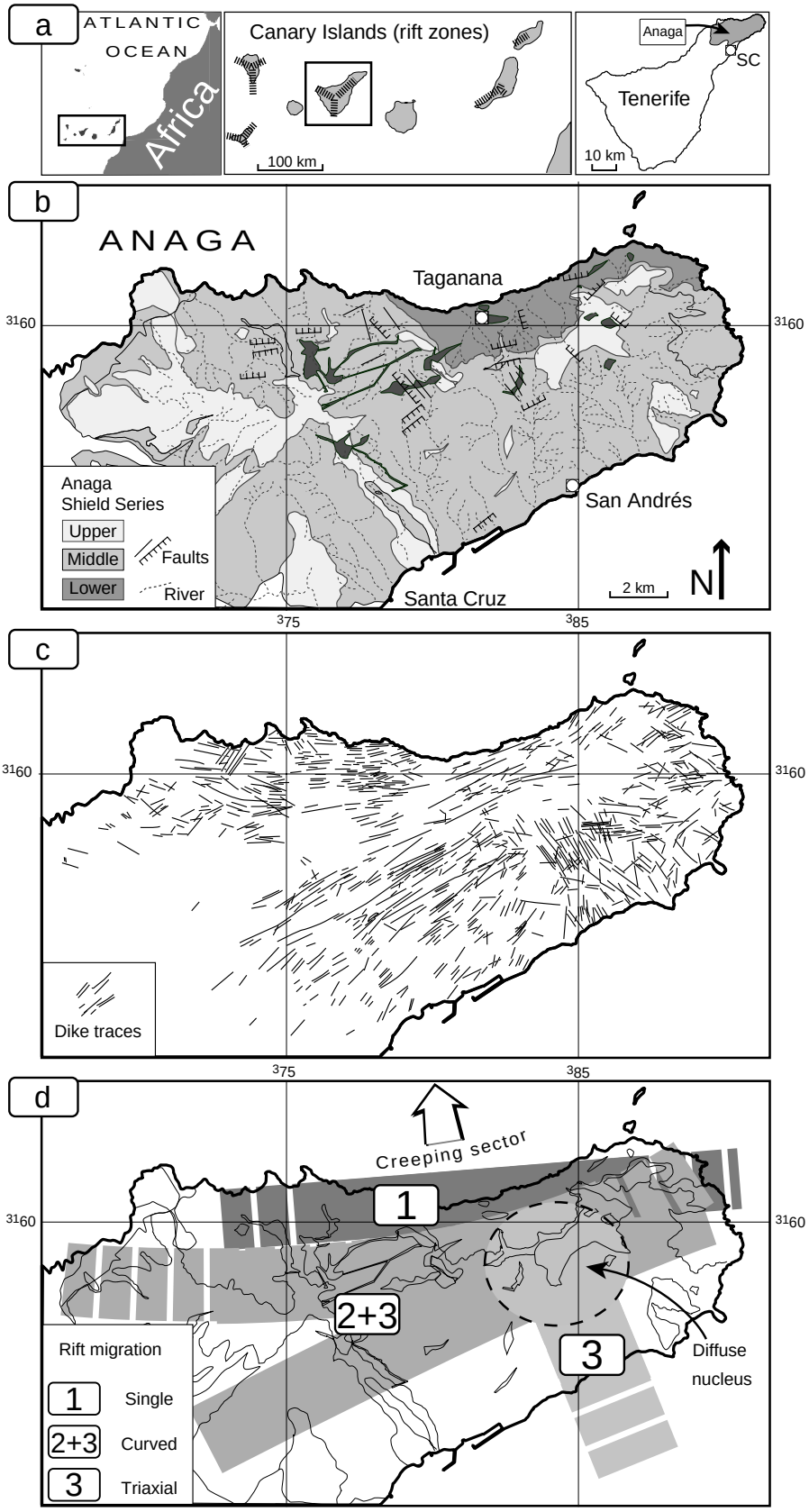

Figure 1.

a. *Location of the study area Anaga (NE Tenerife).*

b. *Simplified map of the geology of Anaga, showing three subseries of the Miocene/ Pliocene "Anaga Shield Series" and major fault traces.*

c. *Dike traces of Anaga, including data from Araña et al. (1979), Féraud et al. (1985), Hernán-dez Pacheco and Rodríguez Losada (1996).*

d. *Rift migration in Anaga. The old dike swarm of the Taganana rift zone (TRZ) intruded E-W or ENE-WSW. Later intrusive axes are curved around the Arco de Taganana (E-W to NE-SW). Based on crosscut-ting relationships of the dikes, the rift of NW-SE direction formed during the late stage of the curved rift.*

Anaga rift zones

Dike orientations were studied using the 1998 aerial photographs of Anaga (1:18.000), and the geological maps (Araña et al. 1979). Geometric parameters of dikes and faults were measured in the field. The high density of the Anaga dikes was noted by Hernández-Pacheco and Rodríguez-Losada (1996), who compared it to the coherent dike complexes on Oahu (Walker 1987). An assortment of dike swarms formed on Anaga (Navarro 1974, Féraud et al. 1985, Hernández-Pacheco and Rodríguez-Losada 1996, Marinoni and Gudmundsson 2000), with three major trends in direction NNW-SSE, NNE-SSW and E-W.

The “Arco de Taganana” is formed by ankaramites and polymict breccias, intruded by an early dense, largely basaltic dike swarm (Hernández-Pacheco and Rodríguez-Losada 1996), and alkali gabbro and syenite intrusives (Rodríguez-Losada and Martinez-Frias 1998). These early dikes define the first stage of rifting, forming the “Taganana rift zone” (TRZ), with dikes constituting more than 80% of the entire rock mass, suggesting a horizontal extension of at least 1.5 km in the direction NNW-SSE. This intrusive complex is also strongly deformed, sheared and altered. The traces of the strata are unclear due to shearing and secondary mineralization. Individual dikes are termed by local geologists as "diques fantasma" (ghost dikes) (Fig. 2). The dip of the Taganana dikes is inconsistent; faults and fragmentation locally show rotational offsets that define blocks with surface areas of more than one km², resulting in a range of dip directions of the dikes. Near the northern shoreline, dikes of the TRZ dip mostly N170°; in upper levels (>300masl) the dip line and the strike line is incoherent, ranging N180° ± 60° with dips between 90° and 40°. Near the shoreline, we found a mean strike direction of the TRZ as ENE-WSW (Fig. 1), similar to the results of Hernández-Pacheco and Rodríguez-Losada (1996).

Numerous faults and fractures indicate a general extensional stress regime (second stage), dissecting the middle AS near this northern sector of Anaga. The area of fracturing is most pronounced in the Arco de Taganana, where many faults cut the intrusions of the first stage (TRZ), which themselves are altered by secondary mineralization. Deformation of the second stage generated fault trends that commonly outline a curved sector, larger than the Arco de Taganana (Fig. 1).

Younger dike intrusions and differentiated domes were emplaced during a third stage following a period of erosion (Araña et al. 1979, Ancochea et al. 1990). These Pliocene intrusions contain generally more differentiated dikes (Hernández-Pacheco and Rodríguez-Losada 1996); trachytic and phonolitic domes intruded into the Taganana area in the early Pliocene, followed by late Pliocene intrusive activity (Carracedo 1975). The orientation of this younger rift is slightly curved from E-W to ENE-WSW to NE-SW around the embayment of Taganana (Fig. 1).

Based on two road profiles, Marinoni and Gudmundsson (2000) compiled a horizontal extension of ca. 160 m for southern Anaga in N60°, and a horizontal extension to N145° direction of ca. 190 m. We confirm their findings, but attribute the direction N60° to a third rift arm, away from the Taganana area, rather than a regional trend. For this NNW-SSE rift, major faulting by dike propagation was not demonstrated, and horizontal extension by dike intrusions was about one order of magnitude greater than that due to faulting (Marinoni and Gudmundsson 2000). Flow direction of the majority of these dikes was sub-horizontal, as indicated by vesicle elongation and imbrication.

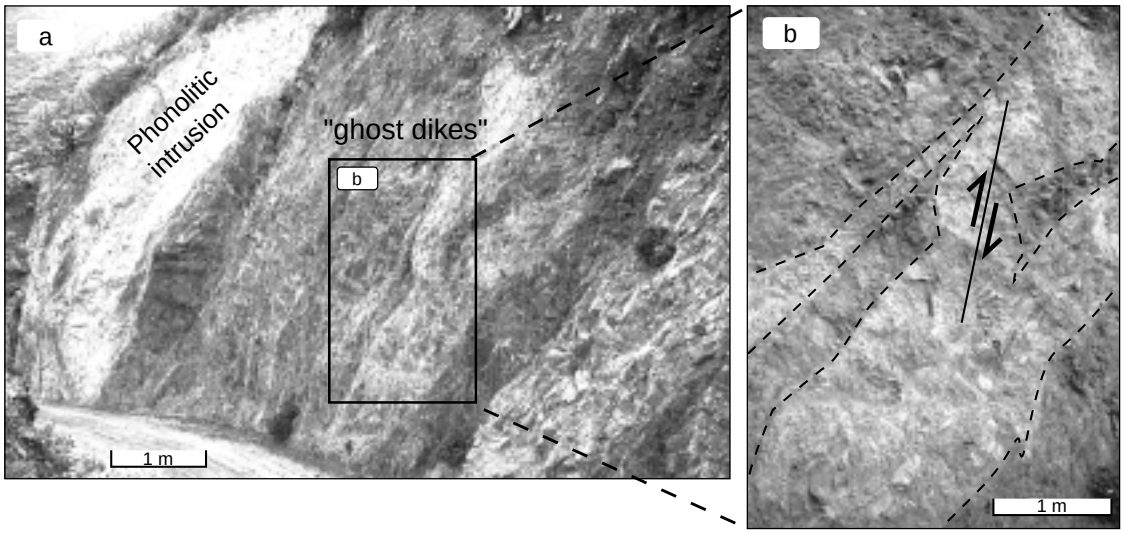

Figure 2. a *Dikes of the oldest dike-swarm of the Taganana rift zone (TRZ) with intrusive volumes reaching partially 90%. Strong shearing and fragmentation leads to structures similar to those of proximal debris avalanche deposits and to diffuse margins of "ghost dikes" (spanish "diques fantasma").* ***b*** *Enlarged inset points up strong shearing by subvertical faults.*

Taganana area - the roots of a landslide?

Rodríguez-Losada et al. (2000) considered a possible dominant extensional fault offshore to the N that influenced the "evolution of the primitive Anaga edifice". Extension faults within the northern sector of Anaga also formed horst and graben structures around the Taganana area and cut earlier dikes, whereas younger dikes intruded into such faults (Fig. 3). Old dikes of the TRZ are strongly sheared and tilted; younger dikes of the middle Anaga Shield Series, especially within the Taganana embayment, are less faulted, and the youngest intrusions are largely intact.

Many of the old dikes were sheared following solidification, producing secondary fractures in the dike and shearing near their (chilled) marginal facies. Some dikes were partially folded by post-emplacement ductile deformation (Fig. 3), as also pointed out by Hernández-Pacheco and Rodríguez-Losada (1996). We observed host rock drag faults

essentially within the creeping northern sector, but also 2 km away from the Arco de Taganana. Many faults showed sliding planes located within a few centimeters from the chilled margin in the entire host rocks, some including slickenlines, and indicate marginal cooling followed by brittle deformation (Fig. 3b).

Secondary mineralization becomes increasingly dominant toward the embayment of Taganana, and commonly seals faults and fractures. Secondary mineralization altered the rocks, forming paragenesis of amorphous SiO_2 veins and diverse mica minerals, associated with hematite, magnetite, siderite, ilmenite and calcite. Rodríguez-Losada et al. (2000) described such an intense silicification and chloritization in Punta Poyata, western Taganana area. The main cause of alteration was hydrothermal, as revealed by the appearance of *celadonite*, suggesting a significant role of heated sea-water (Rodríguez-Losada et al. 2000). Intensity of fracturing and alteration increases in the older rocks.

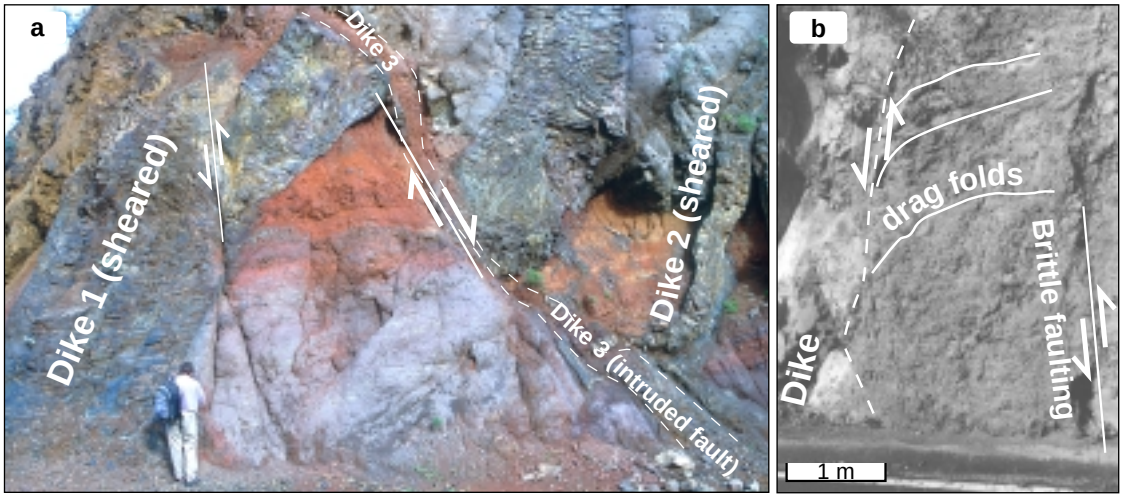

Figure 3. a *Photographs of two sheared dikes (dike 1 is 2 m thick, dike 2 is 50 cm). Faults form a local horst structure, and drag and tilt of the older dikes. Younger dike 3 is emplaced into the fault.* ***b*** *Drag folding near a thick (6 m) phonolitic dike. At a distance of 2.5 m to the right, normal faulting indicates sinistral subsidence.*

Debris avalanche deposits and redeposited breccias, characterizing cyclic slumps into a scarp, are generally inclined to the north and crop out in particular at higher levels in cliffs, as e.g. near Chinobre and Roque de Animas. The intensity of shearing and alteration of post-TRZ dikes gradually increases beneath these breccias, suggesting that the area of Taganana may represent a deep root of a creeping flank. The destabilized flank affected by décollement from the ridge finally resulted in partial removal of the overlying material by lateral failure and erosion. The creeping flank of Kilauea may be a recent analogue of such a structural relation (Hernández Pacheco and Rodríguez Losada 1996).

Physical Models

Physical modeling of complex structures greatly improved the understanding of formation and evolution of natural volcanic complexes (e.g. Komuro 1984, Marti at al. 1994, Walter and Troll 2001). To advance the understanding of processes that cause reconfiguration from single rift to multiaxial/triaxial rift zones, we carried out gelatin analogue experiments. Such models are suitable to study liquid-filled crack propagation (Fiske and Jackson 1972, Pollard et al. 1983, Maaloe 1987, Knight and Walker 1988, Dieterich 1988, McGuire and Pullen 1989, Lister and Kerr 1991, Fialko and Rubin 1999), as they portray the general geometric validity of the hydro-cracks within the highly elastic material as a reasonable analogue to natural dikes and dike-swarms. The analogue experiments are not scaled to natural conditions, because the morphology is oversteepened and the Poisson's ratio is about 0.45 (other than 0.25 in natural systems). They may, however, help to better understand the formation of rift zones in a quantitative way.

Experimental set-up and procedure

Powdered gelatin was dissolved in hot water and filled into stable ridge-shaped moulds, which are positioned on a prepared PVC base. A thin layer of sand grains was glued on a 1 m² PVC plate, except for one half-circular segment, to create a layer of high friction between the gelatin and the PVC-base in a controlling manner (Fig. 4). After hardening of the gelatin-filled moulds, we removed the mould from the cooled gelatin-ridge onto the final position on the PVC plate. Defined by the half-circular sand-free segment (radius ~5 cm), a sector of the ridge was triggered to creep to a greater degree on the basal shear plane from the ridge outward. A soap-based lubricant further reduces the basal friction between the basal PVC plate and the gelatin model. The ridges were 40 cm long with slopes of 30°, 40°, 50°, and 60° respectively and a height of 12 cm. Injection of colored water was accomplished through small holes drilled into the basal PVC-plate, using a thin needle that was connected to a syringe/pipe system.

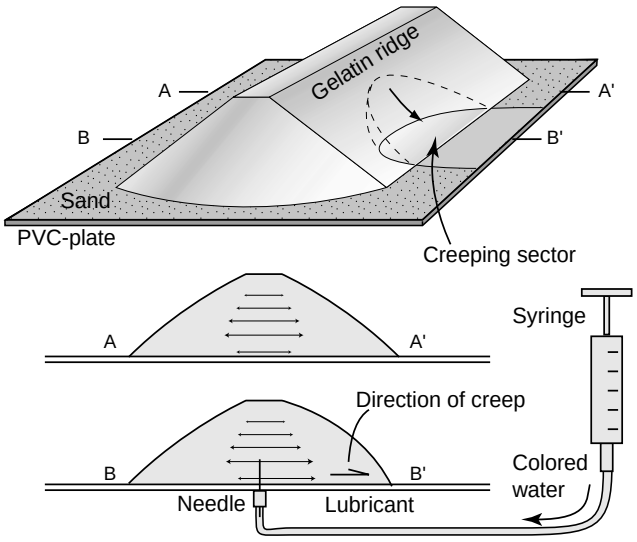

Figure 4. *Experimental set-up. The experiments described here were reproduced ca. 50 times each, yielding similar results in over 90% of experiments. The transparent gelatin and the colored injection fluid allowed to film, photograph and study propagating fractures in three dimensions.*

Experimental results

A. In accordance with previous studies of Fiske and Jackson (1972), injection into a ridge produced fractures that propagated dominantly along-strike. Injection near the edge of the ridge caused less arranged fractures, diverging away from the ridge (Fig. 5b).

B. Injection into the ridge at greater distance (>4 cm) from a creeping sector produced also generally along-striking fractures (Fig. 5c). For 80% of such experiments, the along-strike fractures were linear, and about 15% resulted in sigmoidal "dikes". Injection closer to the creeping sector (2 cm distance) with some excentricity resulted in increasingly sigmoidally curved fractures (55%), i.e. the stress field of the entire edifice became increasingly influenced by the creeping sector (Fig. 5d). Injection closer to the creeping stress field produced curved, sector-tangential fractures for >80% of the experiments (Fig. 5e).

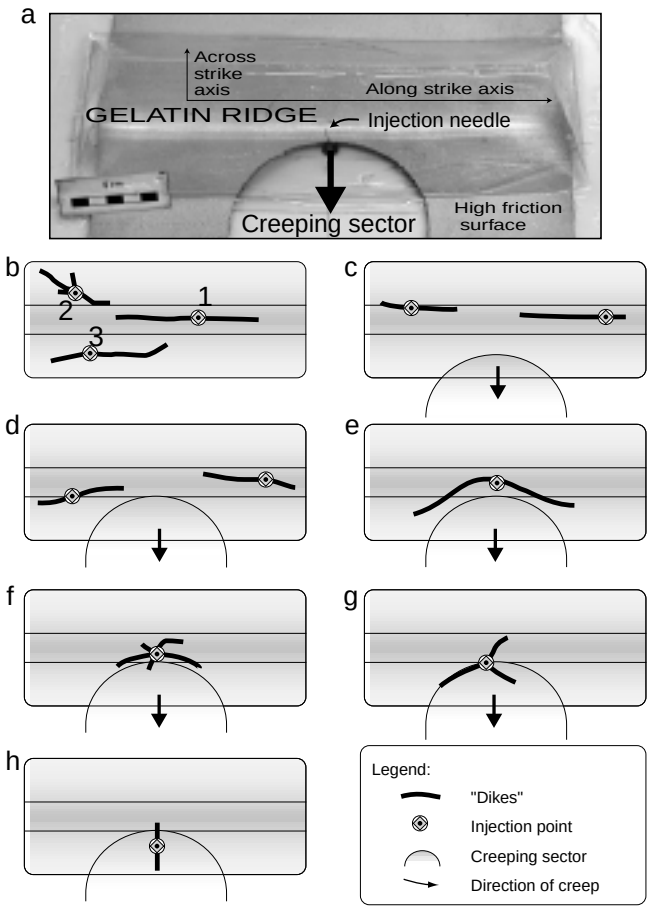

Figure 5. *Photographs and sketches (plan view) of the experiments.*

a *Photograph of unstable situation.*

b *Stable situation; injection in localities 1, 2, 3.*

c *Injection in great distance (>4 cm) from the creeping sector.*

d *Injection in distances of 2-4 cm from the creeping sector.*

e *Injection in distances of 1-2 cm from the creeping sector.*

f-g *Injection above the interface stable / unstable sector.*

h *Injection directly above the sliding surface.*

Injection very close to or directly into the area above the boundary creeping-sector / non-creeping-sector produced mostly complex initial multiple (radial) fractures, which frequently propagated on continuous fluid pressure into a dominant tangential configuration in ~40% of the experiments (Fig. 5f) or into a triaxial configuration (50%) (Fig. 5g). About 5% of these experiments resulted in a biaxial arrangement, and ca. 5% in single

rifts. Injection directly into the area above the sliding surface (i.e. into the creeping sector) resulted in ~90% of these experiments in fractures that were prependicular to the strike direction of the ridge (across-strike) (Fig. 5h). Percentages not mentioned were based on errors by minor defects/irregularities of the set-up, or were alternative situations that were not reproduced.

Discussion

Most major basaltic volcanoes evolve through eruptive fissures that are a) concentrated in dense dike swarms, and b) form the structural and morphological skeleton of a volcano in the form of rift zones. Dikes propagate, comparable to liquid-filled cracks, in pre-existing fractures and/or perpendicular to the least compressive stress. To better understand the formation and propagation of magma-filled cracks, physical and numerical models allow insight into the complexity of the mechanism(s) involved. The level of lateral propagation is defined by the level of neutral buoyancy, which lies at depths of the changing gradient in excess magma pressure (Rubin and Pollard 1987, Ryan 1987, Fialko and Rubin 1998, Lister and Kerr 1991). If the state of stress changes, propagating intrusions may change their orientation when entering from one stress field into another. The structural axis of a rift zone may even migrate laterally, as proposed for some Hawaiian dike swarms (Swanson et al. 1976).

Regional tectonism may also influence the formation and orientation of the rift zones of a volcano and its stability (cf. Lagmay et al. 2000). Regional extensional stress alignments on Tenerife are still debated with two scattered alignments younger than the Anaga massif trending NW-SE and NE-SW with perpendicular extensional stresses (Ruiz et al. 2000), resembling the stress relations in northwest Tenerife (Teno) in part (Marinoni and Gudmundsson 2000). The structural reconfiguration described here for Anaga could have been a supplementary local feature, adding on - or supported by - the regional stress. A major regional tectonic influence in the Canary Islands is elusive, however, and has yet to be documented unequivocally since the rift configuration on the western volcanic edifices does not indicate a consistent regional tectonism (Fig. 1a). The geometrical arrangement of triaxial rift zones in the Canary Islands is thus thought not to follow general structural alignments, but rather form by magma-induced vertical loading (Carracedo 1994). However, since structures related to tumescence and doming of magma chambers produce generally fissural patterns in a radial and concentric arrangement (e.g. Anderson 1936, Komuro 1984, Marti at al. 1994, Walter and Troll 2001), a stand-alone reason of vertical loading for the initiation of rift zones seems doubtful. An overpressurized shallow magma chamber, moreover, may cause detachment on a low angle basal fault while dike swarms may form (Delaney and Denlinger 1999).

Lateral displacement caused by sub-volcanic strata has been proposed for the Hawaiian shield volcanoes (Nakamura 1980, Iverson 1995, Elsworth and Voight 1996). The thickness of the proposed weak layer on Hawaii is very small (1%) compared to the volcano height (Borgia 1994), and acts as a lubrication plane on which deformation of the volcano flank is accommodated. Stratovolcanoes and relatively small stratocones also deform on such weak layers, as proposed for Mount Etna (Italy) and Mombacho (Nicaragua). The eastern flank of Mount Etna creeps on a basal detachment surface, while numerous contemporaneously dikes intruded forming two structural axes around the upper scarp of the continuing surface depression (McGuire et al. 1990, Borgia et al. 1992). The lateral failure of Mombacho volcano resulted from progressive hydrothermal weakening of the cone and consequent flank spreading (van Wyk de Vries and Francis 1997). Volcano deformation starts long before failure, and is indicated by steepening and thrusting of the lower flank and by normal faulting higher up (van Wyk de Vries and Francis 1997).

Spreading in Anaga was preferentially to the north and we propose the creeping-direction to have been influenced by a) high fluid pressures under the northern side of the Anaga shield, and b) persistent rifting and buttressing, and presumable by c) the type and the regional slope of the basement beds. Increasing fluid circulation and fluid pressure by shearing and magma intrusion may have facilitated flank creeping, and provided a progressive destabilizing feedback of the rift-type volcano. For such a destabilized rift volcano, our models indicate that new rift arms initiate by magma injection into a transitional stress field, partially controlled by a creeping flank and partially controlled by the stress field of the stable edifice. This surface-controlled structural reconfiguration is suggested as an alternative or additional model of the formation of new structural rift axes.

Conclusion

Based on field work and physical modeling we suggest that the orientation of extension in across-strike direction of a ridge-shaped edifice reorganizes when the flank stability is reduced or basal friction of a volcano is inhomogeneous, leading to reorientation of intruding dikes and rift zones. Our results suggest that, with onset of a creeping sector, an initial single rift volcano (Anaga) may reconfigurate and produce a) migrating rifts and b) new rift zones. The shape of an edifice and the position of magma injection relative to a creeping sector largely influence the formation of rift zones and the orientation of lasting dike intrusions.

Acknowledgements: Our work was financially supported by the Deutsche Forschungsgemeinschaft (Grants Schm 250/77-1 and Schm 250/72-1). VRT acknowledges a grant from the "Studienstiftung des deutschen Volkes"; AB acknowledges support by the "Alexander von Humboldt" foundation.

References

Anderson, E.M. 1936. The dynamics of the formation of cone-sheets, ring-dykes, and cauldron-subsidences. *Proc R Soc Edinburgh* 56:128-163.

Anguita, F. & Hernan, F. 1986. A propagating fracture model versus a hot-spot origin for the Canary Islands. *Earth Planet Sci Lett* 27: 11-19.

Araña, V., Carracedo, J.C., Fúster, J.M. & Garcia Cacho, L. 1979. Mapa Geologico de España E. 1:25000. *Inst. Geol. Min. España (ITGE)*, Madrid.

Abdel-Monem, M.A., Watkins, N.D. & Gast, P.W. 1972. Potassium-argon ages, volcanic stratigraphy, and geomagnetic polarity history of the Canary Islands; Tenerife, La Palma and Hierro. *Am J of Sci* 272: 805-825.

Ancochea, E., Fúster, J.M., Ibarrola, E., Cendrero, A., Hernan, F., Cantagrel, J.M. & Jamond, C. 1990. Volcanic evolution of the island of Tenerife (Canary Islands) in the light of new K-Ar data. *J Volcanol Geotherm Res* 44: 231-249.

Borgia, A., Ferrari, L. & Pasquare, G. 1992. Importance of gravitational spreading in the tectonic and volcanic evolution of Mount Etna. *Nature* 357: 231-235.

Borgia, A. 1994. Dynamic basis for volcanic spreading. *J Geophys Res* 99: 17,791-17,804.

Carracedo, J.C. 1975. Estudio paleomagnetico de la isla de Tenerife. Thesis, *Univ. Complutense de Madrid*, 265 p.

Carracedo, J.C. 1994. The Canary Islands; an example of structural control on the growth of large oceanic-island volcanoes. *J Volcanol Geotherm Res* 60: 225-241.

Delaney, P.T. & Denlinger, R.P. 1999. Stabilization of volcanic flanks by dike intrusion: an example from Kilauea. *Bull Volcanol* 61: 356-362.

Dieterich, J.H. 1988. Growth and persistence of Hawaiian volcanic rift zones. *J Geophys Res* 93: 4258-4270.

Elsworth, D. & Voight, B. 1995. Dike intrusion as a trigger for large earthquakes and the failure of volcano flanks. *J Geophys Res* 100: 6005-6024.

Elsworth, D. & Voight, B. 1996. Evaluation of volcano flank instability triggered by dyke intrusion. In W.J. McGuire, A.P. Jones & J. Neuberg (eds.), *Volcano instability on the Earth and other planets. Geol Soc London* 110: 45-53.

Féraud, G., Giannerini, G., Campredon, R. & Stillman, C.J. 1985. Geochronology of some Canarian dyke swarms. Contribution to the volcano-tectonic evolution of the archipelago. *J Volcanol Geotherm Res* 25: 29-52.

Fialko Y.A., & Rubin, A.M. 1998. Thermodynamics of lateral dike propagation: Implications for crustal accretion at slow spreading mid-ocean ridges. *J Geophys Res* 103: 2501-2514.

Fialko Y.A., & Rubin, A.M. 1999. What controls the along-strike slopes of volcanic rift zones? *J Geophys Res* 104: 20,007-20,020.

Fiske, R.S. & Jackson, E.D. 1972. Orientation and growth of Hawaiian volcanic rifts: the effect of regional structure and gravitational stresses. *Proc R Soc London* 329: 299-326.

Fúster, J.M., Araña, V., Brandle, J.L., Navarro, J.M., Alonso, U. & Aparicio, A. 1968. Geología y Volcanología de las Islas Canarias: Tenerife. *Inst Lucas Mallada, CSIC*, Madrid, 218 p.

Gudmundsson, A., Marinoni, L.B. & Marti, J. 1999. Injection and arrest of dykes: implications for volcanic hazards. *J Volcanol Geotherm Res* 88: 1-13.

Hernández-Pacheco, A. & Rodríguez-Losada, J.A. 1996. Geología y estructura del Arco de Taganana. *Rev Soc Geol España* 9: 169-183.

Iverson, R.M. 1995. Can magma-injection and groundwater forces cause massive landslides on Hawaiian volcanoes? *J Volcanol Geotherm Res* 66: 295-308.

Knight, M.D. & Walker, G.P.L. 1988. Magma flow directions in dikes of the Koolau Complex, Oahu, determined from magnetic fabric studies. Special section on how volcanoes work. *Am Geophys Union* 93: 4301-4319.

Komuro, H, Fujita, Y. & Kodama, K. 1984. Numerical and experimental models on the formation mechanism of collapse basins during the Green Tuff Orogenesis of Japan. *Bull Volcanol* 47: 649-666.

Lagmay A.M.F., van Wyk de Vries, B., Kerle, N. & Pyle, D.M. 2000. Volcano instability induced by strike-slip faulting. *Bull Volcanol* 62: 331-346.

Lister, J. R. & Kerr, R.C. 1991. Fluid-mechanical models of crack propagation and their application to magma transport in dykes. *J Geophys Res* 96: 10,049-10,077.

Luongo, G., Cubellis, E., Obrizzo, F. & Petrazuoli, S.M. 1991. A physical model for the origin of volcanism of the Tyrrhenian margin: the case of the Neapolitan area. *J Volcanol Geotherm Res* 48: 173-185.

Maaloe, S. 1987. The generation and shape of feeder dykes from mantle sources. *Contr Min Petrol* 96: 47-55.

Marinoni, L.B. & Gudmundsson, A. 2000. Dykes, faults and palaeostresses in the Teno and Anaga massifs of Tenerife (Canary Islands). *J Volcanol Geotherm Res* 103: 83-103.

Marti, J., Ablay, G.J., Redshaw, L.T. & Sparks, R.S. 1994. Experimental studies of collapse calderas. *J Geol Soc London* 151: 919-929.

McGuire, W.J. & Pullen, A.D. 1989. Location and orientation of eruptive fissures and feeder-dykes at Mount Etna; influence of gravitational and regional tectonic stress regimes. *J Volcanol Geotherm Res* 38: 325-344.

McGuire, W.J., Pullen, A.D. & Saunders, S.J. 1990. Recent dyke-induced large-scale block movement at Mount Etna and potential slope failure. *Nature* 343: 357-359.

Merle, O. & Borgia, A. 1996. Scaled experiments of volcanic spreading. *J Geophys Res* 101: 13,805-13,817.

Nakamura, K. 1980. Why do long rift zones develop in Hawaiian volcanoes; a possible role of thick oceanic sediments. *Bull Volcanol Soc Japan* 25: 255-269.

Navarro, J.M. 1974. La estructura geológica de Tenerife y su influencia en la hidrogeología. *Simp Int Hidrol Terrenos volcánicos*. Lanzarote, 20p.

Pollard, D.D., Delaney, P.T., Duffield, W.A., Endo, E.T. & Okamura, A.T. 1983. Surface deformation in volcanic rift zones. *Tectonophysics* 94: 541-584.

Rubin, A.M. & Pollard, D.D. 1987. Origins of blade-like dikes in volcanic rift zones. In R.W. Decker, T.L. Wright & P.H. Stauffer (eds.); *Volcanism in Hawaii. US Geol Surv*: 1449-1470.

Rodríguez-Losada, J.A. & Martinez-Frias, J. 1998. Ancient oxide- and sulphide-mineralization in the islands of Tenerife and La Gomera (Canary Archipelago, Spain). *Mineralium Deposita Letter* 33: 639-643.

Rodríguez-Losada, J.A., Martinez-Frias, J., Bustillo, M.A., Delgado, A., Hernandez-Pacheco, A. & de la Fuente Krauss, J.V. 2000. The hydrothermally alterated ankaramite basalts of Punta Poyata (Tenerife, Canary Islands). *J Volcanol Geotherm Res* 103: 367-376.

Ryan, M.P. 1987. Neutral buoyancy and the mechanical evolution of magmatic systems. In B.O. Mysen (ed.), *Magmatic Processes. Geochem Soc University Park, Pa*: 259-288.

Ruiz, C.R., García-Cacho, L., Araña, V., Luque, A.Y. & Felpeto, A. 2000. Submarine volcanism surrounding Tenerife, Canary Islands: implications for tectonic controls, and oceanic shield forming processes. *J Volcanol Geotherm Res* 103: 105-119.

Staudigel, H. & Schmincke, H.-U. 1984. The Pliocene seamount series of La Palma, Canary Islands. J Geophys Res 83: 11,195-11,215.

Stillman, C.J. 1987. A Canary Islands dyke swarm: implications for the formation of oceanic islands by extensional fissural volcanism. In: H.C. Halls, & W.J. Fahrig (eds.); *Mafic Dyke Swarms. Geol Ass Canada*, Spec Paper 33.

Swanson, D.A., Duffield, W.A. & Fiske, R.S. 1976. Displacement of the south flank of Kilauea Volcano; the result of forceful intrusion of magma into the rift zones. *US Geol Surv Prof Pap* 963: 39p.

Thirlwall, M.F., Singer, B.S. & Marriner, G.F. 2000. 39Ar - 40Ar ages and geochemistry of the basaltic shield stage of Tenerife, Canary Islands, Spain. *J Volcanol Geotherm Res* 103: 247-297.

van Wyk de Vries, B. & Francis, P.W. 1997. Catastrophic collapse at stratovolcanoes induced by gradual volcano spreading. *Nature* 387: 387-390.

Walker, G.P.L. 1987. The dike complex of Koolau Volcano, Oahu; internal structure of a Hawaiian rift zone. In R.W. Decker, T.L. Wright & P.H. Stauffer (eds.); *Volcanism in Hawaii. US Geol Surv*: 961-993.

Walker, G.P.L. 1992. Coherent intrusion complexes in large basaltic volcanoes; a new structural model. *Essays on magmas and other earth fluids; a volume in appreciation of Prof. Peter G. Harris. K. G. Cox and P. E. Baker.* Amsterdam, Netherlands, Elsevier 50: 41-54.

Walter, T.R. & Troll, V.R. 2001. Formation of caldera periphery faults: an experimental study. *Bull Volcanol* (in press.).

Walter, T.R. & Schmincke, H.-U. 2002. Rifting, recurrent landsliding and structural reorganization on Teno, NW-Tenerife, Canary Islands. *Int J Earth Sci* (subm.).

Part II: Volcano flank instability and dike intrusions

Chapter 6

Creeping – rifting – sector collapse

Creeping – rifting – sector collapse
the structural feedback on ocean island volcanoes

Thomas R. Walter[1], Valentin R. Troll[1,2], Hans-Ulrich Schmincke[1]

[1] GEOMAR, Dept. of Volcanology, Wischhofstr. 1-3, D-24148 Kiel, Germany;

[2] Dept. of Geology, University of Dublin, Trinity College, Dublin 2, Ireland;

Abstract. Large ocean island volcanoes comprise high-productive rift zones along with unstable flanks and sites of sector collapse. Gravitation is the key reason of such strained volcano flanks; the site and value of structural instability is biased by weak (substratum) layers. The influence of lubricated and therefore laterally creeping flanks for rift-migration, rift-development, and adjustment of the entire volcanic architecture was studied by analog experiments. We injected colored water from below into gelatine-cones and found systematic orientations of hydro-fractures (dikes) propagating through the "volcano". This allows inferring parameters of gravity-driven cone deformation and resulting dike directions for various basal friction conditions. By varying the setting of basal friction and by lubricating local sectors, we changed the stress field and modeled radial dike swarms, collinear rift zones and three-armed rift systems. Our data suggest that the most common dike patterns on volcanic islands may form in response to the basal creep conditions. Only one creeping volcano flank is sufficient to modify the entire structure, heralding, initiating or adjusting rift volcanism.

Our experiments help to infer the structural conditions for natural systems, as demonstrated for La Palma (western Canary Islands). The unstable and outward creeping south-western sector of La Palma resulted in essential dike reconfiguration from an initially radial swarm to well defined rift zones. This study implies that gravity-driven volcano deformation and flank-creep control the configuration and orientation of the rift zones, are thus symptomatic of the impermanence of dike swarms in general. When a critical load is reached, the distribution of a weak substratum will control the volcano architecture in a major way.

Keywords: volcano deformation, rift zones, flank creeping, dikes, sector collapse, Canary Islands

Introduction

Dikes are the common witnesses of fracture-type pathways ascending magmas produce and use when they propagate through the crust. Most volcanic eruptions start above feeder dikes, but only a small fraction of those dikes ever reaches the surface (Gudmundsson et al. 1999). Driven by high magmatic pressure, the orientation of such a

propagating magma-filled fracture strongly depends on the local stress pattern. Dike orientation is usually perpendicular to the minimum principal compressive stress, hence indicative of the stress field within a volcano (Anderson 1937). If a temporarily steady stress system dominates in a volcanic edifice, dikes may group to form swarms and rift zones (Fiske and Jackson 1972). A volcanic center is defined by nucleating rift zones, forming structurally, morphologically and genetically related axes. Rift zones are basically vertical structures formed by hundreds or thousands of parallel dikes, with individual dikes showing a large variance of dips (Walker 1999). Dikes may contribute to the endogenous growth of volcanic edifices by up to 30% (Annen et al. 2001).

The structural axis of a rift zone is not necessarily stable and can migrate laterally, as proposed for some Hawaiian dike swarms (Swanson et al. 1976). As a dike reflects the stress field, a significant change of the stress field with time may change the rifting dynamics and the position of an entire rift zone of a volcano. Rift zones form in particular within larger volcanic edifices, indicative of the importance of gravitational stresses (Walker 1987, 1992). Since large volcanoes deform under their own weight, the question arises how the volcano stress field and rift directions diverge from each other. We here focus on the dynamic interplay of rift formation, volcano deformation and its response due to weak substrata.

Volcano instability and rifting

The dominant structural phenomena on large volcanic edifices are dike swarms and the zones of structural weakness leading to sector collapse events, episodically destroying the flanks of a growing volcano. Volcano instability and rifting thus appear to be genetically related (Siebert 1984). Seamount studies show that the significance of rifting increases for larger volcanoes (Vogt and Smoot 1984).

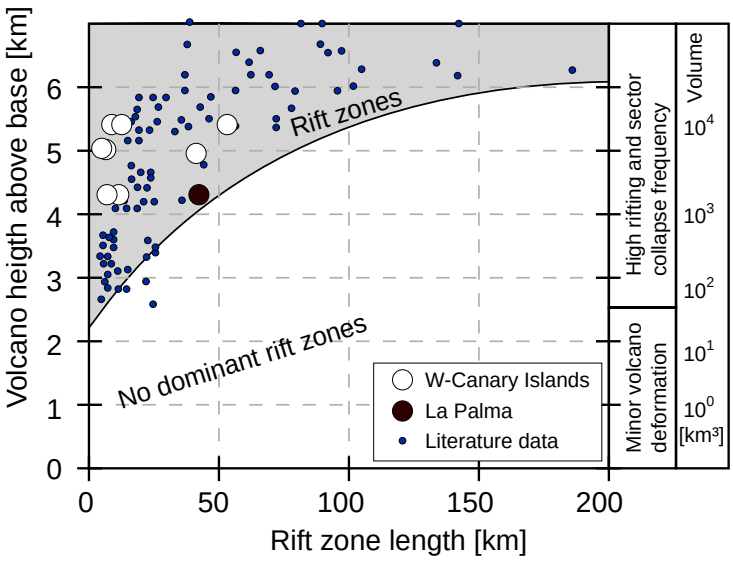

Figure 1. *Rift zone lengths (x-axis) as a function of oceanic volcano height above the base (y-axis) and estimated volume. Rift zone commonly establish and elongate on higher volcanoes (modified, after Vogt and Smoot 1984; Mitchell 2001).*

Figure 1 summarizes morphological data sets of seamounts and volcanic islands, describing the constitution of rift zones on volcanoes taller than 2.5 km (Vogt and Smoot 1984; Mitchell 2001).

The mean rift zone length can be approximated by a function of the form

$$RZ \leq 10^{\frac{3}{8}H},$$

where RZ = rift zone length, and H = volcano height above the base (Fig. 1). The length of rift zones rapidly thus increases with increasing edifice height over 3 km – but the vulnerability for landslides also increases (cf. Mitchell 2001).

The largest volcanic edifices on Earth, volcanic ocean islands, are most susceptible to rifting and structural collapses owing to their immense weight. The well-studied edifices of the Canary Islands and the Hawaiian Chain show various types of structural collapse and rift zone systems. High magmatic and hydrothermal pressures accompanying dike intrusions are thought to force the volcanoes to expand laterally and thus the flanks to creep seaward (McGuire et al. 1990; Iverson 1995; Elsworth and Voight 1995, 1996). The location of lateral collapses and sector-slip of volcanic flanks are thus frequently enclosed by two rift zones (e.g. Siebert 1984). For intrusive flank push and sector-slip along low inclined detachment surfaces, the basal shear resistance and the angle of internal friction must be very low, so that weak substrata constitute lubrication planes (cf. Iverson 1995). It remains unclear, however, at what stage of volcano evolution forceful rift zones are initiated leading to such flank-push, and how the dynamic response to changes in the stress pattern e.g. by flank creep modifies a given rift pattern.

Both, dike directions and volcano flank instability, are a function of a volcanoes' gravitational load. Given that these two processes are linked, changing one of the parameters would then alter the volcano stress field – and thus the controlling environment of the other parameter.

Gravity-driven volcano deformation

Mechanisms for volcano deformation are manifold; the main force for deformation is, however, gravity itself a function of edifice height and mass. Three types of gravity-driven volcano distortion are shown in Figure 2. Fiske and Jackson (1972) illustrated the importance of the volcano load and stress distribution for the formation of rift zones on volcanoes. Accordingly, the topography of a volcano directs the dike paths, while rifting and edifice shape are genetically linked in a dynamic feedback. The gelatine analog models of Fiske and Jackson being highly elastic and oversteepened; Dieterich (1988) recalculated the models and found that a further type of flank deformation is necessary to allow persistent dike intrusions along existing rift zones. The flanks must thus dilate laterally to overcome a plumbing effect. On Hawaii, the presence of weak substrata (e.g. deformable

ocean sediments and possibly olivine cumulates) provides widespread potential décollements (Delaney et al. 1998; Clague and Denlinger 1994; Borgia et al. 2000). The southern Kilauea flank appears to slide on basal faults thus opening the space for (feeder) dikes of the Kilauea rift system (Dieterich 1988). Third, the presence of a low strength or quasi-viscous layer essentially drives the structural arrangement of a deforming volcano (Borgia 1994; Merle and Borgia 1996). Substrates upon which volcanoes are built are often sediments translating a loading stress to outward horizontal displacements around the flanks (Borgia et al. 2000). Volcanic spreading is believed to control the structural evolution of many volcanoes (Borgia et al. 2000; vanWyk de Vries 2001).

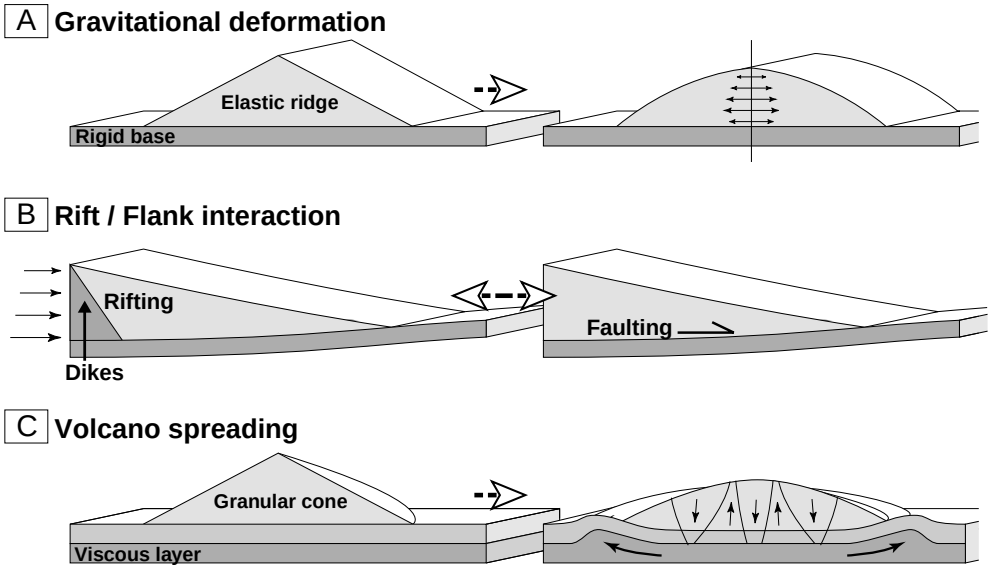

Figure 2. *Selected types of gravity-driven volcano deformation.* ***A.*** *Gravitational de-formation of elastic ridge analog models produces horizontal expansion along the axis of symmetry. After Fiske and Jackson (1972) persistent rifting is gravity-driven.* ***B.*** *Ocean sediments form a weak substratum and facilitate décollement of volcano flanks. Rifting accumulates the driving stress for lateral slide, extension drives rifting persistence (after finite element modeling of Dieterich 1988).* ***C.*** *Volcano spreading describes a specific type of flexure and basal deformability. Granular analog models above thin viscous layer results in lateral expansion, formation of a circumferential bulge, horst and graben structures on the edifice flanks, and apex subsidence (after Merle and Borgia 1996).*

Understanding of the precise influence of weak substratum on volcano stability and rift formation / rift migration remains, however, largely poor. It is an open question to what degree expansion mechanisms, such as creeping and lateral sliding of an existing volcanic edifice control the rift geometry. Since rift zones form the most productive feeder systems of volcanoes, control the lasting magmatic evolution, and direct potential future magmatic sites, understanding of rift generation is essential.

Based on qualitative experiments, our study concerns the initiation of rift zones and the dynamic feedback with flank creeping, a process that changes a volcano's internal stress

field as reflected in adjusted dike patterns. The model builds upon earlier studies on rift zone geometries (e.g. Fiske and Jackson 1972; Swanson et al. 1976; Nakamura 1980; Lipman et al. 1985; Carracedo 1994, 1996).

Experimental procedure

We dissolved powdered gelatine in 60°C water by a concentration ~2.5 wt.%, filled into cone-shaped moulds and then refrigerated for 12 hours. We used various initial moulds and thus cone-geometries to study the fracture geometries, independently of dimension and mass diversity. The base of the cone-shaped moulds were between 50 mm and 300 mm in radius, with heights of 50 mm to 200 mm, amounting to a flank steepness of about 45 and 34 degrees, respectively. The hardened gelatine-"volcanoes" were placed onto a PVC-plate. To simulate intruding magma, we injected colored water into the cones and studied the propagation and direction of fluid-filled fractures.

The underlying PVC surface was prepared in such a way as to simulate a variety of frictional interfaces between the base and the gelatine cones. First, we studied cone deformation with a homogeneous basal friction. In a second setup, we placed the gelatine cones onto a PVC-plate that contained a low-friction sector. These two setups are categorized into a *stable situation* and an *unstable situation*, respectively. In the stable situation experiments, a soap-based lubricant greased the entire gelatine-cone base, so that the entire interface cone/ground represented similar low-friction surfaces. In these experiments, the gravitational stress field of the cone caused uniform spreading of the flanks, the cone spreading outward due to its load (Fig. 3).

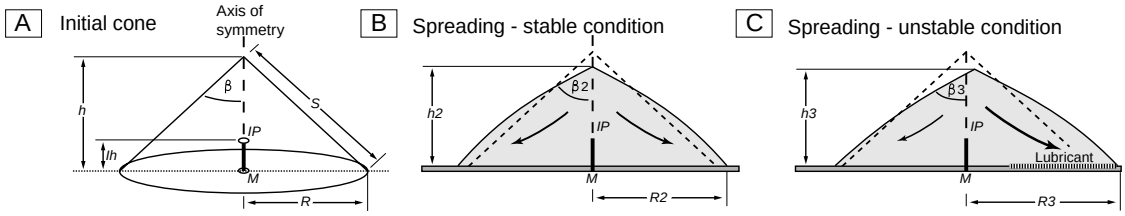

Figure 3. *Geometry of the cones. Sizes of the cones were between 50 mm and 300 mm in radius, with a flank steepness between 45° and 34°. Due to gravity, the cone spread outward, partially sliding on a basal lubricant. In the unstable situation, only one flank is lubricated.*

As a consequence of this gravitational deformation, the cone height was reduced and the plane perimeter increased. By varying the frictional conditions at the base, we customized the flank deformation and regulated flank creeping influences. Accordingly, the stress field changed and the direction of propagating blade-like dikes adjusted, as described in the result section.

In the unstable situation experiments, a different PVC plate was sand-roughened, except for one sector, allowing the mounted cone to glide locally. We consider this unstable situation as a rough analog to a volcano stress field influenced by a flank that slides on a basal detachment surface. The size of this décollement and the sliding direction was varied in different experimental set-ups. Small holes were drilled into the PVC-plates through which injection of the liquid (the magma) was accomplished using a thin needle connected to a syringe. The propagation and orientation of the fractures were measured and recorded (Fig. 4).

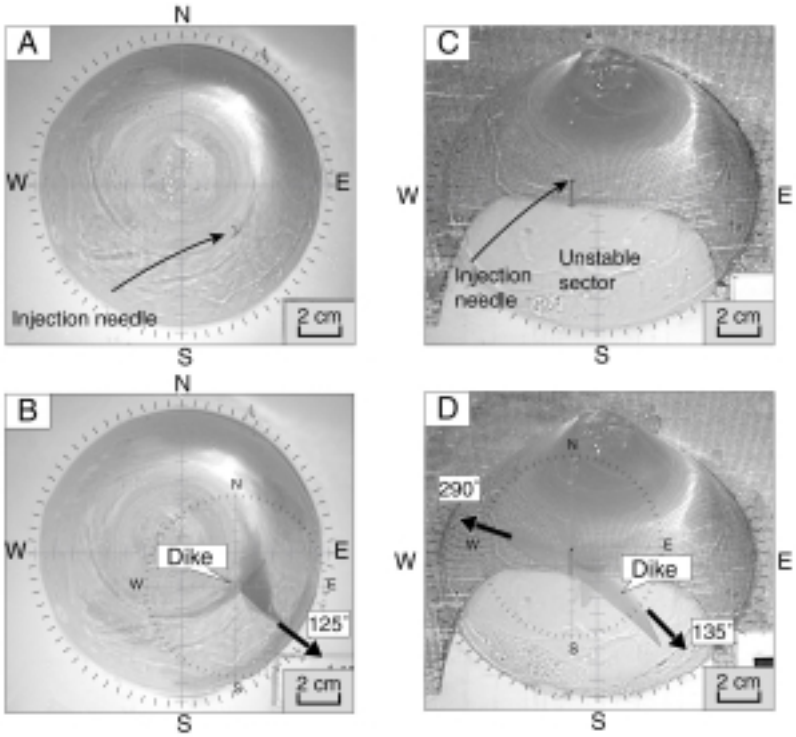

Figure 4. *Photographs of experiments before (a, c) and after injection (b, d).* ***A.*** *Plan view of stable situation, forming* ***B.*** *on injection a radial dike oriented 125° azimuth.* ***C.*** *Oblique view of unstable situation with injection into the interface creeping/non-creeping sector and a slight southwestward eccentricity of the lubricated base.* ***D.*** *Produced fractures to southeast (135°) and northwest (290°).*

Gelatine is characterized by linear viscoelastic behavior at small deformations (Richards and Mark 1966), with a shear modulus G depending strongly on velocity (Bot et al. 1996). The rheological behavior of gelatine was examined in creep tests, indicating a short-term "Voigt body deformation" (elastic behavior) and "Maxwell body flow" for long time duration (Richards and Mark 1966). This means that the stress-strain curve –whose slope is defined as the "Young's modulus"– depends on the rate of strain, resulting in brittle behavior at high strain rates, which we controlled by the injection rates. The strength of gelatine depends upon the concentration and intrinsic strength of the gelatine used (here: bloom strength 170g). Other factors affecting the rigidity of gelatine include its temperature and the thermal history, which was held constant throughout all experi-

ments. The physical parameters of natural rocks were not to scale in our gelatine experiments; the results are considered to be qualitative. To test the influence of various gelatine strengths, we changed the concentration of the gelatine powder and repeated the experiments, generally reproducing the same arrangements of fractures.

The solute gelatine gel has a Poisson´s ratio of nearly 0.5, the condition in gelatine thus being approximately hydrostatic. If fracturing occurs, the finite yield strength is exceeded. On injection, vertical hydraulic fractures form when the injection pressure is greater than the sum of the gelatines yield strength and the minimum compressive stress that acts in the horizontal plane. In profile, the injected liquid caused cracks and propagated mainly laterally under low injection pressure. If the liquid was more viscous, the thickness of the cracks increased. For high injection pressures, the vertical propagation axis amplified. This may be considered analogous to volcanoes, which deform elastically before fracturing occurs and dikes propagate. This is in accordance with magmatic pressure that exceeds the tensile strength of the volcanic rock plus $\sigma 3$, acting in horizontal plane, as reported from Hawaiian volcanoes and numerical models (e.g. Pollard et al. 1983; Ida 1999).

To diminish side effects and pre-experimental strain of the gelatine by, e.g. insertion of the needle from below, upside down turning of the moulds and slightly varying material properties, the experiments were evaluated statistically, based on 200 individual experiments. The large number of experiments allowed evaluation of mean dike directions for a specific geometrical situation. We did not study the details of multiple injections into a sole gelatine edifice, since gelatine rupture is an irreversible process and the early fracture paths acted as free surfaces and generally modified the stress field. A further (background) tectonic influence, such as regional stress, was also not simulated.

Hydro-fractures described in this study stand for the supposed arrangement of dikes in natural systems, propagating perpendicular to the least compressive stress. For experimental descriptions we project the dike trends on imagined compass directions (N-S-E-W) and used standard tools of statistical azimuth analysis in stereographic projections (view Figure 4). The experiments were divided into groups, defined by the locality of the points of injection beneath the cone, and the size and the eccentricity of the creeping sector.

Experimental results: Stable situation

Cone-shaped gelatine volcanoes with homogeneous basal shear resistance are considered as the stable end-member model. We injected the liquid into the cones' flanks or into the axis of symmetry of the cone. If injected into the flanks of the cone, the fractures propagated towards the nearest free surface of the "volcano", i.e. radially away from the cone's center (Fig. 5). When injected very close ($< \sim 2$ cm) to the axis of symmetry, the

azimuth of the fractures seemed to be initially arranged randomly. These occasionally concentric initial orientations were most likely due to the centered plumbing effect of the cone; on further injection and outward directed fracture propagation, the fractures also curved into radial paths.

A radial fracture pattern is plausible for an elastic cone that is placed on a homogeneous base, since the gravity-driven deformation causes circumferential flank extension around the cone, resulting in a circumferential minimum principal stress direction all around the edifice. The sole influence of the cone-load on crack propagation is thus generally in accordance with the findings from experiments by McGuire and Pullen (1989).

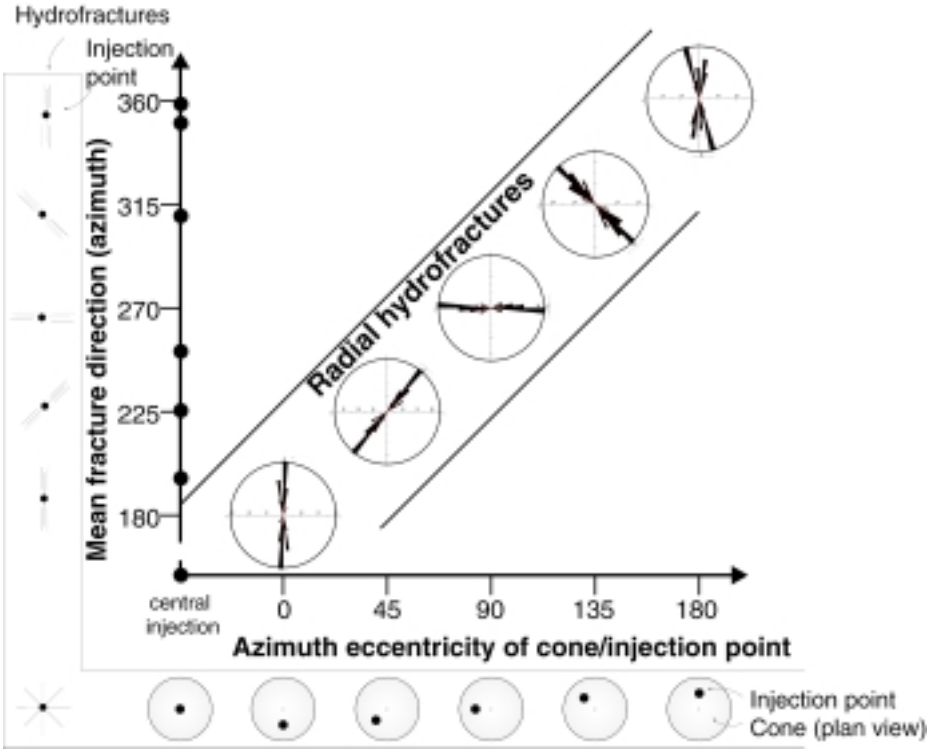

Figure 5. *Stable situation. Relation of mean hydrofracture propagation direction to the eccentricity of injection point (measured in azimuth). Situated on a uniform substratum, the flanks of the gelatine-cone deform by gravity-driven extension. Central injection beneath the apex of a regular cone generates randomly directed fractures (plumbing effect). Injection into the cones flanks produces fractures oriented radial away from the edifice center. The overall dike pattern with various positions of injection into the cone is thus radial.*

Experimental results: Unstable situation

In a second set of experiments, we studied inhomogeneous volcano spreading and the influence of sector-creep on the configuration of rift zones. For these unstable situation experiments, a laterally spreading flank of a volcanic cone was qualitatively simulated by lubricating parts of the gelatine-cones' base. As shown in Figure 4, we enlarged the basal friction of the PVC plate with fine-grained sand, apart from a well-defined lubricated

sector. Hardened gelatine cones were placed on this base, located partially on high-friction surface and partially above the slippery décollement sector. The resulting stress field qualitatively imitates a volcano that partially deforms above a mechanically weak substratum. We repeated these experiments and systematically varied site and size of the unstable sector and, again, the point of injection. Various groups of "dike" directions we observed on injection. First, we studied the importance of the flank-creep direction. We placed the gelatine-cone in such a way that its southern flank glides southward (no E-W-eccentricity). In other words, the north-south axis forms the axis of symmetry of intruded dikes in plan-view. Fractures formed on injection that were similarly oriented on the east and on west part of the volcano (Fig. 6A-1, 6B-1, 6C-1). However, if we changed the creep direction of the sector towards slight eccentricity, basically uneven fractures formed on the west and the east sides of the cone (e.g. Fig. 6A-3; 6C-3). In this case, a lubricated southern sector slipping to the southwest enforced the principal and longest fractures to form into the southeastern sector of the cone. Moreover, the location of the injection point relative to the cone and its unstable sector largely influences the above relations:

a) *Injection into the stable sector* of a partly lubricated cone caused slightly curved fractures, striking mainly tangential to the southward creeping sector (Fig. 6A). The fractures were thus mainly orientated east–west. With further outward propagation, the fractures turned perpendicular to the cones perimeter. This tendency of reconfiguration into a radial direction increased with distance to the lubricated part of the volcano and with increasing distance to the volcano midpoint. The greater the distance of injection from the unstable sector, the larger number of radial trends were observed.

b) *Injection into the creeping sector* of the cone also produced fracture orientations strongly adjusted due to the size and direction of sector creep. When the unstable sector was centered with southward sector-creep direction, slightly curved fractures formed north-south, as well as sector-tangentially (east-west). These dike directions varied with increasing creep influence: when 10% of the cone creeps southward, the main dike direction is north-south, only influenced very close to the unstable flank. When more than ~20% of the cone's base was on a weak substratum, three main axes formed: one into N-S direction, two axes with strong tangential influence, curving around the creeping/non-creeping interface (Fig. 6B). All main axes were restricted to the unstable southern half hemisphere. To the north a more diffuse radial trend formed. The main direction of this diffuse swarm migrates with more eccentric creep directions of the unstable sector. Slight eccentricity of the basal lubricant to the southwest resulted in the major southeast-northwest fracture direction (in analogy eccentricity to the southeast resulted in major southwest-northeast fractures).

c) *Injection directly above the interface* of the creeping sector caused fractures in three major directions (Fig. 6C). This triaxial geometry depends on the eccentricity of the cone

relative to the creeping sector and injection point. Two sector-tangential directions, plus a third trend into the stable cone define these three main trends. The location of the third diffuse trend is a function of the other two tangential ones. When a cone is unstable e.g. in the SW- flank, and injection was in the unstable/stable interface, the main tangential trend is SE, the secondary tangential rift axis is propagating to the W, and a third diffuse swarm formed into the stable area to the NW to NE (Fig. 6C-3). The two principal directions (W and SE) were tangential to the interface stable / unstable cone base, reflecting the approximate size of the lubricated sector beneath.

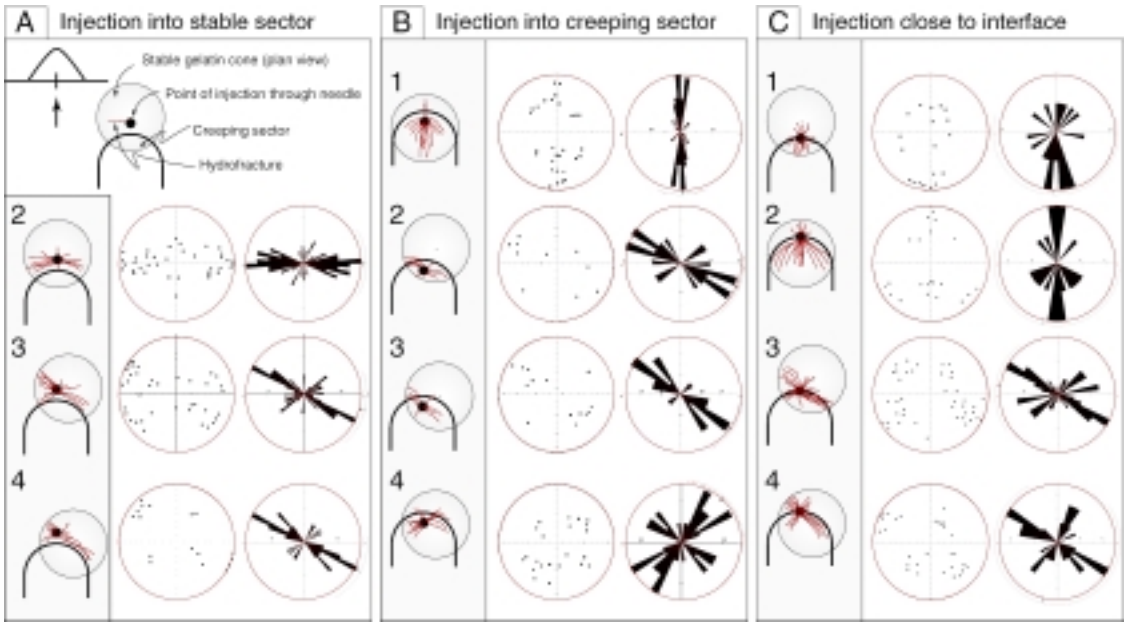

Figure 6. *Summarized arrangement of hydrofractures, propagating in locally destabilized edifices, in relation to injection point and eccentricity of a creeping sector on a weak layer (lubricant), relatively.* ***A.*** *Injection into stable sector,* ***B.*** *Injection into creeping sector, and* ***C.*** *Injection close to the interface stable / unstable sector. Stereoplots illustrate the statistic orientation of fractures: each circle in pole plots refers to the distal locality of fracture, measured in azimuth and distance from the point of injection. Frequency-azimuth (rose) - diagrams using polar lines, sector size = 8°, the length of each rose sector is proportional to the frequency of orientation that lie within that sectors. Two types of 'average directions' are reported by a "preferred direction"; and a vector mean.*

The unstable experiments resulted largely in variable fracture orientations relative to the stable experiments. We regard the two tangential rifts as a non-collinear or strongly curved rift zone. Accordingly, sector creep influences a collinear rift pattern to develop into non- collinearity. The main dike “adjustment” was observed close to the unstable sector. There, dikes are no longer radial but tangential, enclosing an area somewhat smaller than the limits of the detachment surface below.

How many rift axes?

By counting the fracture trends, we get a rough idea on the number of rift zones likely to develop. A collinear trend means that the fracture propagated from the injection point (the eruptive center) into two opposite directions, resulting in the formation of a single rift zone. A collinear trend, however, may develop into a non-collinear or even triaxial configuration.

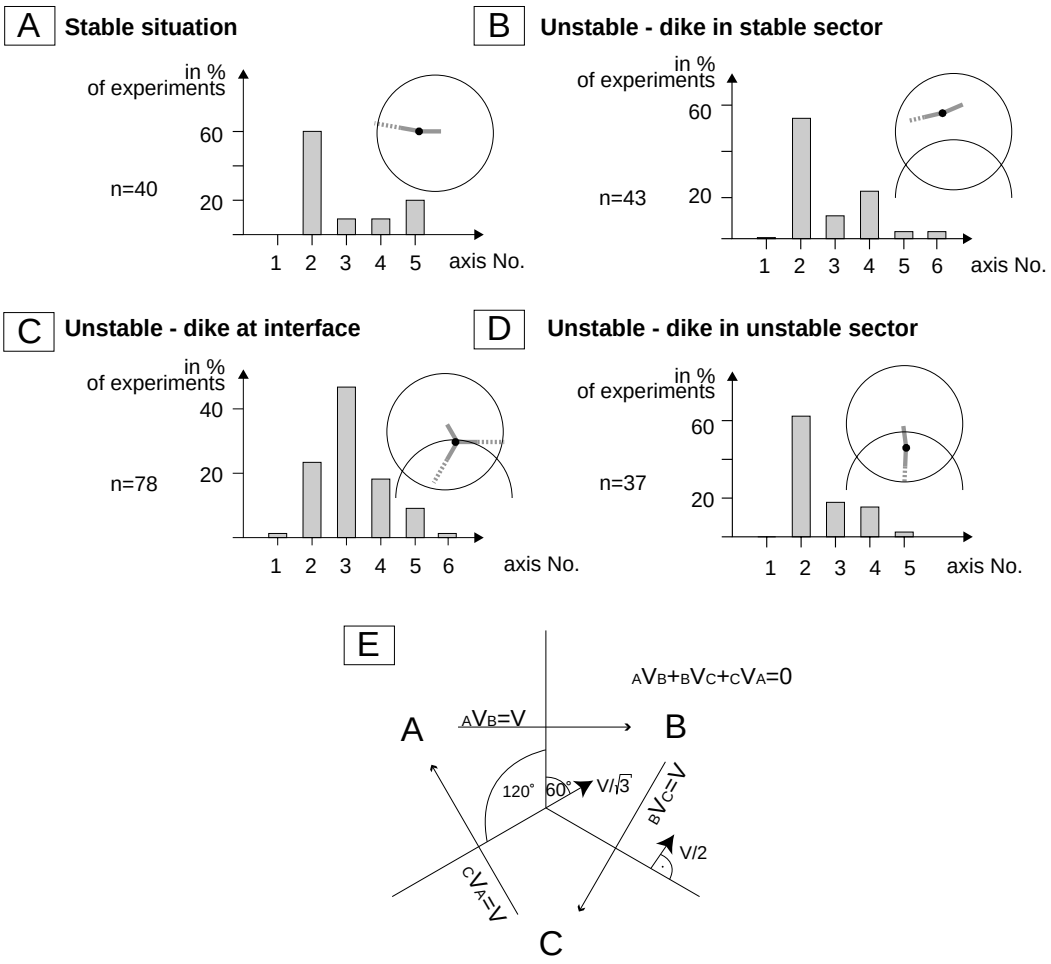

Figure 7. *Amount of rift zones as a function of total number of experiments [in %].* ***A.*** *Stable experiments caused on single injection mainly two radial fractures.* ***B.*** *Unstable situation resulted -when injected into the stable sector- in mainly 2 or 4 emergent directions.* ***C.*** *Injection into the interface stable/unstable sector produced in approximately 60% (n=78) in triaxial rift zones. The angle between fracture azimuths was more than 100°.* ***D.*** *Injection into the creeping sector resulted in most of the cases in two divergently propagating dikes. In a), b) and d) the angle between the two main dike directions was > 130°, suggesting that in nature these will reflect a single or curved rift zone.* ***E.*** *If two rifts develop into a non-collinear trend, a third rift arm forms as a result of their compression. When a flank starts to creep, the result will be that the number of rift zones change.*

The arrangement of the experimental dikes was a function of basal shear resistance, and moreover, of the injection point. In the stable situation, the radial azimuth produced two fracture-directions in 60% of the cases, propagating collinearly from the injection point into opposite directions (Fig. 7A). The unstable situation resulted also in 60% of the cases in two fracture directions (collinear), although with slight trend towards non-collinearity (Fig. 7B). When injected, however, close to, or directly above, the interface stable / unstable sector, three directions developed, two of them well pronounced in curved tangents, and a third arm directed into the stable part of the volcano (Fig. 7C). The transition from collinearity towards two rift zones (sector tangential) is controlled by the presence and size of a creeping sector. This means that weak substratum and slow displacement at a décollement causes the formation of non-collinear rifts.

A third rift arm developed predominantly when the liquid was injected in the vicinity of the interface stable/unstable cone. This, moreover, resulted in a strong tangential (non-collinear) trend. A third arm, developing subsequently, can be the response of the dilation at the tangential rifts. McKenzie and Parker (1967) applied displacement vectors to lithosphere triple junctions – a method well suitable to volcanotectonics: when three rift zones in a volcanic edifice are arranged symmetrically, nucleating in a central point, individual axes are non-collinear. The angle α separates the three sectors *A*, *B*, *C* (Fig. 7E). These sectors dilate with displacement vectors V that are ${}_AV_B + {}_BV_C + {}_CV_A = 0$. Accordingly, the vector of sector B in direction C is ${}_AV_C - {}_AV_B = {}_BV_C$. The common geometry of the younger Canary Islands is assumed to have three-armed rift systems with angles of $\alpha \approx 120°$ in-between (Carracedo 1994). The velocity of dilation across a rift is V, so that the velocity perpendicular to one side of the rift is $V_V = V/2$. Two of such vectors interact on 60° to the sector in-between; the velocity relative to the fixed nucleus is $V_R = V/3^{½}$. This may force a third rift zone to develop, when two (non-collinear) rift-arms do exist. Assuming two rift zones to converge at 120° with horizontal extension rates on the order of 1000 m per 1 million year, given by $\sin \alpha/2 = V_{third}/V_R$, so that $V_{third} = \sin \alpha/2\ (V/3^{½})$. The resulting third rift dilation rate V_{third} is as fast as the initial ones. Consequently, a third arm is likely to develop due to local tension resulting from the compression induced by dilation of the two other main (non-collinear) rift zones. For the Hawaiian volcanoes, Walker (1992) described that two collinear rift zones may become non-collinear, when asymmetric growth occurs e.g. due to buttressing effects. Dike injection into such non-collinear rift zones may cause extension on the opposite side of the nucleus and form extensional stress and the potential site of a third rift arm (Walker 1992).

Implications

Rift zones occur on most oceanic volcanic islands and are characterized by dense dike swarms and a concentration of eruptive centers (Fiske and Jackson 1972; Walker 1992). The accumulating dikes form coherent intrusion complexes, making up the structural framework of large ocean island volcanoes, such as those of the Hawaiian and Canary Archipelagos (e.g. Walker 1992; Carracedo 1996). Walker (1992) termed rift zones as being "possibly an invariant component" controlling the evolution of oceanic island volcanoes. In turn, scarps of giant lateral collapses are often located between two dominant structural axes of a triaxial rift system, as well documented for the Canary Islands (Carracedo 1996). Our models show how the directions of hydrofractures reconfigure due to a laterally creeping flank. Hence, contrasts in basal friction (i.e. flank creep) may modify the propagation direction of dike swarms, but is such a model applicable to natural systems such as the Canary Islands?

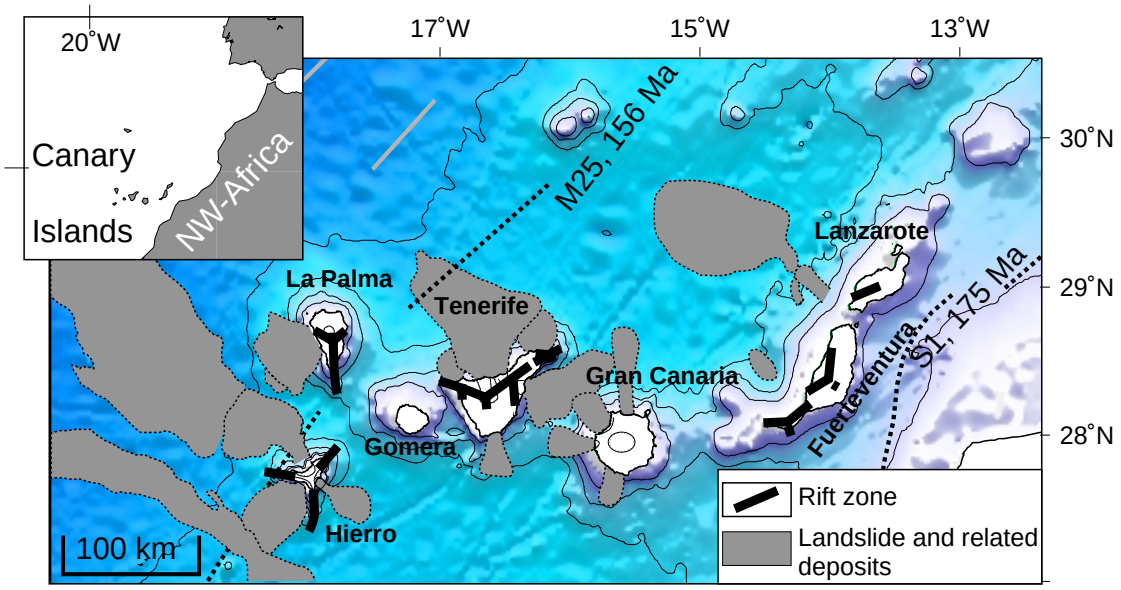

Figure 8. *Canary Islands, structural axes and landslides (after Féraud et al. 1985; Carracedo 1994; Krastel et al. 2001; Masson et al. 2002).*

On each of the younger (western) Canary Islands, rift zones underlie the aligned vent locations and parallel dike orientations (Fig. 8). On Tenerife, La Palma and El Hierro three rift zones are arranged in triaxial configuration (Carracedo 1994), systematically having a ~100 to ~140° angle in-between.

The previous concept of the genesis of regular triaxial rift geometry on the Canary Islands is adapted from plate tectonics, where triple armed junctions are believed to form in response to vertical upward loading (McFarlane and Ridley 1968; Luongo et al. 1991; Carracedo 1994, 1996). In this context, regular triple-armed fractures may result from the least-effort fracturing mechanism of the brittle crust (Carracedo 1996). This least-effort

model (Fig. 9) is considered to explain a) the aligned concentration of eruptive sites on Tenerife, El Hierro and La Palma, b) the stable site and direction of rift zones, and c) the genesis of volcano sector collapses, located in-between two ~120° rift zones (Carracedo 1994, 1996).

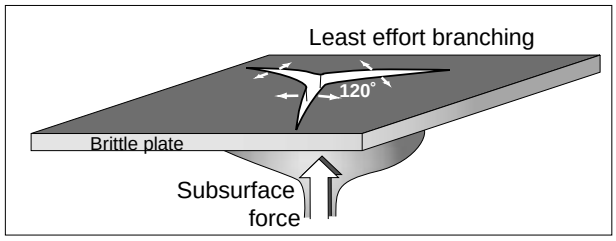

***Figure 9**. Least effort model; previous idea of the origin of triaxial rift geometries on the Canary Islands.*

However, studies that focused on inflating deep and shallow magma reservoirs produced exclusively radial and concentric fracture swarms, narrow or focused (three) rift zones have not been observed (Anderson 1937; Komuro 1984; Marti et al. 1994; Walter and Troll 2001).

Rift zones in the Canary Islands are represented at the surface by strings of aligned eruptions emission vents (Carracedo, 1996). Near the surface, the topographic and slope-loading stress influences the final orientation of vents within the rift (Carracedo 1994, 1996). Both, triple armed rifts and giant landslides are closely associated in the Canaries on single islands (Carracedo 1996). Elsworth and Voight (1996) described extensional stresses in volcanic edifices that are related to phases of intense eruptive activity. These stresses may reach the rupture threshold and trigger massive landslides. More than 50% of the total subaerial volume of the western Canary Islands collapsed laterally into the sea or was eroded during the past million years (Carracedo et al. 1999a,b). The azimuths of the main rift zones in the western Canary Islands (Tenerife, La Palma, El Hierro), as well as the directions of giant landslides are clearly related (Fig. 8). Our models imply that the formation of non-collinear and triaxial rifts may be a function of preexisting volcano sector instability and flank creep. We demonstrate this relation for La Palma, the youngest and most active edifice of the Canary Islands.

La Palma: Taburiente shield volcano

The pear-like outline of La Palma is due to an old circular shield in the north to which is welded the elongate 25-km-long Cumbre Nueva / Cumbre Vieja rift zone to the south (the "Cumbre Ridge"). The rift zone forms a >1700m high ridge of superimposed tephra and spatter cones and lava flows. About six major eruptions occurred in the last 500 years along this ridge, the two youngest in 1949 and 1971. The ridge also extends several kilometers offshore to the south of the island (Urgeles et al. 1999; Schmincke and Graf 2000). Two main geologic units are defined: a) a Pliocene submarine and plutonic core forming a seamount complex exposed in the walls of the "Caldera de Taburiente"

(up to 1500 m asl), uplifted by over 1 km and tilted to the southwest, and 2) subaerial lavas subdivided into three successive volcanoes (Taburiente, Bejenado/Cumbre Vieja) that unconformably cover the seamount (Staudigel and Schmincke 1984; Carracedo et al. 1999a). The Taburiente shield predates the giant landslides, while Bejenado and Cumbre Vieja postdate the collapse (Carracedo et al. 1999a). The 5-km-wide embayment "Caldera de Taburiente" is one of many misinterpreted "calderas" on large volcanoes, being the result of destructive 200 km³ lateral landslides and erosion rather than a classical (vertical) collapse caldera (Ancochea et al. 1994; Carracedo et al. 1999a; Urgeles et al. 1999). Also submarine studies revealed distinct landslide debris fields around western La Palma (Urgeles et al. 1999; Masson et al. 2002). The collapse scars and deep erosion level presently allow deep insights into the base i.e. the seamount complex underneath the younger cover, and form the steep cliffs of the Caldera de Taburiente (Ancochea et al. 1994; Carracedo et al. 1999a).

Northern La Palma was structurally controlled by generally radial fissures (Ancochea et al. 1994), forming a deep-reaching radial dike swarm for about 1 Ma (Day et al. 1999; Carracedo et al. 2001; Guillou et al. 2001), active in the very initial stage of the development of the volcano (Carracedo et al. 1999a,b). Starting of about 0.8 Ma this radial configuration was superseded by two narrow rift zones, one to the west (El Time Rift) while the highly productive "Cumbre-ridge" developed to the south (Ancochea et al. 1994; Carracedo et al. 2001). The unstable flank enclosed by those rifts collapsed ~0.56 Ma ago to the west and southwest (Guillou et al. 2001). Based on borehole and age data, Carracedo et al. (1999b) interpreted the contact between the much older seamount series and the post-collapse Bejenado volcano (0.55 Ma) as the interface of the collapse boundary. Strong shearing was focused in-between those series (K. Roa, pers. commun. 2001), implying the presence of a weak décollement. In our gelatine experiments, a creeping flank of a radial cone caused two main sector-tangential fracture trends. One of these experimental rifts developed more strongly than the other, when the unstable sector was eccentric e.g. to the southwest. In these experiments, hydro-fractures propagated to the west and principally to the south. In La Palma, dike directions thus reflect the plausible response of sector creep to the southwest. The dikes grouped to form a small (to the west) and a major tangential rift (to the south), replacing an initial radial dike swarm; volcanic productivity migrated to the south. Lasting magmatic activity at the south rift formed a ridge, extending up to 25 km south from the summit of La Palma (Cumbre Ridge). Once established, the morphological high aspect ratio caused a steady rifting stress field and flank instability normal to the rift axis (Carracedo et al. 1999b). Dike arrangements and aligned scoria cones indicate the Quaternary position of this rift, although largely destroyed by later westward-directed landslide processes (Carracedo et al. 1999b; Carracedo et al. 2001).

Based on our experiments, we infer that the rifts were initiated during early stages of flank instability due to southwestward sector creep. The sequence above the tilted seamount succession was detached in the southwestern sector. In analogy to the sector-tangential fracture direction in our gelatine cone, the lasting and dominant tangential Cumbre rift zones formed, highly active up to the present.

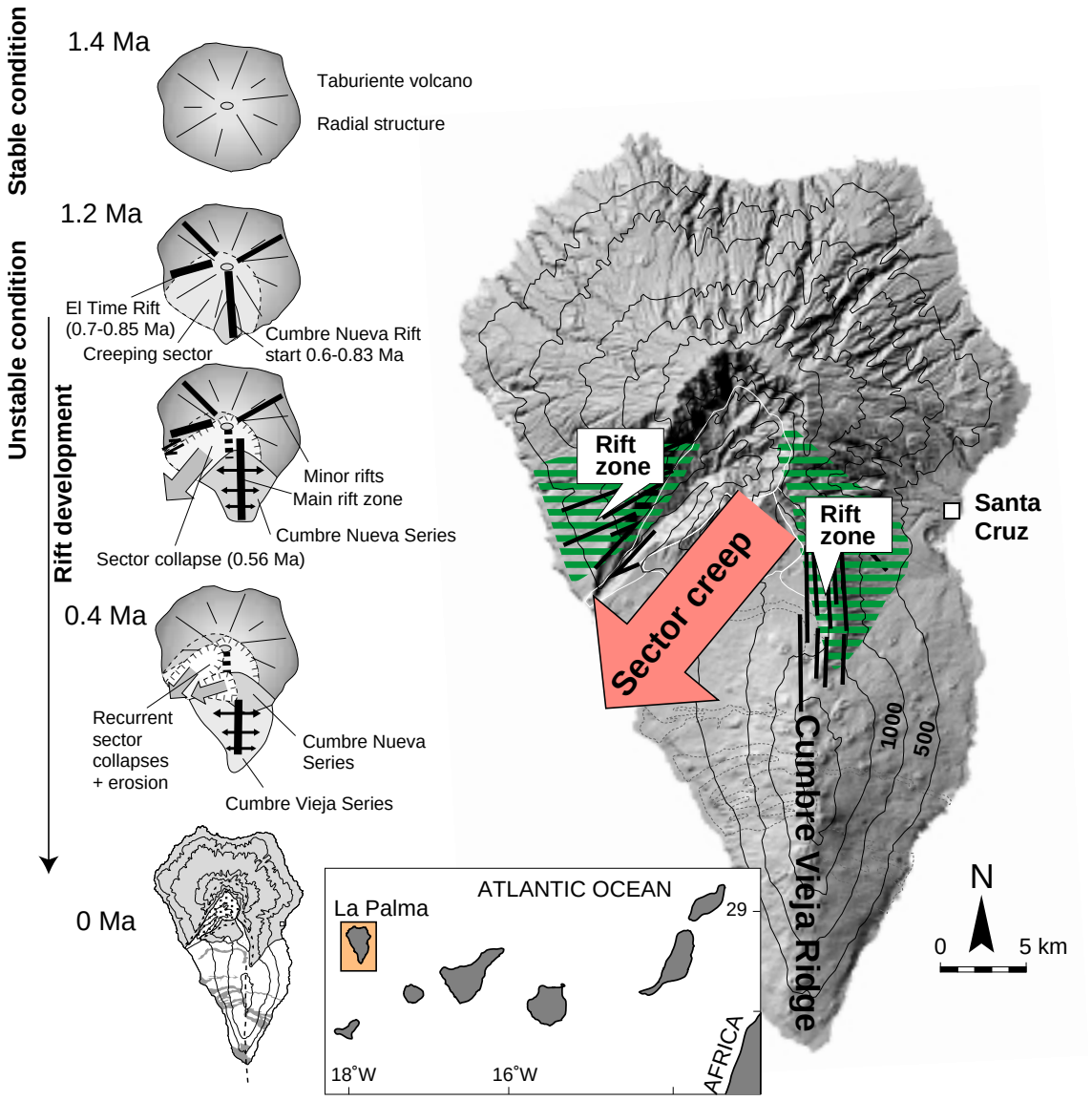

Figure 10. *Structural evolution of La Palma (include data from Ancochea et al. 1994; Carracedo et al. 1999b; Guillou et al. 2001). See text for explanation.*

Discussion

Gelatine-cone models show how the stress field and propagating hydrofractures reconfigurate the internal architecture, when sector creep dominates. By injecting colored water into these gelatine cones we studied the fracture paths and found a systematic pattern reflecting sector creep conditions. Since the cones are branched on injection by a) radial fracture trends when the basal friction is homogeneous, but form b) discrete rift zones when a cones' sector was located on a basal lubricant, we can infer that volcanoes and their intrusive sheets follow similar mechanisms depending on the lubricating potency of detaching sectors above weak layers.

The ancient radial edifice of La Palma was unstable in the southwestern part, since underlying seamount series dip towards south–southwest (Staudigel and Schmincke 1984). The interface of the uplifted seamount complex and the unconformably overlying series formed a potential décollement. Masson et al. (2002) identified much older submarine landslide deposits, being ~1 Ma old and directed also to the southwest; hence the giant landslide 0.56 Ma ago being a recurrent collapse. Although boreholes drilled in the embayment reveal the weak contact between the Seamount series and Bejenado lavas at sea level (Carracedo et al. 1999a), breccias of much older landslides (Masson et al. 2002) may have formed further deeply buried weak mechanical unconformities inclined to the southwest. A submarine effect of flank creep remains speculative. The unstable southwestern La Palma and attended flank creep process and stress field change resulted in structural reconfiguration forming two tangential rift zones; one main rift zone to the south and a minor one to the west. The sector collapse of the unstable flank was dated to ~0.56 Ma (Guillou et al. 2001). Individual dikes of two sector-tangential rifts (El Time Rift and Cumbre Ridge) were dated to about 0.8 Ma (Carracedo et al. 2001), predating the collapse. If these occurrences –tangential rift zones and sector collapse– are genetically related, the unstable southwestern sector of La Palma was creeping laterally for about 250.000 years before sector collapse occurred. The locations of the tangential rift zones indicate the extent of the unstable southwestward creeping flank.

Our models and field evidence for La Palma imply that volcano sector-creep may generate rift zones. The south rift of La Palma is the volcanically most active area in the Canaries, forming the southward-elongated Cumbre Vieja ridge. The question is, whether sector-creep and rift formation influences magma eruption. On the Hawaiian and Canary Islands the most focused, longest and straightest rift zones are those of the shield volcanoes in their most productive stage (Stearns, 1985; Dieterich 1988). The later stages of La Palma show many similarities with the early stages of development of the Hawaiian Islands that are presently in a highly productive juvenile stage (Carracedo et al. 1999a). Interacting rifting and lateral creep is moreover reported from Kilauea, Hawaii (Dieterich 1988). We wonder whether very productive rift volcanism is a consequence of volcano

instability and sector creep. Plumbing effects and thus the magma supply rates may change by flank creep and volcano spreading, and became modified rapidly e.g. by a sudden decrease of basal shear resistance.

Once established, gravitational spreading of the topographic ridges (Fiske and Jackson 1972) and density increase near the dike complex (Walker 1992) contribute to lasting activity of rift zones. The close temporal and genetic relationship between intrusions, ground deformations, moderate to large seismicity and sliding of the south flank of Kilauea over thin décollement planes are discussed (e.g. Dvorak 1994; Ryan 1988; Delaney et al. 1993). The basal Kilauea fault is almost horizontal and roots at depth at the base of the rift. Sliding along this décollement plane is largely aseismic, interpreted to be an effect of large Coulomb stress changes along the fault zone (Tilling and Dvorak 1993; Troise 2001). The site of detachment well fits the location of weak materials close to the interface to the ocean crust at a depth of ~9 km (Clague and Denlinger 1994; Delaney et al. 1998). This lubricating interface extends laterally along ancestral landslide debris and pelagic sediments (Moore et al. 1989). The seaward-directed flank motion is interpreted to be driven by the volcano mass and the "magma push" (Denlinger and Okubo 1995; Owen et al. 1995; Delaney et al. 1998). Of interest is the asymmetric seismicity across the Kilauea rifts, being focused at the seaside and being practically absent north of the rift (Ryan 1988; Tilling and Dvorak 1993). Theoretical studies of dike pressure, however, predict a symmetric pattern of Coulomb stress on either side of the rift (Rubin and Pollard 1987). This discrepancy could be the result of buttressing barrier (Mauna Loa) at the northern onshore side, or an effect of the concave curvature of the rift (Ryan 1988; Troise 2001). An alternative explanation is lateral slip along the lubricated base, focusing the extensional stress on the sector-tangent rifts and the southern sector itself. The Kilauea rift zones also root at a depth of ~9 km, i.e. the root is located in the same depth than the localized detachment plane (cf. Borgia et al. 2000). Our model suggests that the rift configuration is likely to be the result of slow flank creep rather than the causal mechanism of flank instability. According to this interpretation, the southern flank of Hawaii is a restricted creeping flank of a gravitationally spreading volcano (cf. van Wyk de Vries et al. 2001); the sites of intrusions are imposed to form rift zones that established and push the flank further seawards. Weak substratum and gravity-driven creep of volcano flanks may control near-surface rifting of volcanic edifices and thus the structural framework of volcanoes. Later rifting is a result of gravity-driven volcano deformation and its significance, location and direction is a function of partial flank creep. The evolution from flank creep to rift zone forming dikes may hence be the components of a positive feedback pattern.

Summary and conclusions

We designed gelatine analog experiments to simulate the stress field and intrusive patterns of unstable volcanic edifices. The analog volcanoes were cone-shaped and different conditions of basal friction were used in various experimental setups. We injected colored water from below and studied the orientation of fractures (dikes) that propagated through the cones.

Situated on uniform substratum, the flanks of the gelatine-cone deformed by gravity-driven extension. The orientation of the fractures was perpendicular to the minimum principal compressive stress, resulting in a "radial dike swarm". In a further setup, we reduced the basal shear resistance in one sector, to simulate the stress field close to a locally creeping flank. In these experiments, the dike azimuth diverged largely when injected into a) the non-creeping part of the cone, b) the creeping sector, or c) the stable/unstable interface. Case a) produced radial fractures; case b) produced mainly fractures that reflect strong circumferential expansion of the creeping sector. In case c) three main fracture directions formed, two of which were tangential to the stable/unstable interface and a third diffuse one propagated into the stable part of the cone, reminiscent of triaxial rift zones on many volcanoes. The significance and direction of the three rift zones varied systematically with size, eccentricity and creep direction of the unstable sector. As shown in Figure 11, three main types of rift zone configurations may accordingly develop from an initially radial volcanic cone. Slight eccentricity of the creeping sector focuses dike intrusion along two curved axes tangential to the stable/unstable interface. In contrast, strong eccentricity resulted in only one main tangential rift, very similar to the S-rift observed on La Palma.

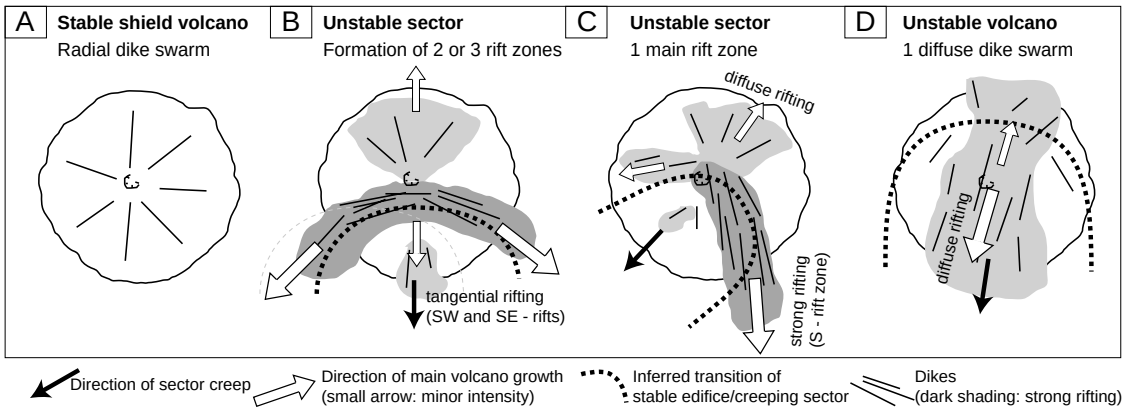

Figure 11. *The persistence and direction of three main rift zones varied systematically in size, eccentricity and creep direction of the unstable sector.* ***A.*** *Radial volcano; spreading with homogeneous basal shear resistance.* ***B-D.*** *If a sector of a radial volcano starts to creep laterally, we can expect one of three principal structural configurations. Case* ***C.*** *illustrates the projected structural development of La Palma.*

With initiation of a creeping sector, an initial radially structured volcano is likely to reconfigurate and produce rift zones composed of two or three axes. Based on the experimental results, we propose that the formation and configuration of triaxial rift zones may be a response to near-surface volcano-deformation such as volcano-flank creep rather than a simple function of vertical upward loading as commonly assumed for volcanic rifts on ocean islands.

Acknowledgements: The authors thank G. Alvarado and T. Hansteen for critical comments on earlier versions of the manuscript and N. Mitchell for discussion. Financial support was provided by the Deutsche Forschungsgemeinschaft to H.-U. Schmincke (Schm 250/77-1,2), a grant from the Studienstiftung des deutschen Volkes to VRT and travel support by the Trinity College Dublin.

References

Anderson, E.M., Cone sheets and ring dykes; the dynamical explanation, *Bull. Volcanol., 1*, 35-40, 1937.

Ancochea, E., F. Hernan, A. Candrero, J.M. Cantagrel, J.M. Fuster, E. Ibarrola, and J. Coello, Constructive and destructive episodes in the building of a young oceanic island, La Palma, Canary Islands, and genesis of the caldera de Taburiente, *J. Volcanol. Geotherm. Res., 60*, 243-262, 1994.

Annen, C., J.-F. Lénat, and A. Provost, The long-term growth of volcanic edifices: numerical modelling of the role of dyke intrusion and lava flow emplacements, *J. Volcanol. Geotherm. Res., 105*, 263-289, 2001.

Borgia, A., Dynamic basis of volcanic spreading, *J. Geophys. Res., 99*, 17,791-17,804, 1994.

Borgia, A., P. Delaney, and R.P. Denlinger, Spreading Volcanoes, *Ann. Rev. Earth Planet. Sci., 28*, 539-570, 2000.

Bot, A., R.D. Groot, and W.G.M. Agterof, Non-linear elasticity and rupture of gelatine gels, in *Gums and stabilisers for the food industry 8*, edited by G.O. Phillips, P.A. Williams, and D.J. Wedlock, *IRL Press, Oxford*, 117-126, 1996.

Carracedo, J. C., The Canary Islands; an example of structural control on the growth of large oceanic-island volcanoes, *J. Volcanol. Geotherm. Res., 60*, 225-241, 1994.

Carracedo, J. C., A simple model for the genesis of large gravitational landslide hazards in the Canary Islands, in *Volcano instability on the Earth and other planets*, edited by W. J. McGuire, A. P. Jones, and J. Neuberg, *Geol. Soc. London., 110,* 125-135, 1996.

Carracedo, J.C., S. Day, H. Guillou, and F.J.P. Torrado, Giant Quaternary landslides in the evolution of La Palma and El Hierro, Canary Islandsm, *J. Volcanol. Geotherm. Res., 94*, 169-190, 1999a.

Carracedo, J.C., S. Day, H. Guillou, and Gravestock, P., The later stages of the volcanic and structural evolution of La Palma., Canary Islands: The Cumbre Nueva giant collapse and the Cumbre Vieja volcano, *Geol. Soc. Am. Bull., 111*, 755-768, 1999b.

Carracedo, J.C., R. Badiola, and H. Guillou, Norte de La Palma, *Mapa Geológico Nacional de España (MAGNA)*, Hojas 1083-I-1083 IV, 2001.

Clague, D.A., and R.P. Denlinger, Role of olivine cumulates in destabilizing the flanks of Hawaiian volcanoes, *Bull. Volcanol., 56*, 425-434, 1994.

Day, S.J., J.C. Carracedo, H. Guillou, and P. Gravestock, Recent structural evolution of the Cumbre Vieja volcano, La Palma, Canary Islands: volcanic rift zone reconfiguration as a precursor to volcano flank instability? *J. Volcanol. Geotherm. Res., 94*, 135-167, 1999.

Delaney, P.T., A. Miklius, T. Arnadottir, A.T. Okamura, and M.K. Sakao, Motion of Kilauea volcano during sustained eruption from the Puu Oo and Kupaianaha vents, 1983-1991, *J. Geophys. Res., 98*, 17,801-17,820, 1993.

Delaney, P.T., R.P. Denlinger, M. Lisowski, A. Miklius, P.G. Okubo, A.T. Okamura, and M.K. Sako, Volcanic spreading at Kilauea, 1976-1996, *J. Geophys. Res., 103*, 18,003-18023, 1998.

Denlinger, R.P., and P. Okubo, Structure of the mobile south flank of Kilauea Volcano, Hawaii, *J. Geophys. Res., 100*, 24,499-24,507, 1995.

Dieterich, J.H., Growth and persistence of Hawaiian volcanic rift zones, *J. Geophys. Res.*, 93, 4258-4270, 1988.

Dvorak, J.J., An earthquake cycle along the south flank of Kilauea Volcano, Hawaii, *J. Geophys. Res., 99*, 9533-9541, 1994.

Elsworth, D., and B. Voight, Dike intrusion as a trigger for large earthquakes and the failure of volcano flanks, *J. Geophys. Res., 100*, 6005-6024, 1995.

Elsworth, D., and B. Voight, Evaluation of volcano flank instability triggered by dyke intrusion, in *Volcano instability on the Earth and other planets*, edited by W. J. McGuire, A. P. Jones, and J. Neuberg, *Geol. Soc. Ldn., 110*, 45-53, 1996.

Féraud, G., G. Giannerini, R. Campredon, and C.J. Stillman, Geochronology of some Canarian dyke swarms. Contribution to the volcano-tectonic evolution of the archipelago, *J. Volcanol. Geotherm. Res., 25*, 29-52, 1985.

Fiske, R.S., and E. D. Jackson, Orientation and growth of Hawaiian volcanic rifts, *Proc. R. Soc. London, Ser. A, 329*, 299-326, 1972.

Gudmundsson, A., Marinoni, L.B., and Marti, J., Injection and arrest of dykes: implications for volcanic hazards, *J. Volcanol. Geotherm. Res., 88*, 1-13, 1999.

Guillou, H., Carracedo, J.C., and Duncan, R.A., K-Ar, 40Ar-39Ar ages and magnetostratigraphy of Brunhes and Matuyama lava sequences from La Palma Island, *J. Volcanol. Geotherm. Res., 106*, 175-194, 2001.

Ida, Y., Effect of the crustal stress on the growth of dikes: Conditions of intrusion and extrusion of magma, *J. Geophys. Res., 104*, 17,897-17,909, 1999.

Iverson, R.M., Can magma-injection and groundwater forces cause massive landslides on Hawaiian volcanoes? *J. Volcanol. Geotherm. Res., 66*, 295-308, 1995.

Komuro, H, Fujita, Y., and K. Kodama, Numerical and experimental models on the formation mechanism of collapse basins during the Green Tuff Orogenesis of Japan, *Bull. Volcanol. 47*, 649-666, 1984.

Krastel, S., H.-U. Schmincke, C.L. Jacobs, R. Rihm, T.P. La Bas, B. Alibés, Submarine landslides around the Canary Islands. *J. Geophys. Res., 106*, 3977-3997, 2001.

Lipman, P. W., R. Y. Lockwood, R. T. Okamura, D.A. Swanson, and K. M. Yamashita, Ground deformation associated with the 1975 Magnitude-7.2 earthquake and resulting changes in activity of Kilauea volcano, Hawaii, *U.S. Geol. Surv. Prof. Pap., 1276*, 1-45, 1985.

Luongo, G., E. Cubellis, F. Obrizzo, and S.M. Petrazzuoli, A physical model for the origin of volcanism of the Tyrrhenian margin: the case of the Neapolitan area, *J. Volcanol. Geotherm. Res., 48*, 173-185, 1991.

Marti, J., G.J. Ablay, L.T. Redshaw, S. Sparks, Experimental studies of collapse calderas, *J. Geol. Soc. London, 151*, 919-929, 1994.

Masson, D.G., A.B. Watts; M.J.R. Gee, R. Urgeles, N.C. Mitchell, T.P. Le Bas, and M. Canals, Slope failures on the flanks of the western Canary Islands, *Earth Sci. Rev. 57*, 1-35, 2002

McFarlane, D.J., and W.I. Ridley, An interpretation of gravity data for Tenerife, Canary Islands. *Earth Planet. Sci. Lett., 4*, 481-486, 1968.

McGuire, W. J., and A. D. Pullen, Location and orientation of eruptive fissures and feeder-dykes at Mount Etna; influence of gravitational and regional tectonic stress regimes, *J. Volcanol. Geotherm. Res., 38*, 325-344, 1989.

McGuire, W.J., A.D. Pullen, and S.J. Saunders, Recent dyke-induced large-scale block movement at Mount Etna and potential slope failure, *Nature, 343,* 357-359, 1990.

McKenzie, D.P., and R.L. Parker, The North Pacific as an example of tectonics on a sphere, *Nature, 216*, 1276-1280, 1967.

Merle, O., and A. Borgia, Scaled experiments of volcanic spreading, J. Geophys. Res., 101, 13,805-13,817, 1996.

Mitchell, N.C., Transition from circular to stellate forms of submarine volcanoes, *J. Geophys. Res., 106*, 1987-2003, 2001.

Moore, J.G., D.A. Clague, R.T. Holcomb, P.W. Lipman, W.R. Normark, and M.E. Torresan, Prodigious submarine landslides on the Hawaiian Ridge, *J. Geophys. Res., 94*, 17,465-17,484, 1989.

Nakamura, K., Why do long rift zones develop in Hawaiian volcanoes; a possible role of thick oceanic sediments, *Bull. Geol. Soc. Jpn., 25*, 255-269, 1980.

Owen, S., P. Segall, J. Freymueller, A. Miklius, and R. Denlinger, Rapid deformation of the south flank of Kilauea volcano, Hawaii, *Science, 267*, 1328-1332, 1995.

Pollard, D. D., P.T. Delaney, W.A. Duffield, E.T. Endo, A.T. Okamura, and T. Delaney, Surface deformation in volcanic rift zones, in Processes of continental rifting, edited by P. Morgan and B. H. Baker, Elsevier, 94, 541-584, 1983.

Richards, R. Jr., and R. Mark, Gelatin models for photoelastic analysis of gravity structures, *Exp. Mech., 6*, 30-38, 1966.

Rubin, A.M., and D. D. Pollard, Origins of blade-like dikes in volcanic rift zones, *in Volcanism in Hawaii*, edited by R. W. Decker, T. L. Wright, and P. H. Stauffer, U. S. *Geol. Surv. Prof. Pap., 1350*, 1449-1470, 1987.

Ryan, M.P., The mechanics and three-dimensional internal structure of active magmatic systems: Kilauea Volcano, Hawaii, *J. Geophys. Res., 93*, 4213-4248, 1988.

Schmincke, H.-U, and G. Graf, DECOS/OMEX II, Cruise No. 43, *Meteor Reports, No. 2000-1*, Univ. Hamburg, pp.1-99, 2000.

Siebert, L., Large volcanic debris avalanches: characteristics of source areas, deposits and associated eruptions, *J. Volcanol. Geotherm. Res., 22*, 163-197, 1984.

Staudigel, H., and H.-U. Schmincke, The Pliocene seamount series of La Palma, Canary Islands, *J. Geophys. Res., 89*, 11,195-11,215, 1984.

Stearns, H.T., *Geology of the State of Hawaii* (2nd edition). Pacific Books, Palo Alto, California, 1985.

Swanson, D.A., W.A. Duffield, and R.S. Fiske, Displacement of the south flank of Kilauea Volcano; the result of forceful intrusion of magma into the rift zones, *U.S. Geol. Surv. Prof. Pap., 963*, 39pp, 1976.

Tilling, R.I., and J.J. Dvorak, Anatomy of a basaltic volcano, *Nature, 363*, 125-133, 1993.

Troise, C., Stress changes associated with volcanic sources: constraints on Kilauea rift dynamics, *J. Volcanol. Geotherm. Res., 109*, 191-203, 2001.

Urgeles, R., D.G. Masson, M. Canals, A.B. Watts, and T. Le Bas, Recurrent large-scale landsliding on the west flank of La Palma, Canary Islands, *J. Geophys. Res., 104*, 25,331-25,348, 1999

Vogt, P.R., and N.C. Smoot, The Geisha Guyots: Multibeam bathymetry and morphometric interpretation, *J. Geophys. Res., 89*, 11,085-11,107, 1984.

vanWyk de Vries, B., S. Self., P.W. Francis, and L. Keszthelyi, A gravitational spreading origin for the Socompa debris avalanche, *J. Volcanol. Geotherm. Res.*, 105, 225-247, 2001.

Walker, G.P.L., The dike complex of Koolau Volcano, Oahu; internal structure of a Hawaiian rift zone, in *Volcanism in Hawaii*, edited by R.W. Decker, T.L. Wright and P.H. Stauffer, *U.S. Geol. Surv.,* 961-993, 1987.

Walker, G.P.L., Coherent intrusion complexes in large basaltic volcanoes; a new structural model, in *Essays on magmas and other earth fluids; a volume in appreciation of Prof. Peter G. Harris*, edited by K.G. Cox and P.E. Baker, *Elsevier, 50*, 41-54, 1992.

Walker, G.P.L., Volcanic rift zones and their intrusion swarms, *J. Volcanol. Geotherm. Res., 94*, 21-34, 1999.

Walter, T.R., and V.R. Troll, Formation of caldera periphery faults, an experimental study, *Bull. Volcanol., 63*, 191-203, 2001.

Conference contributions

Walter TR, Troll VR and Schmincke H-U (2000) Flank destabilization of cyclic caldera volcanoes. *EOS, Transactions of the American Geophysical Union* 81: 1386-1387

Walter TR, Troll VR, and Schmincke H-U (2001) Rift architecture in volcanoes: from single rift to triaxial rifts. *Fourth international dyke conference (IDC4), South Africa, p 8*

Walter TR, Troll VR and Schmincke H-U (2001) Modeling volcano structures: the usage of gelatin, flour, and sand as tools to improve understanding of volcano deformation. *Workshop on "New techniques in analog modeling" GFZ Potsdam.*

Walter TR, Troll V.R. (2001) Flank creeping, sector collapse and formation of volcanic rift zones. *EOS, Transactions of the American Geophysical Union* 82: 1299

The following abstract summarizes a presentation at the annual conference of the
American Geophysical Union (fall meeting) in Dezember 2000, San Francisco, USA
published in
EOS, Trans. Am. Geophys. Union 81: 1386-1387

Flank Destabilization of Cyclic Caldera Volcanoes

TR Walter, VR Troll, H-U Schmincke

Since the failure of Mount St Helens' northern flank on May 18th 1980, lateral collapses of volcanic flanks are recognized as a fundamental process during the evolution of volcanoes on land and on oceanic islands. No consensus exists, yet, concerning the mechanisms responsible for initial structural destabilization, prompting to fail suddenly once triggered by e.g., earthquakes, weathering, hydrothermal alteration.

One scenario allowing prediction of flank collapses is dome intrusion (e.g., Mt. St. Helens). A further mechanism responsible for flank weakening is rifting, directing the locations of flank collapses between two main active axes of a three-armed rift system, e.g., as on Western Canary Islands. Caldera volcanoes, however, which do not fit the above models, are also affected by major flank collapses, suggesting that additional mechanisms causing flank destabilization must be assumed.

An example for weakening of volcanoes flanks is Gran Canaria (Canary Islands), structurally dominated by the multicyclic ca. 20 km-wide Miocene Tejeda Caldera. The extra-caldera lava and ignimbrite series are dissected by radial faults and dike swarms, crosscutting and crosscut by circumferential faults and dikes. In-between, at 5-7 km distance from the caldera rim, a complex horst and graben system is formed, peripheral to the caldera wall. A prominent embayment of the northwest coastline corresponds to a giant landslide scarp, likely to be genetically related to Miocene episodes of caldera collapse.

We carried out analog experiments to simulate cyclic doming, evacuation collapse, and resurgence. Our preliminary conclusions include: (a) Magma chamber inflation results in radial (mode I) fractures and subordinate cone-sheet (mixed mode) fractures accompanied by a steepening of the volcano flanks and subsidence of the broadening apex. (b) Chamber evacuation causes the chamber roof to collapse along outward-dipping ring faults; and (c) the combined mechanisms of doming and subsequent evacuation collapse produce a network of overlapping concentric and radial structures. Relaxations of the initially steepened flanks create circumferential en-echelon faults propagating downwards deeply with main- and reverse-sense to form horst and graben structures at their intersections.

Combining field observations and the results of analog experiments, we suggest the collapse of northwest Gran Canaria to have been a consequence of intersecting radial doming structures and circumferential relaxation faults in the caldera's periphery.

This newly recognized category of flank cracking allows identification of former collapse events in ancient multicyclic caldera terrains and helps to predict potential flank collapses at recent caldera volcanoes.

This abstract goes over the main points of a presentation at the quadrennial conference
Fourth International Dyke Conference (IDC4) in June 2001, Durban, South Africa
published in
IDC4 2001, In: Watkeys M (ed), Fourth international dyke conference, South Africa, p8

Rift architecture in volcanoes: from single rift to triaxial rifts

TR Walter, VR Troll, H-U Schmincke

Creeping flanks of ocean island volcanoes are commonly thought to be triggered by dike intrusion into axial rift zones, the position of huge landslides is recognized to be located between two axes of a three-armed (triaxial) rift system. The genetic and temporal relationship between flank creep and intrusive rift formation remains poorly understood, however.

In Anaga, the deeply eroded northeastern shield volcano of Tenerife (Canary Islands), we reconstructed the palaeostress-vectors and structural changes of dike intrusions with time. During an early stage, a single rift zone dominated the growth of the edifice. A second stage was marked by faulting and dike reorientation, gradually developing a curved (biaxial) structure, located around the northern creeping sector. During a third stage, a third rift-arm developed to the south; all these three axes nucleated in a poorly defined central area. A fourth stage is characterized by a major lateral collapse of parts of the northward creeping sector.

To better understand the mechanisms of dike intrusion and reconfiguration, with respect to creeping sectors of an edifice, we carried out physical models using ridges of gelatin and colored water injected from below, following a method described by Fiske and Jackson (Proc.R.Soc.London, 1972). Liquid-filled crack propagation into the ridge (re-)produced along strike *dikes* (the stable situation). We then enlarged the basal friction of the gelatin ridge by fixing sand onto the basal PVC plate on which the gelatin ridge was placed, with one spherical sector free of this basal sand-layer. In this spherical sector, basal friction was further reduced using a soap-based lubricant. The gelatin ridge was positioned partially on this sector and was thus forced to locally creep due to its own gravitational load. Injection of the fluid caused fractures to propagate in various orientations, relative to (1) the geometric position of the creeping flank, (2) the *edifice* morphology, (3) the center of injection and its eccentricity relative to the gelatin edifice. With greater distance from the unstable and lubricated sector, hydro-fractures were curved around the unstable sector or orientated in along strike direction if injected far away from this sector. Injection of the fluid nearer to, or at the marginal plane of the unstable sector, however, produced mostly biaxial and triaxial arrangements of the hydro-fractures.

The experimental results suggest that the number and orientations of structural axes in volcanic edifices are largely controlled by the near-surface imbalance that arises from the instability of the volcano flanks. With onset of the creeping of a sector that interferes with the stress field of a pre-existing rift system, the structure of a single rift volcano (e.g. Anaga) reconfigurates to a biaxial or triaxial rift. The location of flank failures is consequently situated between these intrusive axes, as dilation of the basal detachment surface is at a maximum in-between.

An international workshop focusing on "New techniques in analog modeling" was held at the GeoForschungsZentrum (GFZ) Potsdam in Oktober, 2001

Modeling volcano structures: the usage of gelatin, flour, and sand as tools to improve understanding of volcano deformation

T.R. Walter, V.R. Troll & H.-U. Schmincke

The general shape and detailed morphology of volcanoes commonly reflect their structural configuration and their preceding episodes of construction and destruction. Probably all of the Canary Islands experienced large destructive sector collapses (up to several tens of cubic-kilometers) during their life time, i.e. landslides that occur by the lateral failure. The trigger mechanisms of these flank failures are poorly constrained, since the rapidly changing structure of a volcano leads to potential misinterpretations of the initial mechanisms. In order to better understand the structural evolution of large oceanic volcanoes, we used physical modeling to simulate the magmatic processes and resulting stress paths, and compared the structural configuration and arrangement of fractures in experiments and nature:

(i) A large Miocene caldera on Gran Canaria formed by partial subsidence of the edifice's surface into an evacuating shallow magma chamber. Magma-pathways (dikes) on the island are generally radial, trending away from the caldera, while faults are distributed mainly concentrically. To model the Gran Canaria caldera, an inflatable balloon - simulating magma chamber dynamics - was placed into an analog edifice and connected to a pipe-system. Scaling was chosen to be $1:10^{-5}$. For mechanical control, we used two very different materials, flour and sand. Flour allowed to study fault propagation without collapse of steep structures; sand was used to study landslide effects. Both materials allowed to reproduce the structures of Gran Canaria, when the balloon was repeatedly inflated and deflated.

(ii) The triangular shape of Tenerife is defined by three dominant rift zones. The sites of flank collapses are generally located between two axes of the triaxial rift system. The intervening areas commonly creep, possibly triggered by concomitant pressures of intruding dikes along the rift zones. The relationship between volcano load, creep of flanks and intrusive rift-formation remains poorly understood, however. We used the orientation of dike swarms on Tenerife to reconstruct the paleo-stress field at the time of dike emplacement, and carried out gelatin experiments to improve constraints on rift zone development. Gelatin is highly elastic and the experiments were not to scale. We used ridges of gelatin and injected colored water from below. Defined by lateral spreading, injection of the fluid into a morphological triangular-prismatic ridge caused hydro-fractures (dikes) to propagate parallel to the ridge elongation. In a further experimental setup, the gelatin ridge was positioned partially on a lubricated sector that was allowed to creep locally due to its own gravitational load. Injection of the fluid then caused fractures to propagate in new directions, suggesting that volcano deformation has a major influence on reorganization of rift zones in volcano systems.

In both cases, (i) the scaled and (ii) the unscaled experiments, we simulated volcano deformation mechanisms, reproducing structures that correlate with the field data. Moreover, the very different experimental setups showed that volcano construction and destruction take place essentially synchronously. The choice of gelatin, flour or sand used for modeling was based on the requirements of the different approaches and the specific mechanisms addressed.

AGU 2001 fall meeting: EOS, Transactions of the American Geophysical Union 82(47): 1299

Flank creeping, sector collapse and the formation of volcanic rift zones

T.R. Walter, V.R. Troll

The structural skeleton of ocean island volcanoes is commonly formed by rift zones that are marked by abundant dike intrusions and sites of volcanic eruptions. Field data on Tenerife, La Palma and El Hierro (Canary Islands) reveal that single and radial dike swarms form early during volcano evolution and are rearranged to become triaxial rifts during later stages of volcano growth. These rifts are commonly associated with unstable flanks in-between two axes, however, the relationship between rift initiation and flank instability remains poorly resolved.

Due to rising awareness of local flank creeping, dynamic volcano spreading and the recognition of weak substratum at volcanoes worldwide, we designed analog experiments to simulate the stress field and intrusive patterns of unstable volcanic edifices. The analog volcanoes were cone shaped and made of gelatine, whereby different conditions of basal friction were used in various experimental setups. From below we injected colored water and studied the orientation of fractures (dikes) that propagated through the cones.

Situated on uniform substratum, the flanks of the gelatine-cone deformed by gravity-driven extension. The orientation of the fractures was perpendicular to the minimum pricipal compressive stress, resulting in a ″radial dike swarm″. In a further setup, we reduced the basal shear resistance in one sector, to simulate the stress field close to a locally creeping flank. In these experiments, the dike azimuth diverged largely if injected into a) the non-creeping part of the cone, b) the creeping sector, or c) the stable/unstable interface. Case a) produced radial fractures; case b) produced mainly fractures that reflect strong circumferential expansion of the creeping sector. In case c) three main fracture directions formed, two of which were tangential to the stable/unstable interface and a third diffuse one propagated into the stable part of the cone, reminiscent of triaxial rift zones on many natural volcanoes (e.g. El Hierro, Tenerife). The significance and direction of the three rift zones varied systematically with size, eccentricity and creep direction of the unstable sector. Slight eccentricity of the creeping sector focused dike intrusion along two curved axis that were tangential to the stable/unstable interface; a relationship comparable to N Anaga, Tenerife. In contrast, strong eccentricity resulted in one main tangential rift, very similar to the S-rift observed on La Palma.

Based on the experimental results, we propose that the formation and configuration of triaxial rift zones may be a response to near-surface volcano-deformation such as volcano-spreading or flank creeping rather than a simple function of vertical upward loading as commonly assumed for volcanic rifts on ocean islands.

Acknowledgements

Firstly, my profound thanks go to my supervisor, Prof. Hans-Ulrich Schmincke. He engaged me in the first place, kindly introduced me into the field of Gran Canaria and Tenerife, and gave untied stimulating discussions, suggestions, and ... critique. Next on my list of thanks are the colleagues of the department at GEOMAR, I appreciated and largely benefited from lots of discussions with them, especially Matthias Hort, Thor Hansteen, Ralf Seyfried, Alexander Belousov, Paul v.d. Boogard, Carsten Schirnick and Peter Sachs. I profited from numerous discussions on various occasions with Pete Lipman, Falk Amelung, John Stix, Ram Weinberger, Akira Takada, Andreas Klügel, Juan Carlos Carracedo, Doug Masson, Valerio Acocella and Djordje Grujic. Special thanks go to Val Troll for experimental co-working and conjointly field work on the Canary Islands, and for the technical discussions we had on Playa del Chiquas. On Tenerife I thank J.M. Navarro (actually Pepe) for showing me the island and sharing his hammock with "Mietschy the cat". Pepe y Mercedes, muchas gracias por vuestra hospitalidad! Thanks go to the miners and geologists of ITER, particularly Ricardo Balcells and Juan Coello. On Gran Canaria I acknowledge help by Beate Wenskowski, Kiko and Gabriella, Manolin Léon, José Escubar & his family, Señor Palmero and those plenty killer-bees for allowing bypass. My colleagues in the Graduate School and associates are thanked for discussions, manuscript proofreading, data conversions and lots of coffee breaks, namely Ralf Schmidt, Buddy Krastel, Lothar Schwarzkopf, Nico Urbanski, Michael Abratis, Volker Karpen, Barbara Teichert, Stefan Urpi, Alexander Schimanski, Axel Mohr, Jenny Kandiano, Britta Lissina, Richard Heath, Jörg Geldmacher, Susanne Fretzdorf, Nicole Stroncik and Angelika Schmidt. My credits go to Sandra wie das Bollwerk for being my office mate, and sharing tons of chocolates. Special thanks go to Beatrice Cailleau for any support, patience, fun and also for room sharing. PC-man Alexander Heuser very much helped me to finger plenty of computer bugs. During the sample preparation I benefited from help by trainees Sascha Staubach, Elke Hanenkamp, Sven Krein, Marlies Engelmann, Ute Thurow and Ken Heyhold. Technical support was provided by Dagmar Rau. Thanks go to Volker Feeser (IFG) for letting me to test triaxial deformation rigs and get insights into rock mechanical apparatus evolvement. Angelika Finke for rapid organization of inaccessible paper copies. Finally I would like to thank my parents for their warm interest and continuous support at any times.

This work was funded by grants of the Deutsche Forschungsgemeinschaft (DFG), providing a stipend during the first 18 Months by the Graduate School "Dynamics of Global Cycles" (DFG Schm 250-49) and for the following time from the DFG grants (Schm 250/77-1 and Schm 250/77-2) to H.-U. Schmincke.

This work would have been poorer without the contribution of each of them.

Curriculum Vitae

Name:	Thomas Ingo Rafael Walter
Date of Birth:	June 20, 1972
Sex:	Male
Nationality:	German

05/2002	Disputation
11/2000	Dept. of Volcanology and Petrology, GEOMAR Research Center in Kiel
04/1999	PhD – Stipend, Graduate school "Dynamics of Global Cycles" at Christian-Albrechts-University Kiel
1999	Diploma thesis (MS-level), Dept. of Geology - Structure and Tectonics Group, Albert-Ludwigs University Freiburg i. Brsg.
1998	Trainee in engineering geophysics at "Terratec", Heitersheim
1997	Internship at SOEST, Dept. of Geophysics, HI, USA
1994 - 1999	Studies in Geology, Dept. of Geology, University Freiburg
1993 - 1994	Studies in Mineralogy, Dept. of Mineralogy, University Freiburg
1983 - 1993	High school in Konstanz and Überlingen, A-level
1979 - 1983	Primary school Insel Reichenau